Carbon Monoxide Oxidation at the Interface of a Direct Barrier Discharge and a Thin Layer of Yttria-stabilized Zirconia - Characterization of Discharge Properties and Determination of Reaction Rates

Dissertation

by

Dipl.-Phys. Sven Ole Steinmüller

for the degree of

Doctor rerum naturalium

- Dr. rer. nat. -

submitted to the
Faculty of Biology and Chemistry
Justus-Liebig-Universität Gießen, Germany

Gießen 2014

Mr. Spock, all new facts seem to make our situation even more complex.
This is an inevitable risk in any scientific efforts, Captain.

Star Trek: The Original Series
Dreams of the Raven
Novel written by Carmen Carter

Ich erkläre: Ich habe die vorgelegte Dissertation selbständig und ohne unerlaubte fremde Hilfe und nur mit den Hilfen angefertigt, die ich in der Dissertation angegeben habe. Alle Textstellen, die wörtlich oder sinngemäß aus veröffentlichten Schriften entnommen sind, und alle Angaben, die auf mündlichen Auskünften beruhen, sind als solche kenntlich gemacht. Bei den von mir durchgeführten und in der Dissertation erwähnten Untersuchungen habe ich die Grundsätze guter wissenschaftlicher Praxis, wie sie in der "Satzung der Justus-Liebig-Universität Gießen zur Sicherung guter wissenschaftlicher Praxis" niedergelegt sind, eingehalten.

(Sven Ole Steinmüller)

Contents

Abstract

This thesis investigates the carbon monoxide oxidation at the interface between a Direct Barrier Discharge (DBD) and a thin layer of Yttria-stabilized Zirconia (YSZ), which is an oxygen ion conductor. The thin film is deposited on a dielectric consisting of fused silica. The aim of this work was to investigate the reaction rates of the carbon monoxide oxidation according to the new concept of heterogeneous plasma catalysis with an oxygen ion conducting catalyst.

In this work the uncoated fused silica dielectrics were used as reference system and compared with coated dielectrics with a thin YSZ film. The temperature dependent behavior of this system and the discharge itself was monitored as there should be differences according to the thermally activated electrode kinetics and oxygen transport processes in the bulk. A second aspect of the investigations was the frequency dependent behavior of the discharge and the influence of the discharge frequency on the catalytic rate enhancement.

The different discharge setups were investigated according to the distribution of the ionic and excited species with Optical Emission Spectroscopy (OES). Theses results were compared with data obtained by Quadrupol Mass Spectroscopy (QMS). Additionally plasma ignition voltages according to the different discharge compositions at room and elevated temperatures were measured.

The QMS signal intensities were used to compare carbon dioxide reaction rates of the reference and the YSZ coated discharge setups. The obtained data was used to discuss possible kinetic models.

The OES investigations showed that the discharge is strongly influenced by the carbon monoxide gas. The dominant lines recorded are related to CO^+ ions, only at very low CO partial pressures lines of Ar^+ occur. Only rarely and with decreasing intensity at higher oxygen partial pressures oxygen emission lines can be found. This might be a clue to increased concentrations of negatively charged oxygen ions.

With all performed observations it can be concluded that the thin film deposition of a YSZ layer on a fused silica dielectric enhances the reaction rate of the carbon monoxide oxidation due to a discharge YSZ surface interaction or to a YSZ surface restructuring, which takes especially place at room temperature conditions. Possible kinetic models were proposed.

Chapter 1

Introduction

Nowadays there is usually not a solely physical, chemical or biological etc. view of a scientific problem. Instead there is often an interdisciplinary way of solving a scientific problem, which combines the natural sciences and form new interdisciplinary viewpoints. The combination of old concepts leads mostly to new fields of science or even new industrial applications. This work focuses on such an interdisciplinary viewpoint by combining standard knowledge of (plasma) physics and (electro)chemistry, leading to a new perspective to a well known industrial application (carbon monoxide oxidation). This introduction will show the different starting (view)points of the interdisciplinary approach and after this it will lead to the aim and deeper concept of this work.

Plasma discharges are investigated since the 19^{th} century [1, 2, 3, 4] and today different kind of discharges [5, 6, 7, 8] are well known and the results became basic knowledge in plasma physics respectively plasma chemistry. Different applications of plasma discharges can be found today, e.g. in cleaning and disinfection [9, 10, 11], thin film deposition [12, 13], surface modification of materials [14, 15, 16], gas discharge lamps [17], electronic devices as plasma display panels [18] or even ion thrusters [19]. The underlying sometimes very complex processes in discharges are still under investigation [20], but for an empirical description of the behavior of a discharge and the use in the noticed applications this basic atomic or molecular knowledge is often not necessary.

Taking chemical considerations more into account different aspects of an discharge are more interesting. Consisting of electrons, ions, and radicals discharges are well suited for investigations of gas phase reactions or interactions with other phases (liquid or solid) when charged particles offer faster reaction paths. With this in mind the plasma-electrochemical interaction with an ion-conductive solid state material seems to give opportunities for

new approaches. The controlled reactions of electrons and/or ions from a discharge at surfaces of liquid [21, 22, 23, 24] or solid electrolytes [25, 26, 27] are of interest. Otherwise for a solid state chemist also the reverse case of analyzing a discharge with an solid electrolyte seems to be a possible analytical technique [28], where physicists normally use the well adapted Langmuir probes [29, 30, 31, 32].

Taking electrochemistry into a closer focus the possibility to manipulate with a solid electrolyte the concentration of ionic species in a discharge seems to be a promising idea for different technical applications. For this purpose an ion conducting material like yttria-stabilized zirconia (YSZ) seems to be the right candidate. In a work of Torimoto at the end of 20^{th} century [33] the observation of a DC glow discharge during the experiment of a fuel cell with a solid electrolyte of YSZ led to first investigations of the discharge characteristics and the influences of temperature and applied voltage on the solid electrolyte.

Electrochemical properties of YSZ are well known (see sections 3.4 and 5.1 for details) and it is used for example in automobiles in the lambda probe to control the oxygen partial pressure in the engine. In addition it is known for about ten years that YSZ can emit negative oxygen ions into the vacuum. This was shown by Torimoto et al. [34, 35, 36] and Fujiwara et. al [37, 38, 39]. These results encouraged to use YSZ as electrode material in different discharge systems. The surface oxygen exchange of YSZ with a RF discharge was studied by Rohnke et al. [40] and the use of YSZ as electrode material in a DC discharge was investigated by by Steinmüller et. al [41]. All these results showed that an interaction of an oxygen discharge with a solid electrolyte as YSZ is possible and can influence the discharge itself.

The arising question with this information in mind was: Is it also possible to influence a chemical reaction itself by adapting these results into a new concept? From catalysis it is known that the presence of a heterogeneous catalyst can positively influence the reaction rate of a chemical process. This is well known from different industrial applications (see section 3.2). The combination of discharges with the use of heterogeneous catalysts is already adapted in science (see section 3.3). With the use of an ion conducting material as heterogeneous catalyst it should be possible to influence the discharge composition itself and accelerate a chemical reaction. In the case of the mentioned YSZ, used as solid electrolyte, an increase of the oxidation rate of a gas like carbon monoxide to carbon dioxide might be enhanced. This will lead to the new concept of heterogeneous plasma catalysis with an oxygen ion conducting catalyst. This new interdisciplinary concept will be introduced in the next section.

Chapter 2

Concept and Aim

A large variety of discharge systems is well known and different applications have been established with different kinds of discharge systems over time. For the new concept of this work especially a Direct Barrier Discharge (DBD) (see section 3.1) offers the technical requirements which are needed. DBDs can be ignited at atmospheric pressure, which makes them well suitable a lot of technical and medical applications. In this work the DBD technology used in Plasma Display Panels (PDP, known from the television market) is adapted to perform electrochemical gas phase experiments. The usual PDP architecture (batch discharge system) is transferred into a flow through discharge reactor. The usually used dielectric material that is essentially for the discharge ignition is exchanged by an ion conducting material (YSZ), which shall work as a heterogeneous catalyst for a gas phase reaction under discharge conditions.

In the case of YSZ, which is an oxygen ion conductor, the plasma catalytic increase of an oxidation reaction rate of for example carbon monoxide to carbon dioxide will be monitored and compared with non functionalized dielectric material. The advantage over normal heterogeneous catalyst systems with or without discharge assistance lies in the interaction of the ion conductor and the alternating applied potential of the DBD. Figure 2.1 shows a schematic overview of such a discharge system with ion conducting catalyst used for heterogeneous plasma catalysis. In the upper half of the figure a dielectric barrier discharge system with he metal electrodes (black) which cover two YSZ dielectrics (orange) is shown. Between the dielectrics a discharge is ignited (pink). The discharge consists of oxygen and carbon monoxide and the corresponding ions. Inside of the discharge ions are accelerated according to their charge to the opposite charged electrode. This leads to two different "working" interfaces.

The yellow arrow in the upper left shows the incorporation of negative

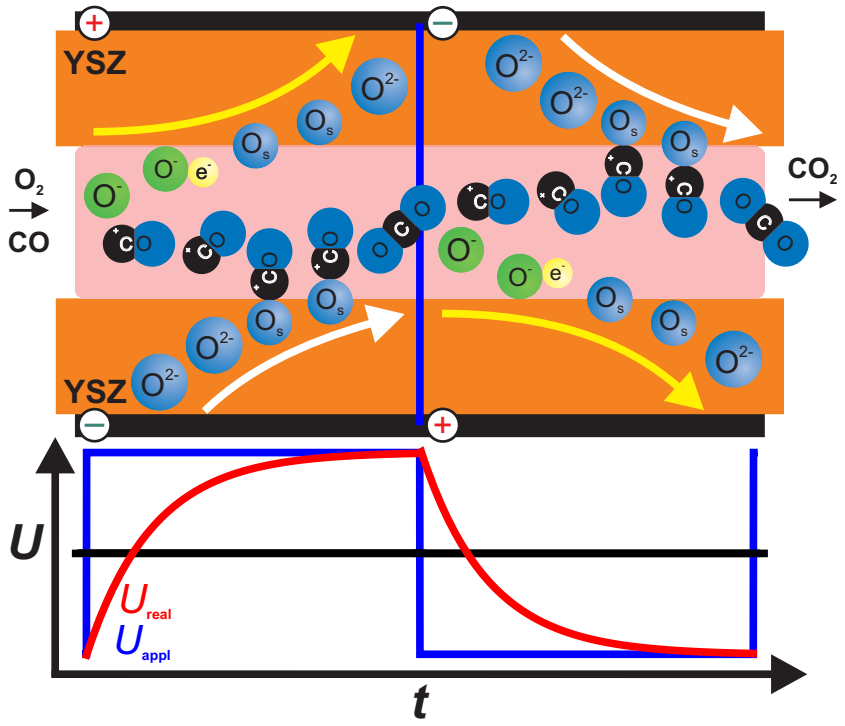

Figure 2.1: The figure shows the reaction (white arrow) and regeneration (yellow arrow) cycle of the ion conducting heterogeneous catalyst during one full AC generator cycle. The alternating potential leads to a reaction and recovering cycle for both YSZ dielectrics as explained in detail in the text. At the bottom the progression of the applied potential by the square waveform function generator (blue) and the calculated real potential according to the charging of a capacitor system (red). The black line indicates the ground potential level. At the vertical blue line in the middle of the schematic drawing of the discharge system the square wave function is reversed. The processes at the surfaces of the YSZ coating on top of the fused silica dielectric are reversed as discussed in the text.

oxygen ions O^- at the electrode with the positive potential into the top surface oxygen layer O_s of the YSZ. If the oxygen is incorporated into the anion lattice of the bulk material double negatively charged oxygen ions O^{2-} are formed . The white arrow below shows the second interface reaction steps. Bulk O^{2-} forms a surface layer oxygen ion O_s and has then the possibility to react with adsorb carbon monoxide CO at the surface to form CO_2.

As long as the DBD frequency is at an appropriate value the oxygen ions (O_s) stay near the surface unless the potential is switched due to the alternating current generator, which usually is used for a DBD. In this case a surface oxygen ion O_s should easier react with adsorbed molecules of the used reaction gas and pushed afterwards back into the discharge. The alternating potential hereby influences the binding of surface or near surface oxygen on the YSZ thin film. Taking this into account the white arrow shows the reaction steps and the yellow arrow shows the regeneration steps of the dielectric heterogeneous catalyst system. Due to the potential switch of the AC generator (blue line in the dielectric system) the "functions" of the YSZ coatings are exchanged and alternating reaction and regeneration cycles are established on each functionalized electrode.

With this behavior as in a "normal" heterogeneous catalyst system the activation energy for a chemical reaction should be reduced and therefore the reaction rate increased. This concept may be named as "ion supported DBD driven heterogeneous plasma catalysis". In figure 2.1 additionally is the applied potential by the square waveform function generator (blue) and the calculated real potential according to the charging of the whole capacitor system is shown (red) below the schematic overview of the dielectric system. The zero potential is indicated by the black line.

The aim of this work is to show that the use of an functional ion conducting layer in a DBD can influence the plasma chemistry inside the discharge and work as a heterogeneous catalyst according to reaction rates of an oxidation reaction. This is from an industrial viewpoint, for example for exhaust cleaning (carbon monoxide is often a by product, which has to be removed from gas streams), of interest. A reduction of costs and an increase of effectivity could be attractive from a technical viewpoint.

To reach this aim a special reactor had to be designed and the DBD system characterized. This includes to find preparation routines for the "dielectric electrodes", to investigate the influence of the gas composition and the interaction of the alternating current reactor with the dielectric system. As the ionic conductivity of YSZ is a temperature dependent function the influence of temperature on the reaction rates had to be examined. Reference experiments without functional layers had to be performed and compared with experiments with functional YSZ layers.

Chapter 3

State of Research

This chapter shows the current state of research in the topics related to this thesis. First a short introduction on Direct Barrier Discharges (DBD) and their operation conditions is given in section 3.1. Beginning with possible electrode arrangements in 3.1.1. DBD are closer introduced and the different modes of this discharges are presented in 3.1.2.

Examples of usages of DBD in science and industry are shown in section 3.1.3 to give an overview of the field of applications. After this a closer look to the concept of heterogeneous catalysis is given in section 3.2 and followed by the concept of heterogeneous plasma catalysis in section 3.3.

The material properties of the ion conducting yttria stabilized zirconia (YSZ) material which is used in this work follows in section 3.4. The topic of electrochemical promotion is explained by the example of the Non-Faradaic Electrochemical Modification of Catalytic Activity (NEMCA) in section 3.5. The last section 3.6 gives a short introduction to the optical emission spectroscopy and the literary sources of emission line data and the theoretical concepts of the used analytical methods.

3.1 Dielectric Barrier Discharges (DBD)

Plasma discharges were known and examined since the 19^{th} century. Different ways of ignition of a discharge were found and for all kinds of systems basic knowledge of the plasma physical properties is available, nowadays. Usually the requirements for a plasma discharge are very simple. Either two electrodes (Direct Current (DC) discharge) or a coil for inductive energy coupling (RF) or microwave excitation is used to ignite a gas discharge. In more special applications these simple systems can be altered and the ignition of the discharge follows modified excitation processes.

In this work a Dielectric Barrier Discharge (DBD) is used. This kind of discharge is a modified DC discharge setup with certain specifications. An insulating dielectric material is used to separate the electrodes from each other. The dielectric limits the current flow through the system, which is important for a proper functioning of the DBD [8]. The applied voltage that is needed for a discharge is increased generally in the range from a few hundred V up to several kV. The discharge operates usually at frequencies of several Hz to 50 kHz depending on the application of the used DBD. In contradiction to DC and RF discharges a DBD operates at atmospheric pressure and is a highly non-equilibrium plasma.

The discharge properties can be influenced by the experimental setup, which basically includes the gap distance of the electrodes and the dielectric material. Typical operation conditions of DBD's in air are summarized by Wagner et. al in [42]. A closer view to volume and surface barrier discharges is given by Kogelschatz [7]. He also discusses collective phenomena like filament arrangement, regular and ring patterns depending on the kind of discharge used.

First experimental investigations of a DBD were performed by W. Siemens in the middle of the 19^{th} century [1]. Siemens investigated the generation of ozone which was the first application of DBD's. A brief historic introduction of DBD's is given by Kogelschatz at the beginning of [43]. In the following subsections the basic properties and discharge behavior of DBD's will be discussed and the special needs for this work carried out briefly.

3.1.1 Possible Arrangements for DBDs

DBD experiments usually include one electrode that is used as high voltage electrode and another electrode which is grounded. For a DBD a dielectric layer in the current path between the electrodes is essential. Figure 3.1 shows typical electrode setups as discussed by Wagner et. al in [42]. Planar reactors (subfigures a) to c)) are very simple DBD systems with a strong similarity to a capacitor system with a dielectric material in between the electrode "plates" and a constant electric field between both electrodes. A cylindrical reactor (subfigure d)) uses the same simple arrangement concept but the radial electric field distribution is not that easy to handle. The surface discharge (subfigure e)) is easier to prepare because both electrodes are put directly on the dielectric material, but at least one of the electrodes is in direct contact with the discharge itself. This is also true for the "one-sided" planar DBD systems (subfigures a) and b)). The benefit of the coplanar discharge is that both electrodes are embedded into the dielectric material. This electrode setup is used in plasma display panels.

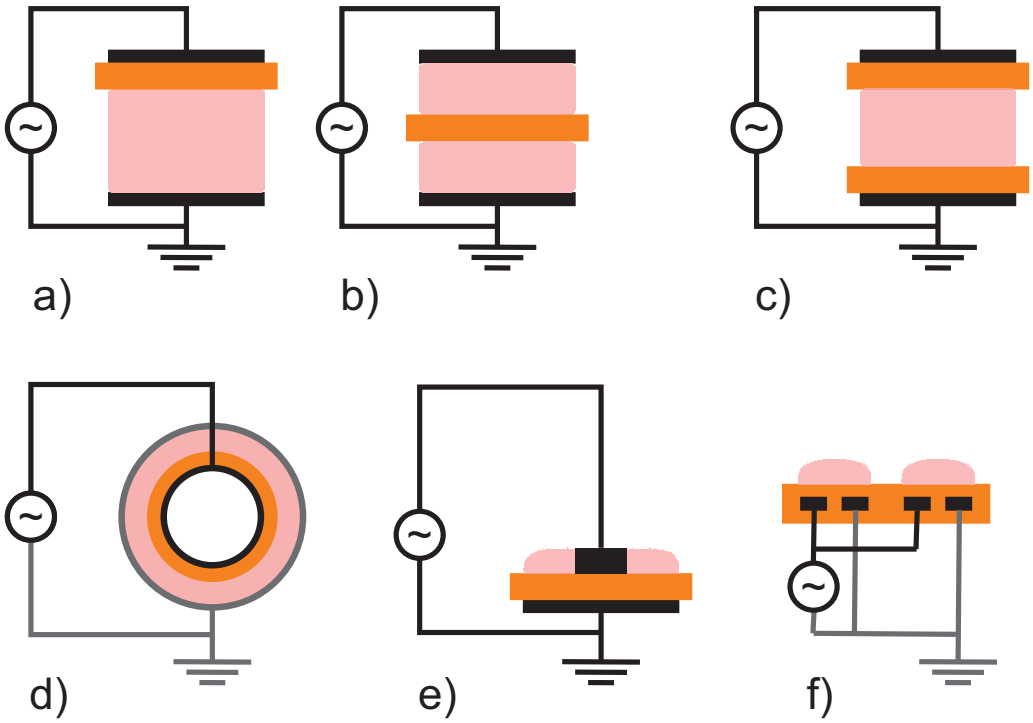

Figure 3.1: The figure shows possible arrangements for DBD setups with conducting wires (black and grey smaller lines), electrodes (thick black lines), dielectric material (orange), and discharge (pink): Subfigure a) to c) show planar reactors. Specific reactor setups can be divided into a) one-sided DBD reactor with dielectric on top of high voltage electrode, b) one-sided DBD reactor with dielectric between both electrodes and two ignited discharges, c) two-sided DBD reactor with dielectric on top of both electrodes. Subfigurs d) to f) show special arrangements of DBD reactor systems d) cylindrical DBD reactor with dielectric material directly on the high voltage electrode, e) surface discharge with both electrodes placed directly on opposite sides of the dielectric material, and f) coplanar discharge with both electrodes embedded into the dielectric material. For detailed explanations see references [42, 43]

Garamoon et. al [44] investigated a "two-sided" planar DBD reactor discharge and compared it with a "one-sided" planar DBD reactor. They examined in both DBD setups four different dielectrics (Pyrex glass plates of 1.1 mm thickness, Mylar sheets of 0.1 mm thickness, porous alumina Al_2O_3 plates of 3.5 mm thickness, and ceramic Al_2O_3 plates of 3.5 mm thickness). In the "one-sided" experiments just the electrode were the potential was applied (life electrode) was covered by dielectric material. They found that no changes occurred for the filamentary mode of the Pyrex glass and the Mylar sheets. The use of the Al_2O_3 dielectrics instead changed the discharge behavior of the two half cycles (plus resp. minus). The density of filaments and the glow component were different in the both half cycles.

Taking into account that in this work catalytic effects are investigated some of the DBD electrode arrangements seem to be imperfect for use in catalytic experiments. The "one-sided" reactor (as shown by Garamoon) and the surface discharge have the problem of direct contact of the metallic electrode with the discharge which can influence the catalytic behavior of the functional layers of YSZ used in this work. Therefore the "two-sided" planar reactor and the coplanar discharge reactor appeared to be a reasonable choice for the experiments performed in this work.

3.1.2 Filamentary and Glow Mode of DBD

In general the discharge behavior of a DBD can be divided into two modes of operation. Similar as known from DC discharges one glow mode exists under certain experimental conditions for a DBD discharge. The intensity of this glow mode varies from a quasi-glow mode to a atmospheric pressure glow mode. Another discharge characteristic is the occurrence of micro discharges, which are described usually as filamentary mode of DBD plasma. Kogelschatz gives an overview in [45] of filamentary, patterned, and diffuse barrier discharges investigated in literature. The wide range of applications accessible for barrier discharges makes an understanding of the different discharge types necessary. A deeper discussion of the "Applications of Microplasmas and Microreactor Technology" is given by him in [46].

The filamentary mode consisting of several micro discharges is the result of simultaneously electrical breakdown of the gas gap [42, 45, 46, 47]. If the electric field is high enough a large number of micro discharges can be established. The densities of microdischarges per electrode area depends on the power coupled into the discharge, which depends on the applied frequency and the peak voltage, but not on the waveform of the applied voltage [45] (see also subsection 3.1.4).

The electrical conductivity and therefore the discharge itself is only re-

stricted to the micro discharges. The surrounding gas is not ionized and therefore absorbs the energy dissipated in the micro discharges as explained by Kogelschatz [43]. Wagner et al. state in [42] that the dielectric barrier limits the amount of the transferred charge and energy deposited in a micro discharge channel. They add that if the potential of the applied voltage is reversed also the micro discharge formation processes reverse. With intact dielectric barriers and micro discharges well distributed over the whole electrode area the amount of charge transported by one micro discharge is limited and no spark or arc can occur in the discharge gap [43].

Especially for surface treatment a DBD consisting of micro discharges is not suitable. For a better plasma-surface interaction a uniform glow discharge is preferred. The size of a micro discharge channel (also called streamer channel) depends on the used gas. Kogelschatz [43] gives an order of the streamer channel for several gases: oxygen < carbon dioxide < air < nitrogen < xenon < helium. He explaines that due to the large streamer channels of helium a glow discharge can often be established by overlapping of the propagating electron avalanches during micro discharge generation. Wagner et. al [42] describe the efforts of the work group of Okazaki who investigated from the late 1980's on barrier glow discharges with special kind of electrodes. The term atmospheric pressure glow discharge (APGD) was proposed by Okazaki.

Wagner et al. conclude that for a stable glow DBD special operation conditions are required. The glow of DBD's is sensitive to impurities, admixtures and residual ions in the gas discharge. Depending on the discharge conditions a transition from glow mode to filamentary mode is possible. Brandenburg et al. [48] investigated the behavior of nitrogen DBD with admixtures of different gases (H_2, He, Ne, and Ar) according to the transition from different glow modes to filamentary mode and according to the burning and transition voltages of the DBD. At the burning voltage the ignition of the DBD takes places and at the transition voltage the glow mode changes into the filamentary mode. They found that for lower admixtures of the named gases a wider range of applied voltages feeds a glow discharge even if up to 90% of the nitrogen gas was exchanged.

Garamoon et. al [44] also investigated the DBD discharges from the previous subsection according to the obtained glow modes. They found that depending on the dielectric material the mode of the discharges varies from filamentary to quasi glow mode or atmospheric pressure glow discharge (APGD) mode. They stated that with higher capacitance of the barrier a higher probability of obtaining uniform discharges is given.

3.1.3 DBD used in Scientific Investigations and in Technical Applications

DBDs are used in a wide field of applications. The influence of different parameters on the DBD behavior and general examples of the usage of DBD in literature will be explained briefly in this section.

Aghamir et al. used a DBD discharge for the conversion of methane to methanol [49]. They found that the conversion rate increases with the applied voltage and decreases with the flow rate of the methane gas, which leads to higher residence time of the methane gas in the DBD. The selectivity of the generated products was almost independent of the applied voltage in their experiments. But they also showed that the presence of oxygen has a significant effect on the conversion of methane and product selectivity.

The existence of oxygen above certain voltages led to the production of methanol. A different behavior of the addition of oxygen in a DBD onto the nitric oxide conversion was found by Yin et al. [50]. The removal efficiency of NO was reduced by adding even small volume portions of O_2. But nevertheless the NO_2 generation rate increased with higher oxygen content.

Additionally they found that the side product creation of N_2O was also reduced by adding higher oxygen volume fractions. They also reported lower discharge currents at higher oxygen volume additions which seems to be caused by the electronegative character of the oxygen gas itself. Due to electron attachment several negative ion species as O^-, O_2^- or O_3^- are formed and influence the discharge which causes the reduced discharge current.

The influence of frequency, different oxygen pressure, and gap distance of a DBD on surface etching of a photoresist was investigated by Falkenstein [51]. He found that the etching rate and efficiency of the DBD increased with higher applied frequencies. In addition he found that for the oxygen pressure and the gap distance an optimum exists. The surface of the etched photoresist showed decreasing material damage and an increased surface roughness at higher frequencies.

Falkenstein summarizes that high frequency DBD's are an efficient, alternative plasma source at atmospheric pressure for general surface processing. The temperature dependency on Benzene oxidation in DBD was examined by Li et al. [52]. They found that the rate of conversion of benzene correlated linearly with the gas temperature. At higher gas temperature higher conversion rates could be achieved. They also found that the gas temperature raises without additional heating depending on the energy input into the discharge system. With higher energy input the heating effect on the gas was greater.

Yu and Chang studied the oxidative conversion of CF_4 via Plasma pro-

cessing with DBD [53]. Their study showed that higher applied voltage, gas residence time, oxygen content, and frequency influenced positively the removal efficiency of CF_4. It was also shown that higher power input enhanced the conversion and that the use of an additional catalyst (see section 3.3) also increases the efficiency of the conversion of CF_4.

The medical application of a Floating Electrode (FE) DBD for blood coagulation and living tissue sterilization was demonstrated by Fridman et al. [9]. The FE-DBD was used to hasten blood coagulation without harming the living tissue around a cut performed on a human spleen. They also showed the inactivation of bacteria grown on a blood agar and the tissue sterilization by FE-DBD without any harm to the treated skin.

Borcia et al. examined the influence of different reactive oxygen species onto the surface modification of polymers [15]. They investigated the effect of different DBD duration exposure on the investigated polymer film to the surface roughness, wettability, and surface funtionalization. They showed that the comparison of the gathered data leads to an optimum DBD exposure time to obtain best results on the investigated polymer. They also added that the DBD exposure time is different for other polymers and therefore for each material the best parameters has to be chosen.

An opposite effect of DBD can also be investigated: The decomposition of molecules within a DBD system. Li et al. reported on the influence of different dielectric barrier materials used in DBD on the decomposition rate of CO_2 [54, 55]. They compared the influence of a $Ca_{0.7}Sr_{0.3}TiO_3$ material that was prepared by using $Li_2Si_2O_5$ as a sintering additive with commercial alumina and silica glass barriers. They found that the commercial alumina and silica barriers only decomposed CO_2 to 4.7% respectively 3.8% where as the $Ca_{0.7}Sr_{0.3}TiO_3$ material could achieve up to 15.6% CO_2 decomposition. They stated additionally that the CO_2 decomposition is correlated with the permittivities of the dielectric barrier materials used.

3.1.4 Charging Behavior of the DBD System

The DBD system used in this work can be described in a simplified way as an ordinary plate capacitor according to the electric properties. The charging of such a capacitor follows a time-dependent behavior with a time constant τ that is characteristic for the capacitor system and therefore for the DBD system used in this work. τ is given by the capacity C_{total} of the dielectric plate system and the ohmic resistance R_{total} of the capacitor system.

$$\tau = C_{\text{total}} \cdot R_{\text{total}} \tag{3.1}$$

The value of R_{total} used in calculations was $R_{\text{total}} = 100\ \text{k}\Omega$, for further explanation of this resistor value take a look in section 5.5.1 where the assembly of the AC generator is described. After a charging time of $t = 5\tau$ the maximum of the applied voltage U is reached (about 99% of U_{max}). The value of τ is not frequency and therefore time-dependent but the applied voltage U_{C} at the capacitor system follows a time-dependent function.

$$U_{\text{C}} = U(t) \tag{3.2}$$

Therefore using the dielectric system at different frequencies may lead to the problem of not charging the plates fully in the time t above a frequency of $f(\tau)$ which can be easily calculated if τ is known. This implies that the maximum applied voltage can not be reached during charging. For the amount of power transferred into the discharge during the charging this means that less power P is incorporated into the discharge system. Due to this fact for higher frequencies than $f(\tau)$ the ignition voltages increases. With this increase of the applied voltage the power transferred in the time interval t into the discharge system is still of the same value according to:

$$P = U_{\text{C}} \cdot I(t) \tag{3.3}$$

For a better understanding of this frequency-dependent charging effect a closer look to the DBD capacitor system is necessary. The capacity C_{DBD} of the DBD system depends on the size, the thickness, and the kind of the dielectric material used. For a simple capacitor the capacity C is calculated with the size A and the distance d of the capacitor plates by

$$C = \varepsilon_0 \cdot \frac{A}{d} \tag{3.4}$$

respectively with one dielectric between the plates with

$$C = \varepsilon_0 \varepsilon_{\text{r}} \cdot \frac{A}{d} \tag{3.5}$$

with ε_0 being the vacuum permittivity of $8.8542 \cdot 10^{-15}$ As/Vmm and ε_{r} being the relative permittivity. Increased temperatures and different frequencies can have a direct influence on the value of ε_{r}. The extent of the effect depends on the used material.

In this work the capacitor consists of two electrodes with several dielectric materials X in between. The dielectric materials sequence is fused silica/SiO_2, (YSZ), gas phase, (YSZ), and fused silica/SiO_2 again with their correspondent values of d_{X} and ε_{r}(x). YSZ is put in brackets because it is only present

on the coated dielectric plates. For a constant gap between the electrodes without an ignited discharge equation 3.5 has to be adapted for a series of capacitors taking into account the different dielectric materials. The gas gap distance d_{gas} has to be reduced for the YSZ coated dielectric plates according to the film thickness of the YSZ layers. These leads to

$$\frac{1}{C_{\mathrm{DBD}}} = \frac{1}{\varepsilon_0 \cdot A} \cdot \left(\frac{d_{\mathrm{SiO_2}}}{\varepsilon_{\mathrm{SiO_2}}} + \frac{d_{\mathrm{YSZ}}}{\varepsilon_{\mathrm{YSZ}}} + \frac{d_{\mathrm{gas}} - 2 \cdot d_{\mathrm{YSZ}}}{\varepsilon_{\mathrm{gas}}} + \frac{d_{\mathrm{YSZ}}}{\varepsilon_{\mathrm{YSZ}}} + \frac{d_{\mathrm{SiO_2}}}{\varepsilon_{\mathrm{SiO_2}}} \right) \tag{3.6}$$

for the complete dielectric system and to

$$\frac{1}{C_{\mathrm{DBD}}} = \frac{1}{\varepsilon_0 \cdot A} \cdot \left(\frac{d_{\mathrm{SiO_2}}}{\varepsilon_{\mathrm{SiO_2}}} + \frac{d_{\mathrm{gas}}}{\varepsilon_{\mathrm{gas}}} + \frac{d_{\mathrm{SiO_2}}}{\varepsilon_{\mathrm{SiO_2}}} \right) \tag{3.7}$$

without YSZ coated fused silica plates. With an applied voltage that is high enough to ignite a discharge the term of the gas can be neglected and equations 3.6 and 3.7 are simplified to

$$\frac{1}{C_{\mathrm{DBD}}} = \frac{2}{\varepsilon_0 \cdot A} \cdot \left(\frac{d_{\mathrm{SiO_2}}}{\varepsilon_{\mathrm{SiO_2}}} + \frac{d_{\mathrm{YSZ}}}{\varepsilon_{\mathrm{YSZ}}} \right) \tag{3.8}$$

respectively without YSZ coated dielectric plates to

$$\frac{1}{C_{\mathrm{DBD}}} = \frac{2}{\varepsilon_0 \cdot A} \cdot \left(\frac{d_{\mathrm{SiO_2}}}{\varepsilon_{\mathrm{SiO_2}}} \right) \tag{3.9}$$

Computed values at room temperature (300 K) of C_{total} due to equations 3.6 to 3.9 show only small differences in the capacity of the dielectric system (with $\varepsilon_{\mathrm{YSZ}} = 30$ [56], for 400 °C $\varepsilon_{\mathrm{YSZ}} = 70$ with $d_{\mathrm{YSZ}} = 500$ nm layers, $\varepsilon_{\mathrm{SiO_2}} = 3.8$ [57] with $d_{\mathrm{SiO_2}} = 1$ mm and $\varepsilon_{\mathrm{gas}} = 1.00059$ for Air with $d_{\mathrm{gas}} = 1$ mm). The computed values of capacity and τ are given in table 3.1. A measured value of the system discussed in equation 3.8 is also given in table 3.1 and shows that the complete DBD capacitor system has a much higher capacity value and time constant τ than the theoretical calculations implicated.

For the discharge the applied voltage and the stored charge on the capacitor is more important. The maximum charge Q of the capacitor can be easily calculated if the dielectric capacity and the applied voltage are known:

$$Q = C_{\mathrm{DBD}} \cdot U_{\mathrm{C}}(t) \tag{3.10}$$

Although the AC generator uses a square wave function for the high voltage U_{C}, the value of the applied voltage U is reached by following an exponential function of the time t with the maximum potential of the square

Dielectric System	Equation	Capacity C/pF	τ /μs
SiO_2 | YSZ | Gas | YSZ | SiO_2	3.6	7.114	0.7114
SiO_2 | Gas | SiO_2	3.7	7.109	0.7109
SiO_2 | YSZ | YSZ | SiO_2	3.8	20.607	2.0607
SiO_2 | YSZ | YSZ | SiO_2	3.8 at 400 °C	20.608	2.0608
SiO_2 | SiO_2	3.9	20.608	2.0608
experimental measurement	3.8	320	32

Table 3.1: Comparison of computed values for the dielectric base plates and measured values. Calculations show no great differences of the dielectric system with and without YSZ coating. The comparison of theoretical calculation and experimental measurement (the corresponding calculations are marked red) confirmed a higher time constant of τ and therefore a larger capacity of the whole DBD system is caused by the summary of capacities from cable connections, high voltage feed through, dielectric plates etc.

wave function of the AC generator applied at $t = 0$ and then changing the potential of U from plus to minus with the frequency used. If the charging time exceeds the time of $t = 5\tau$ than the dielectric plates are fully loaded and the maximum of the applied voltage is reached.

$$U_{\mathrm{C}}(t) = U \cdot (1 - e^{-\frac{t}{\tau}}) \tag{3.11}$$

An ignition of the DBD is only possible during a flow of current I in the dielectric plate system. The current in the DBD system can be derived from the following equation

$$I = \frac{\mathrm{d}Q_{\mathrm{max}}}{\mathrm{d}t} = C\frac{\mathrm{d}U_{\mathrm{C}}(t)}{\mathrm{d}t} \tag{3.12}$$

From the differential equation of $U_{\mathrm{C}}(t)$ follows for a constant applied voltage that the current in the system is zero. This situation is reached when $U_{\mathrm{C}}(t)$ reaches the applied voltage of U_{max}. Figure 3.2 shows calculations of the frequency-dependent charging behavior of the capacitor of the whole DBD system. For the experimental setup used in this work a value of $f(\tau) =$ 3125 Hz could be obtained. Therefore a full charging of the capacitor is not possible at frequencies greater than 3125 Hz which leads to the need of applying higher maximum voltages to ignite the discharge.

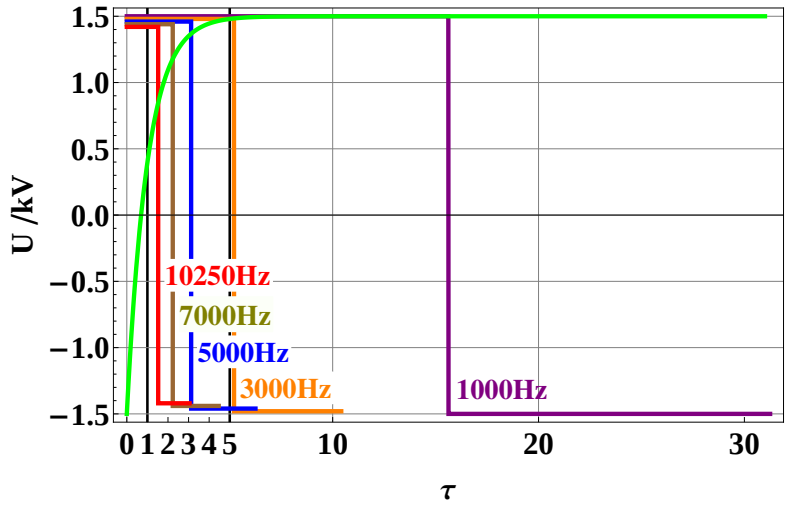

(a)

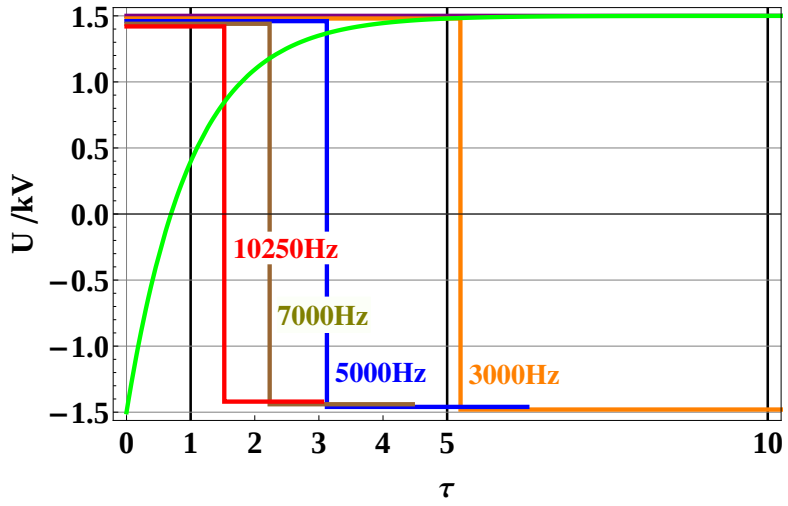

(b)

Figure 3.2: Both figures show the computed values of $U_C(t)$ according to equation 3.11 (green) and of a square wave function profile with an amplitude of 1.5 kV at different frequencies: 1000 Hz (purple), 3000 Hz (orange), 5000 Hz (blue), 7000 Hz (brown), and 10250 Hz (red) in correlation to the value of τ measured. The switch of the potential is performed at $\tau = 0$, therefore the charging of the dielectric system takes places over the total potential range of 3 kV. A fully applied high voltage is only reached for times $t \geq 5\tau$ which correlates with frequencies lower than 3125 Hz. Figure 3.2(a) gives an overview of the whole frequency range and figure 3.2(b) gives a closer look on the relevant time around 5τ.

3.1.5 Frequency Related Influences of the DBD System

As discussed in the last section 3.1.4 the frequency influences the charging behavior of the base plate system capacitor. As explained in detail in section 4.1 the difference of the equilibrium intensity of the CO_2 signal was measured before each discharge experiment and again after a maximum of CO_2 reaction rate is reached. Comparing the absolute difference of base plates with and without YSZ film coating a rate enhancement factor could be obtained for each frequency used in the experiments.

The direct comparison of rate enhancement factors of different frequencies is not reasonable. The definition of a frequency-dependent rate enhancement factor seems to be the logical alternative. Due to this consideration the efficiency of CO_2 generation should be correlated with the discharge frequency. With this consideration in mind a discharge operating at 6000 Hz should be double efficient than a discharge operating at 3000 Hz, because the possibility of a collision of reactive atoms inside the discharge or with the wall is doubled according to the change of the potential of the dielectric plates.

Theoretically a maximum of the reaction rate should be observed if the time constant of the gas reaction is equal to the frequency of the applied high voltage. Another point taken into account is the later discussed energy coupling into the discharge according to Planck's law, (see later section 6.1.3). Therefore the rate enhancement factor R as discussed in section 4.1 given by

$$R = \frac{\triangle \text{ YSZ}}{\triangle \text{ SiO}_2} \tag{3.13}$$

has to be adapted to a frequency-dependent rate enhancement factor $R(\nu)$ as follows:

$$R(\nu) = \frac{\frac{\triangle \text{ YSZ}(\nu)}{\triangle \text{ SiO}_2(\nu)}}{\text{f}(\nu)} \tag{3.14}$$

where $\text{f}(\nu)$ stands for a function correlated to the discharge behavior at different frequencies. With this correction different frequencies can be compared due to their catalytic rate enhancement factors.

3.2 Heterogeneous Catalysis

The reaction rate of a chemical reaction depends on different variables as the concentration of the reactants, rate constant, and usually temperature or pressure. The activation energy E_A of a chemical reaction is often in the order of several hundred kJ/mol. Keeping this in mind usually energy is

necessary to start the reaction. In industrial applications therefore a lot of effort is taken into the research for catalysts that reduce E_A of a specific chemical reaction. The reduced value of E_A increases the reaction rate and therefore the amount of the reaction products. An ideal catalyst itself is neither consumed by the reaction nor alters the thermodynamic equilibrium. It is a partner within a new reaction mechanism which uses the catalyst for an new (less energy intense) route for the generation of the products.

In heterogeneous catalysis the reactants and the catalyst are not in the same phase in comparison to homogeneous catalysis, which is not discussed here. The most used combination is a solid catalyst with liquid or gaseous reactants. Important examples for heterogeneous reactions are for example the Haber-Bosch process [58] (Ammonia synthesis with iron oxides as catalyst) or the sulfuric acid synthesis (contact process with vanadium oxides as catalyst).

An important model case is the heterogeneous CO oxidation. Ertl [59] discusses the CO oxidation at pressures below 10^{-5} mbar on a Pt (111) catalyst and the difference to a Ru (0001) catalyst. He states among other things the following two points which are of greater interest for this work, too: The surface state of a catalyst is crucial for the catalytic reaction and undergoes profound alterations. Impurities of other elements may have strong effects on the reactivity either supporting or poisoning the reaction. In addition the surface state of a catalyst can also be influenced by the use of a supporting material on which the catalyst is dispersed.

The use of ion conducting support materials gives the possibility to influence the catalyst behavior in different ways. For example the influence of surface reactions by near surface vacancy formation or the kind of terminal (oxygen) ions on the catalyst surface can be influenced by ion conducting supports and lead therefore to increased reaction rates. The importance of surface science investigations of heterogeneous catalysts is accentuated by Ertl [59] and a review to the CO oxidation is given by Freund [60].

Another possibility to increase reaction rates is the catalyst respectively support material preparation or the combined preparation of catalyst with supporting material. Often it is possible to find perfect conditions for a maximum output of a special chemical reaction. This fits very well with the often observed lift-off temperatures (temperature where the percentage of conversion of the reactants increases strongly) of a heterogeneous catalyst. At elevated temperature the catalyst shows a strong increase of reaction rate if the lift-off temperature is reached.

These considerations are in good agreement with the work of Hutchings [61] who focused on the question what kind of promoters on catalyst surfaces can be used and which kind of influence on the reaction rate they have. For

different catalysts (with promoters) which are used in the carbon monoxide oxidation often ZrO_2 or YSZ are taken as supporting materials. For a brief overview the following examples from literature are presented:

In the case of a ZrO_2 support Fernandez-Garcia et al. [62] investigated $Pd/Ce_xZr_{1-x}O_2/Al_2O_3$ three way catalysts for their catalytic behavior in the CO oxidation. They show lift-off plots (which give the percentage of CO conversion as a function of the temperature) for all different investigated support systems covered with a 1 wt% Pd loading. As a result they found that the use of $Ce_xZr_{1-x}O_2$ as single support or the combined use of $Ce_xZr_{1-x}O_2/Al_2O_3$ as support increased the catalytic behavior and reduced the lift-off temperatures observed with respect to the pure alumina supported catalyst. In a consecutively work of this group Martinez-Arias et al. [63] investigated the same catalysts in a CO+NO+O_2 gas mixture. Again they could show with lift-off plots that the ceria-zirconia support showed best catalytic activity at lower temperatures.

Another ZrO_2 supported system was investigated by Zhang et al. who presented a study [64] of Au/ZrO_2 catalysts. They investigated the influence of different gold loadings to the catalytic CO conversion. It was found that the highest used loading of 0.76% Au showed the best CO conversion level of about 59.3%. In addition they investigated the effect of the calcination temperature of the 0.76% Au/ZrO_2 catalyst and found that best results were achieved at 473 K.

Craciun et al. [65] used 10 wt% MnO_2 catalyst with YSZ support to investigate the adsorption of CO on the catalyst at reduced temperatures. The adsorption on oxidized and reduced samples was monitored by FTIR spectroscopy. Craciun et al. concluded that the adsorption at low temperatures of 85 K is correlated to the generation of $Mn^{3+} - CO$ species on the oxidized sample, respectively to $Mn^{2+} - CO$ species on the reduced sample. In addition they stated that labile lattice oxygen from the YSZ is also important for the oxidation process, if the CO was adsorbed on the active sites (formation of $Zr^{4+} - CO$ bond). They also compared the catalytic activity of the MnO_x/YSZ catalyst with the pure YSZ support and found that the rate of the CO oxidation was comparatively higher in the case of MnO_x/YSZ.

Another YSZ supported system was reported by Dow et al. [66]. They applied copper oxide on the YSZ support. As a result they found that the surface oxygen vacancies of the YSZ have a direct impact on the interfacial terminal oxygen ions of copper oxide and therefore on the catalytic behavior. In addition they show in [67] the light-off plots of different catalysts. The rate of CO conversion increases strongly depending on the used catalyst at a temperature between 175°C and 250°C. With the YSZ support the copper oxide catalyst shows a lift-off characteristic at a temperature of about 175°C

which is normally not observed for copper oxide catalysts. Dow et al. state that this is caused by the oxygen-ion support and the existing oxygen vacancies on the YSZ surface. The differences of catalyst composition and support material for the lift-off temperatures can be seen for example in [68, 69, 70].

3.3 Heterogeneous Plasma-Catalysis

Different possibilities for the use of DBDs were shown in section 3.1.3. The benefit of a DBD for chemical reactions in the gas phase is often a key aspect for their use. It was also shown in section 3.2 that heterogeneous catalysts can speed up reactions and the output of the product(s). In special applications it was also shown that the combination of DBD and heterogeneous catalysis could improve product selectivity and reaction rates while the single treatment with a DBD or the use of a catalyst had no great influence to product selectivity or reaction rate. The existing excited molecules, radicals, and ions inside the DBD are often responsible for the selectivity of the experimental system by affecting the generation of specific reaction products. They interfere with the catalyst inside of the discharge zone, which supports the reaction to the designated product(s) resulting in higher output values.

In a combined experiment the catalyst is placed into the region of the discharge and held there in a fixed position. In summary the key aspects of combining conventional heterogeneous catalysis with a DBD treatment gives the opportunity of higher conversion rates for the oxidation of different molecules at lower temperatures. For a brief overview the following examples from literature are presented:

Wang et al. showed the results of NO_x removal in a DBD with selective catalytic reduction by C_2H_5OH [71]. The direct influence of the power of the DBD onto the catalytic activity was shown in their work. They stated that the DBD creates strongly oxidizing species as O radical and OH radical that oxidize NO to NO_2 which is then selectively reduced to N_2 by the used catalyst.

Chang et al. investigated the elimination of carbon monoxide in gas streams (air respectively nitrogen) by dielectric barrier discharge systems with a MnO_x catalyst [72]. It was possible in their investigations to obtain higher CO removal at room temperature without heating. They found that the DBD was not able to eliminate the CO without the MnO_x catalyst.

The difference of single DBD and a combined DBD with a Cu/Mn catalyst onto the production of hydrogen and preferential CO oxidation from methanol was presented by Rico et al. [73]. The gap distance between the electrodes was filled with $BaTiO_3$ particles of an average size of 3 mm for

easier DBD ignition. They compared the reactor only filled with $BaTiO_3$ and the reactor with catalyst filled with $BaTiO_3$ + Cu/Mn catalyst (XRD determined a $Cu_{1.5}Mn_{1.5}O_4$ spinel structure) without DBD and found only in the last mentioned system a 2% conversion rate of methanol.

In case of pure $BaTiO_3$ with ignited discharge a selectivity of 92% conversion of methanol only to carbon monoxide and hydrogen was detected. With additional catalyst the conversion rate could be enhanced to 97% but the selectivity for CO and H_2 was lower. Instead the catalyst favored the oxidation of CO to CO_2 with a partial oxidation of hydrogen to water. Rico et al. stated that with the copper-manganese catalyst oxygen ions from the catalyst itself participate in the partial oxidation of CO and H_2. This led during the experiments to a malfunction of the reactor due to the reduced catalyst.

In another experiment the methanol gas stream was enriched with water to prevent the reduction of the catalyst and to enlarge the CO_2 generation. Again the difference of the ignited DBD with and without catalyst was measured. Best hydrogen selectivity of 97% and the lowest selectivity to carbon monoxide of 10% were achieved with the catalyst and the reactor malfunction could be prevented with the additional water supply.

A similar approach was performed by Roland et al. [74]. They used as Rico et al. the ferroelectric material ($BaTiO_3$) to reduce the energy input level and added a catalytically active material ($LaCoO_3$) which should improve the conversion of air pollutants in an air gas stream and a higher selectivity to CO_2 generation. Roland et al. showed that especially at higher energy input a conversion rate to CO_2 of about 60% could be detected with the use of a catalyst during DBD ignition.

A different application of the use of DBD with catalysts was shown by Harling et al. [75]. They investigated the temperature dependence for the destruction of aromatics with normal catalysis and plasma catalysis experiments. They could show that depending on the used catalyst small differences in the temperature dependent destruction rate occurred and that in all investigated materials the plasma catalytic experiment could obtain higher destruction values at lower temperatures as within the solely catalytic experiments. Harling et al. stated that plasma catalysis is more effective than conventional thermal catalysis or plasma treatment itself.

3.4 Ionic Conductivity of Yttria Stabilized Zirconia (YSZ) Thin Films

The mechanism of ion conductivity in solids is well known and relies either on vacancy motion (Schottky defects) or on interstitial ions (Frenkel defects). The dominant type of mobile defect in an ion conducting material depends on the size of the different ions and the coordination number of the different ions. A wide variety of mobile anions and cations can be found in different materials.

In this work the oxygen ion conducting YSZ is used, which shows at temperatures above 300°C pure oxygen ion conductivity in the anion sublattice by a vacancy mechanism. Undoped zirconia ZrO_2 is a stoichiometric material with a small oxygen deficiency especially at low oxygen partial pressures [76]. To obtain higher conductivity, which correlates to higher vacancy concentration zirconia is usually doped with yttria (Y_2O_3). In the Kroeger-Vink notation for point defect reactions this is formulated by:

$$Y_2O_3 + 2\,Zr_{Zr}^{\times} + O_O^{\times} \rightleftharpoons 2\,Y'_{Zr} + V_O^{\bullet\bullet} + 2\,ZrO_2 \tag{3.15}$$

Zr^{4+} is substituted by Y^{3+} in the cation sublattice. For two Zr^{4+} ions substituted by two Y^{3+} ions one oxygen vacancy ($V_O^{\bullet\bullet}$) is created. The concentration of vacancies is therefore half the concentration of yttrium ions. According to literature the highest oxygen conductivities occur at a doping level of 9 to 10 mol% yttria [77, 78, 79, 80].

Empirical estimations for lower temperatures as in [77] are possible but have to be taken with care, because it was shown [78, 79] that at temperatures between 550°C and 650°C structural reorganization inside of the ion conductor changes the value of the ion conductivity. Higher doped materials show decreasing conductivities due to the formation of defect associates [79, 80].

With Y_2O_3 doping contents above about 7 mol% of Y_2O_3 the cubic phase can be kinetically stabilized at room temperature by fast quenching from elevated temperatures. A transition into the tetragonal phase does not happen at lower temperatures [81]. A phase diagram of YSZ can also be found in [81].

The value of the ionic conductivity of YSZ is different depending on whether a single crystal or a polycrystal is used [82, 83, 84]. The oxygen conductivity of a single crystal depends only on the orientation of the YSZ crystal (usually (100) or (111)). In a polycrystalline YSZ ceramic the total conductivity is composed of the bulk conductivity and the grain boundary

conductivity. Thin film deposition of YSZ (as used in this work) leads to polycrystalline films with a usually columnar structure [85, 86, 87] and a preferred orientation of (111). Detailed information on the YSZ target material and the deposited films that were used in this work is given in section 5.1.

3.5 Non-Faradaic Electrochemical Modification of Catalytic Activity (NEMCA)

Especially in the case of YSZ the amount of transferred ions respectively current is essential for an electrochemical reaction. One may expect that the rate of enhancement of a catalytic reaction by an ion-conducting substrate is equal to the supply or removal of the reaction supporting ion. The increase or decrease of reaction rates then follows strictly a Faradaic behavior, which means that the rate enhancement R_{NEMCA} is proportional to the applied current I divided by the Faraday constant F and z the number of elementary charges transferred per ion:

$$R_{\mathrm{NEMCA}} \sim \frac{I}{z\mathrm{F}} \tag{3.16}$$

The effect therefore should be strictly limited to the transferred elementary charges. In 1970 Wagner [88] was the first who realized that by varying the electrical potential of an electrode the possibility is given to control the chemical potential of a surface species. Solid electrolyte interfaces with metal electrodes offer this possibility.

About 30 years ago the group of Vayenas showed that the reaction rate of a catalytic reaction at a metal electrode deposited on an ion conducting solid as YSZ can be influenced by electrochemical promotion by one of the participating ions (oxygen in the case of YSZ). The result was a non-faradaic electrochemical modification of catalytic activity (NEMCA) that was then introduced as a concept for accelerating catalytic reactions by Vayenas et al. [89].

As source of the NEMCA effect spillover ions were proposed [90]. Experiments showed that different ions can be used for electrochemical promotion and that a key aspect of the effect is the change of the catalyst work function [91, 92]. The selectivity of a platinum catalyst on a YSZ ceramic for the CO oxidation in correlation to the applied voltage to the Pt|YSZ electrode was investigated by Tsampas et al. [93]. They found that at applied voltages of

more than 0.4 V had a more than three times higher influence on the CO_2 generation in the experiment.

Today the electrochemical promotion of heterogeneously catalyzed reactions (EPOC) includes the NEMCA effect as a special case. EPOC is a more general description of the electrochemical promotion by ions and is still not fully understood. A critical review of the last 25 years of EPOC and NEMCA is given by Imbihl in [94].

In this work the concept of electrochemical promotion is adapted, to be used in plasma-catalytic cells. Instead of a Direct Current (DC) electrochemical promotion an Alternating Current (AC) supply is established and the degree of electrochemical promotion follows an oscillating behavior. This new concept was introduced in section 2. The key aspect is here likewise to promote (by reducing the binding energy of atoms and molecules on the YSZ surface) the reaction rate and to use the YSZ as an heterogeneous catalyst for a gas phase reaction. In this work a metal electrode on top of the YSZ film is not necessary in contrast to the NEMCA and EPOC experiments presented in literature. The discharge itself is a kind of "perfect gaseous electrode" and in direct contact with the YSZ surface. The interaction at the YSZ and plasma interface therefore could have a comparable significance for the promotion process such as the influence of the metal catalyst surface usually used in contact with the gas phase.

3.6 Optical Emission Spectroscopy: In-Situ Monitoring of Gas Discharges

For the investigation of a DBD different methods are used to identify the ionized or excited states of atoms or molecules. Usually it is very useful to compare Optical Emission Spectroscopy (OES) and Laser-Induced Fluorescence (LIF) results with gas phase mass spectrometry data. The two methods [95] give direct information on the ionic, excited atoms, and molecular composition and beyond that they are in-situ techniques.

Thereby the OES investigations are limited to positive ions or excited states in contradiction to the LIF technique, which also can detect negative ions. Due to experimental predictions and the simpleness of the OES technique the direct identification of negative ions is often not performed. Gases with an electronegative character always show a certain concentration of negative ion formation due to electron attachment [96, 97]. If the concentration of electrons in the discharge is reduced due to electron attachment the interaction of negative ions with molecules has also to be considered. In

an early work of Davis [98] this topic was already addressed.

For a DC discharge we could show that the concentration of positive oxygen ions is reduced by using YSZ electrodes [41]. This leads to the assumption that the ion conducting YSZ increases the concentration of negative oxygen ions in a oxygen discharge. It can be seen that the role of negative ions inside a discharge has to be taken into account under certain circumstances.

If a gas phase reaction is investigated it is sufficient to detect the products by OES. The benefit by using OES for atom and molecule identification is a large data base of emission line data. A general source of emission lines of ions and excited states of single atoms as argon or carbon can be found in the National Instiute of Standards and Technology (NIST) Atomic Spectra Database [99]. Several work for different discharge setups was performed in the literature. An example for a Argon discharge generated in air can be found in [100].

For more complicated molecules a lot of literature data can be found. For example data for nitrogen can be found in a review written by Lofthus and Krupenie [101]. The same kind of review for oxygen was also written by Krupenie [102]. Additional data for oxygen lines can be found for example in [103]. Optical emission data for CO_2 discharges can be found in [104, 31]. In combination with own OES spectra measurements the identification of most of the atomic and molecular lines is possible.

Chapter 4

Analytical Methods

Different analytical methods were applied to examine the gas phase and the dielectric plates used. For the gas phase analysis a Quadrupol Mass Spectrometer (QMS) (section 4.1) and Optical Emission Spectroscopy (OES) (section 4.2) were used. The combination of both techniques allowed a better understanding of the processes inside the discharge.

Discharges are always interacting with the walls present in a discharge setup. In this work the interaction at the plasma | functional layer (YSZ) interface is of interest. It is necessary to monitor the surface structure and surface contamination of the functional layer before and after discharge treatment. Scanning electron microscopy (SEM) in combination with Energy Dispersive X-ray Spectroscopy (EDX) (section 4.3) were used to analyze the surface composition and structure. Time of Flight Secondary Ion Mass Spectrometry (ToF-SIMS) was used to detect impurities on the surface and investigate the YSZ layer stability (section 4.4).

4.1 Quadrupol Mass Spectrometry (QMS)

Quadrupol mass spectrometry (QMS) is a standard technique to investigate the composition of gas mixtures. In this work signals were investigated that corresponds to the gases oxygen, argon and carbon monoxide or the reaction product of the carbon monoxide oxidation, namely carbon dioxide. The mass signals which were correlated to the atoms or molecules mentioned before were recorded over long time.

After filling of the flow through reactor (described in section 5.5.3) with the gas, at least an hour was waited to get a constant pressure and composition inside the discharge cell and therefore stationary intensities of the gas signals in the QMS. The stationary intensities of the gas species were

measured and taken as reference values.

After switching the discharge on the increase and decrease of signals was recorded. The measured data was then normalized to the ion intensity/sccm of the carrier gas argon. After normalization the difference of the absolute values of the CO_2 signal intensity before discharge ignition and the stationary value obtained with ignited discharge was calculated. This difference $\triangle$ of the signal increase of mass 44, which correlates to the CO_2 signal was calculated for uncoated dielectrics ($\triangle$ SiO_2) and YSZ film coated fused silica dielectrics ($\triangle$ YSZ). With this both $\triangle$ values for each analyzed gas mixtures an enhancement factor R for the YSZ coated dielectrics can be calculated by division of the absolute values:

$$R = \frac{\triangle \text{ YSZ}}{\triangle \text{ SiO}_2} \tag{4.1}$$

A schematic how the ratio was taken from the measurement data is shown in figure 4.1. The increase of the CO_2 signal until a reaction rate equilibrium was reached took, depending on the experimental conditions, from several minutes until about one hour. The quadrupol mass spectrometer used during experiments is explained in section 5.5.5.

4.2 Optical Emission Spectroscopy (OES)

Optical Emission Spectroscopy (OES) is an in-situ technique that can be used for the measurement of the gas composition directly in the discharge zone. Excited or ionized states of atoms or molecules can be detected and compared with self-recorded reference spectra or literature data as given in section 3.6.

In this work a SpectraPro 2500i triple grating monochromator respectively spectrograph (manufactured by Acton Research Corporation) was used to record spectra in the wavelength range from about 325 nm to 875 nm. Figure 4.2 shows a variety of recorded reference spectra at a frequency of 44 kHZ for later comparison with experimental data. The purities of the used gases are given in table 4.1.

With this data an identification of the reactive atoms and molecules in the combined oxygen, carbon monoxide and argon discharge becomes possible. During the time until stationary reaction rates inside the discharge were reached several OES spectra were taken at certain times from the start of the discharge experiment. They were stopped if a constant value of the CO_2 signal was reached. The signal intensities of CO related lines in the optical emission spectra were recorded.

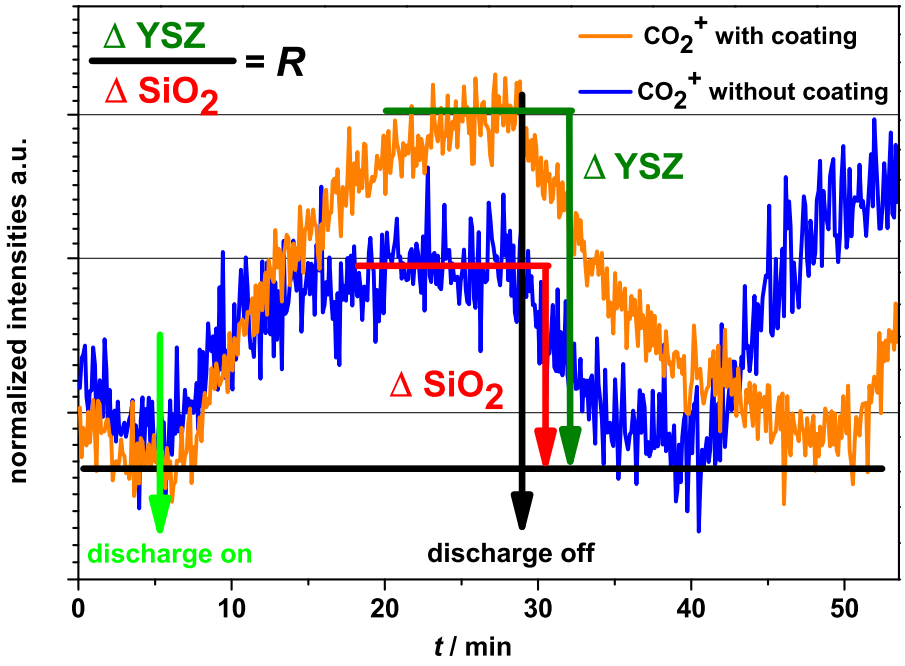

Figure 4.1: Schematic diagram of the determination of the reaction rate enhancement factor R of pure fused silica dielectric plates and with YSZ functional layer coated fused silica dielectric plates. CO_2 signals are normalized to the ion intensity/sccm of the carrier gas argon. The value of R is determined by division of the absolute value of $\triangle$YSZ by $\triangle SiO_2$ as explained in the text.

Gas	Purity of Gas	in %
Argon (Ar)	5.0	99.999
Carbon monoxide (CO)	4.7	99.997
Oxygen (O_2)	5.0	99.999
Nitrogen (N_2)	5.0	99.999
Carbon dioxide (CO_2)	4.5	99.995

Table 4.1: The table gives the purities of the used gases in the experiments.

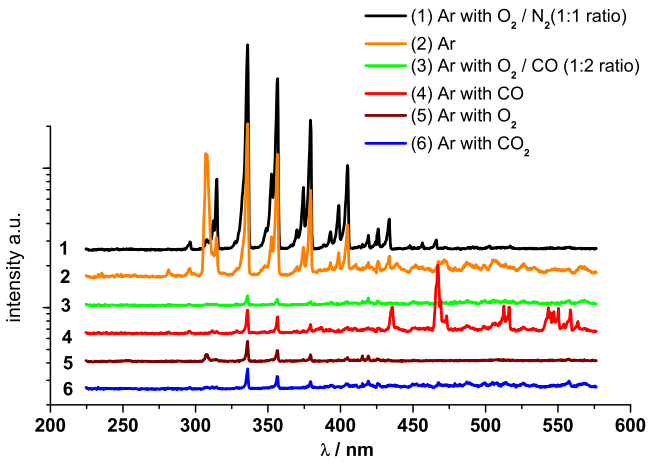

(a)

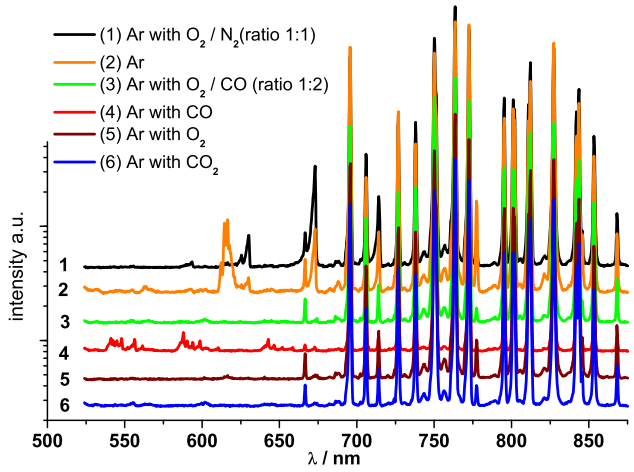

(b)

Figure 4.2: Optical Emission Spectra recorded of different gas mixtures. It can be seen that the optical emission spectra of argon (2) is influenced even by small addition of other gases (4, 5, 6). The Ar^+ lines in the range between 300 nm and 450 nm are strongly reduced in the optical emission spectra. Especially for the CO addition new lines of CO^+ or CO vibrational bands are visible. The situation is even more complex if more than one gas is added (1 with increased Ar lines and 3 with decreased Ar lines). Ar flux was constant in all experiments at 67.15 sccm and the pressure was around 500 mbar: 1) Ar, 2) with 0.5 sccm O_2, 3) with 0.34 sccm O_2 and with 0.66 sccm CO, 4) with 0.5 sccm O_2 and with 0.5 sccm N_2, 5) with 0.5 sccm CO and 6) with 0.35 sccm CO_2. The spectra show that OES is a very sensitive analysis technique even if only small amounts of gases are added to the carrier gas.

4.3 Scanning Electron Microscopy (SEM) and Energy Dispersive X-ray Spectroscopy (EDX)

Two different field emission scanning electron microscopes (FESEM respectively SEM) were used in this work. A Leo Gemini 982 SEM (manufactured by Zeiss GmbH) equipped with an INCA EDX detector (manufactured by Oxford instruments) was used in the beginning of the experiments. Later a MERLIN SEM (manufactured by Zeiss GmbH) equipped with an INCA X-Max EDX detector (manufactured by Oxford instruments) was installed at the university of Gießen and used for the further analysis. The MERLIN is better suited to investigate isolating samples. Acceleration voltage (200 V till 30 kV) and emission current can be adjusted according to the surface charging of the sample. In addition isolating samples can be analyzed without the need of sputtering a conductive material (as platinum or carbon) on the samples, because the MERLIN has a nitrogen gas compensation method to avoid sample charging at all. A maximum surface resolution of about 1 nm can be achieved with the MERLIN SEM.

The dielectric plates were investigated before and after discharge experiments to record changes in the surface structure. EDX measurements were used to obtain the layer composition after the YSZ film deposition or to check whether any surface contaminations were detectable.

4.4 Time of Flight-Secondary Ion Mass Spectroscopy (ToF-SIMS)

A Time of Flight-Secondary Ion Mass Spectrometer ToF-SIMS 5-100 (manufactured by ION-TOF GmbH) was used to monitor the different production steps of YSZ layer and electrode deposition, surface analysis of functional YSZ layers after preparation, after annealing and after discharge experiments and stability investigations of the whole dielectric sample with depth profiling. The ToF-SIMS was equipped with a bismuth Liquid Metal Ion Gun (LMIG) for secondary ion generation and three sputter ion guns (oxygen, cesium, C_{60}) for material removal during three dimensional profile investigations. In most profile measurements of dielectric plates a 2 kV Cs sputter beam was used. Measurements can be performed in negative and positive polarity depending on whether negative or positive ions are examined. The ToF-SIMS is in addition equipped with a electron flood gun which is used to avoid sample charging. In combination with EDX measurements the surface composition could be analyzed and surface contamination detected. The

depth of craters from three dimensional profiles was (if possible) measured with an Alpha-Step IQ Surface Profiler (manufactured by Tencor). Samples with very rough surface structure were not suitable for the depth calibration. This was especially a problem with the PDP test cells (section 5.2).

4.5 X-Ray Diffraction (XRD)

X-Ray Diffraction (XRD) was used to determine the orientation of the YSZ films and the platinum electrodes. A Diffrac 500 powder diffractometer (manufactured by Siemens) was used to analyze the platinum electrodes during the optimization process on smaller fused silica samples. The dielectric base plates were for the verification of the designated YSZ film structure after deposition (due to their size) investigated with a D5000 powder diffractometer (manufactured by Siemens), for detailed YSZ film results see [87].

Chapter 5

Experimental Preliminaries

Some preliminary studies were necessary for the success of the experiments performed in this work. First a method for large scale YSZ thin film preparation had to be established. The analysis and the selection of deposition parameters for first tests is explained in section 5.1. The first tests of YSZ coated PDP cells are presented in the next section 5.2.

The results of thin film stability and the effect of different deposition parameters on the discharge itself led to the presumptions that were necessary to choose dielectric material, section 5.3, electrode material, section 5.4 and the specifications for the dielectric base plates for the discharge setup.

The complete experimental setup is described in section 5.5. This includes the assembly of the Alternating Current (AC) generator, the design specifications for the flow trough reactor, the temperature calibration of furnaces, and the assembly of the Quadrupol Mass Spectrometer (QMS) used for the gas analysis.

5.1 Thin Film Deposition of Yttria Stabilized Zirconia Films

At the beginning of this work two deposition methods were tested. Since several years the deposition of YSZ films with Pulsed Laser Deposition (PLD) has been investigated [105, 106, 107, 108], in consequence, deposition parameters are well known. A problem of the PLD deposition is that samples usually do not exceed sample sizes of about 1 cm into square. Large scale PLD applications are only possible with special equipment as shown in [109]. For the DBD application YSZ films of more than 3 cm into square are needed.

A YSZ polycrystal was used as target material (doped with 9.5 mol% Y_2O_3, purity 99.99 %, manufactured by HTM Reetz GmbH Berlin, Ger-

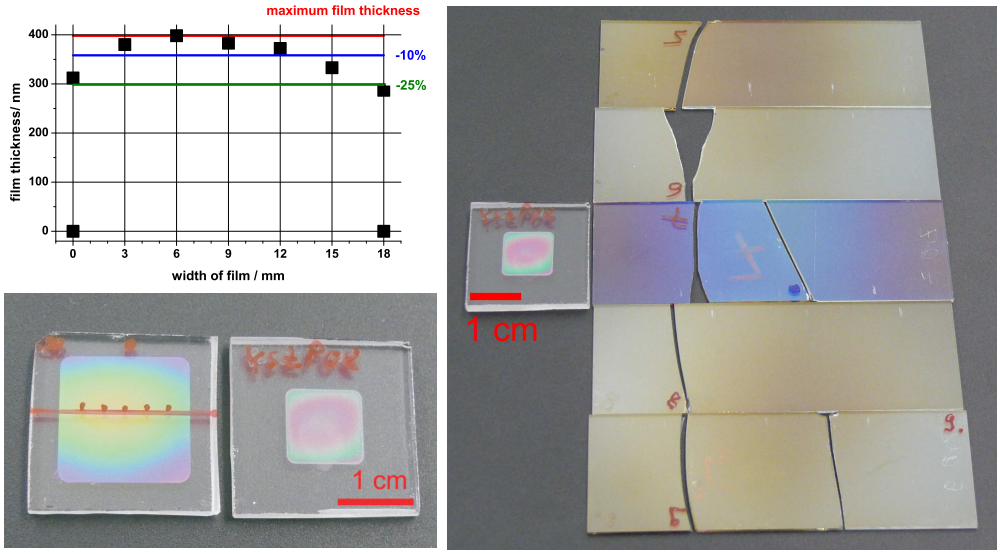

(a) (b)

Figure 5.1: Comparison between PLD 5.1(a) and magnetron sputtered 5.1(b) YSZ films. Red marks in 5.1(a) show position were film thickness was measured by ToF-SIMS depth profiling. The film profile is shown above. Equal film thickness over large scales is much better achieved with magnetron sputtering which can be seen by the homogeneous colored films in figure 5.1(b). For better comparison a small 1 cm square PLD deposition is shown in both pictures.

Series	P(RF)/W	Ar/sccm	O_2/sccm	Furnace T/°C	Surface T/°C
"2X"	100-200	200	0	0	210-250
"3X"	160	200	0.5-10	0	260-290
"4X"	160	200	0	100-800	210-600
"5X"	160	200	10	100-850	270-670
"6X"	160	50-350	0	0	200-240
"7X"	160	45-395	5	0	260-270
"8X"	160	45-395	5	700	550-570
"9X"	160	50-350	0	700	530-570

Table 5.1: Summary of YSZ deposition parameters for the different magnetron sputtering series according to [87]. Parameters in red color are changed within the series.

many). For testing the possibility of large scale PLD deposition samples of 18 mm into square were manufactured. Figure 5.1(a) shows the comparison of a 18 mm and a 10 mm square PLD deposition sample. The 18 mm square sample showed no constant layer thickness over the whole deposition area, see 5.1(a). The difference of layer thickness between the sample center and the edge of the deposition was about 25 %.

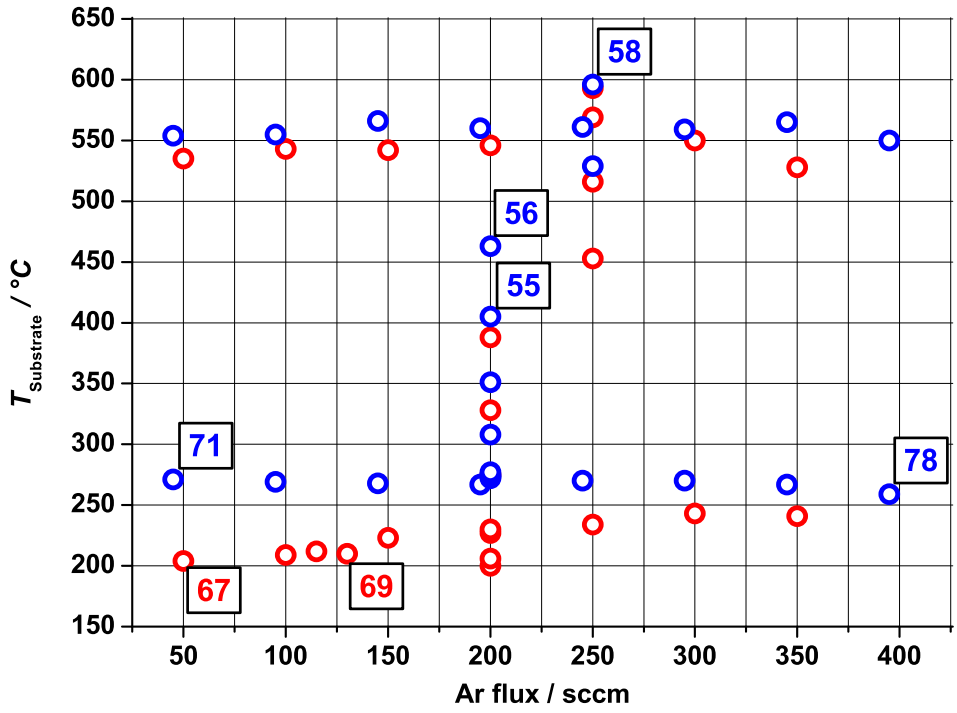

Figure 5.2: Overview of samples prepared with 160 W sputtering power in the series of table 5.1. Samples are shown in dependence of argon gas flux and dielectric surface temperature. Non-reactively sputtered films are indicated by ○ and reactively sputtered films with an oxygen gas flux between 5 and 10 sccm by ○ . Above 5 sccm oxygen gas flux no difference of film deposition could be detected [87]. The □ shows the sample conditions which were used in this work. Colors for the sample numbers are chosen according to the conditions of sample deposition (without or with oxygen).

Alternative YSZ film deposition methods are plasma spraying and different film sputtering techniques [110, 111, 112, 113, 114, 115]. In this work a radio frequency (RF) magnetron sputter machine (process chamber from Pfeiffer Vacuum GmbH with three 3" target holder, I. Institute of Physics of the Justus-Liebig-University Gießen) was used for making larger samples. The dielectric plates were positioned 6 cm below the target on top of the

substrate holders. The whole substrate holder was heatable with a heating element (Thermocoax) to temperatures of up to 700°C. Deposition could be performed under pure argon gas flux of up to 400 sccm or under reactive sputtering conditions with an additional oxygen gas flux of up to 10 sccm.

The RF power was applied by a CESAR 133 generator (from Dressler) with a VM 700 A impedance matching unit (also from Dressler). A three inch diameter YSZ target was used (doped with 9.5 mol% Y_2O_3, purity 99.9 %, manufactured by Kurt J. Lesker Company Ltd Hastings, United Kingdom) for the thin film YSZ deposition. First sputter tests showed much better layer thicknesses over the whole deposition area. The difference between sample center and edge ranged only between 10 % to 15 % which can be seen by the homogeneous color of the deposited films in figure5.1(b), (measured with test samples, not shown here).

For preparing well defined YSZ layers, the sputter process had to be optimized first. Therefore the best parameters for gas composition, RF-power, pressure and temperature had to be found.

For the DBD discharges the surface condition of the YSZ films [116] does probably have a great influence on the plasma properties. In an associated project to this work a diploma thesis with the title "Production and Characterization of YSZ Thin Films" was written by B. Pachner from the I. Institute of Physics [87]. The variation of one parameter led to different YSZ film series which are listed in table 5.1. Figure 5.2 summarizes the different sputtering series from table 5.1 for non reactive sputtered YSZ films (only Argon gas flux, purity 5.0 from Air Liquid) and for reactive sputtered YSZ films (Argon and Oxygen gas flux, both purity 5.0 from Air Liquide). Pachner showed that different film orientations and grain sizes could be obtained on float glass substrates in dependence of the sputter parameters.

It is known that polycrystalline and single crystalline YSZ electrodes interact different with a DC discharge [41]. Thus the surface conditions of the YSZ films may have a great influence on the plasma behavior in the DBD discharge. A possible interaction between surface and discharge should especially occur at low frequencies below 10 kHz due to the charging behavior of the capacitor system induced by the alternating current generator as explained earlier, see section 3.1.4. Figures 5.3, 5.4, and 5.5 show the different deposited films according to the mentioned parameter series from 5.1. Proof of principle experiments for YSZ coated PDP cells with different film orientations and surface modifications were performed. The experimental setup and the results of the PDP cell investigations is shown in the next section 5.2.

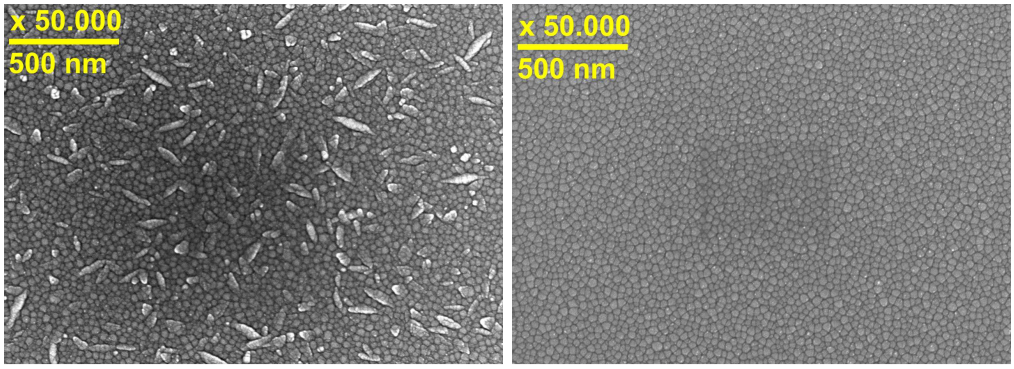

(a) (b)

Figure 5.3: SEM images of two different high temperature film depositions from the "5X" serie (see table 5.1). Figure 5.3(a) shows a deposited film at a surface temperatures of about 475 °C and figure 5.3(b) of about 620 °C. All films of this series are (111) orientated, pictures taken from [87].

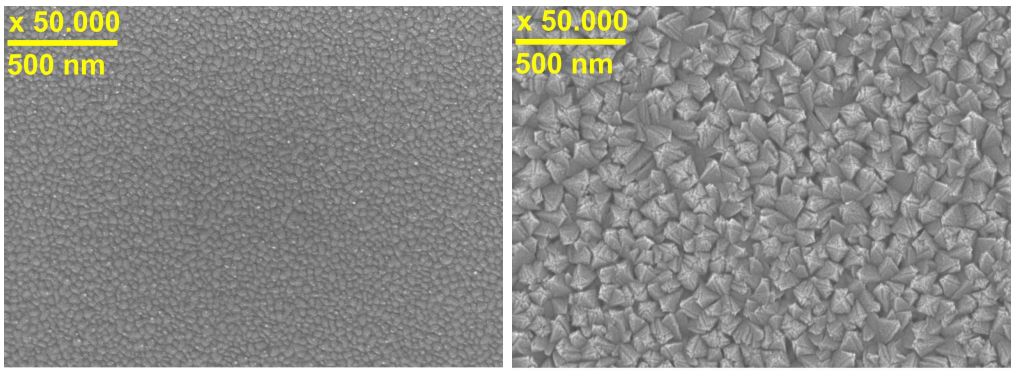

(a) (b)

Figure 5.4: SEM images of two different Ar flux depositions from the non-reactive sputtered "6X" series (see table 5.1). Figure 5.4(a) shows a deposited film at 50 sccm Ar flux and figure 5.4(b) at 130 sccm Ar flux. The difference in the surface structure can be seen clearly and measured in XRD measurements. Film orientation is shifting from (111) Figure 5.4(a) to a mixture of (111) and (200) in figure 5.4(b), pictures taken from [87].

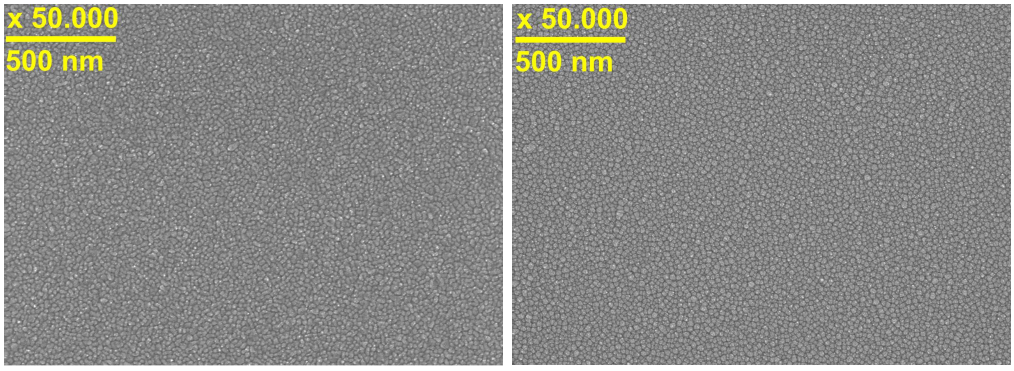

(a) (b)

Figure 5.5: SEM images of two different Ar flux depositions from the reactive sputtered "7X" series (see table 5.1). Figure 5.5(a) shows a deposited film at 45 sccm Ar flux and figure 5.5(b) at 395 sccm Ar flux. The deposition at higher Ar flux shows slightly greater grain size of the YSZ film. All films of this series are (111) orientated, pictures taken from [87].

5.2 YSZ coated PDP Cells for Proof of Principle and Stability Investigations

In collaboration with the working group of Prof. Whang from the Seoul National University standard PDP test cells were used to examine several aspects of dielectric barrier discharges in combination with a YSZ coating on top of the dielectric material instead of the MgO coating that is normally used. YSZ coated standard PDP cells filled with a mixture of Xe and Ne gas were used to test plasma ignition voltages and stability of the YSZ films. Ignition voltages and sustain voltages were measured at Seoul National University by Tae Ho Lee and compared with MgO PDP test cells usually used.

For applications of electrochemically induced plasma catalysis a long time stable YSZ film without larger impurities is needed. The same condition applies to standard plasma display panels. In a collaborative work [18] the interaction of the MgO/SrO coating layers with the dielectric material was investigated with ToF-SIMS. It was found that some elements of the dielectric material diffused into the coating layers under operation conditions. In the first examined YSZ-PDP test cells the same diffusion effect could be detected.

To ensure that no diffusion occurs directly at the dielectric and coating layer interface the idea of a diffusion barrier layer of fused silica (SiO_2) was introduced by the Whang group [117]. ToF-SIMS analysis showed that this

diffusion barrier was capable of avoiding the diffusion of dielectric materials into the functional layers and increased film stability and life time. Even an improvement of aging time of the standard PDP cells could be achieved [117].

The complete experimental work with the YSZ-PDP test cells can be subdivided into four milestones. First the PDP baseplates were prepared at Seoul National University (SNU). Figure 5.6(a) shows the design of a standard PDP test cell as sent to Gießen by Tae Ho Lee. At the beginning of the collaboration the diffusion barrier layer was not introduced.

The second step was the deposition of an approximately 500 nm thick YSZ layer (as described in section 5.1). Figure 5.6(b) shows the schematics of the YSZ coated PDP baseplate. A sample of the first two coated base plates (without diffusion barrier) can be seen in figure 5.7. After deposition the coated base plates were sent back to SNU. As diffusion barrier coated PDP test cells were available the YSZ coating was applied on the fused silica layer as shown in figure 5.6(c).

Thirdly in the Prof. Whang group the PDP test cells were fully assembled. A top plate with the phospor and a grid system to complete the PDP cell was combined with the base plates by an ceramic glue [117]. This preparation step ensured that the same gap distance between electrodes and phosphor was held along the complete PDP cell. A pressure of 400 Torr was applied in the fully assembled YSZ-PDP cells with a mixture of Xe (4%) and Ne (96%) gas. The cells were sealed afterwards by melting the gas supply glass tube. Then experiments were performed to obtain ignition and sustain voltages. The range of ignition voltage of a PDP cell starts if the first pixel of the PDP is ignited and ends if the last pixel of the PDP is ignited. When the whole PDP is ignited the sustain voltage range is determined by reducing the applied voltages till the first pixel extinguishes. The end of the sustaining voltage range is given if the ignition of the last pixel ends. PDP cell sustaining voltages are always lower than the ignition voltages. YSZ-PDP cells could be successfully ignited with a direct barrier discharge. Table 5.2 shows the measured ignition and sustain voltages of the different coated base plates.

After the experiments the YSZ-PDP test cells were sent back to JLU Gießen for ex-situ YSZ film analysis. For the electrochemical dielectric barrier discharge reactor the stability of the YSZ films was of particular interest. The different sets of base plates prepared led to several conclusions according to optimal YSZ film deposition parameters and the choice of dielectric material. For further analysis prototype sample P01 and the reference sample P03 were cut into small pieces perpendicular to the conducting paths for cross section investigation. Two pieces of the same sample were glued together and

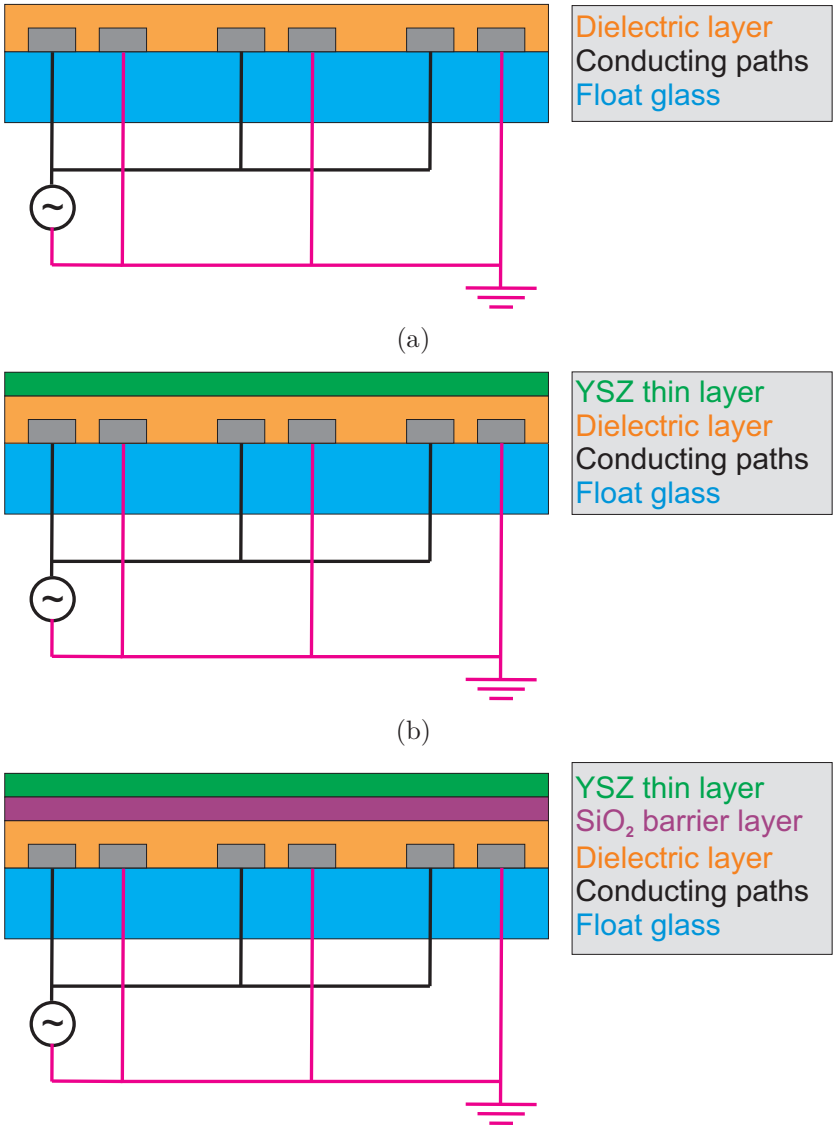

Figure 5.6: a) shows the layer sequence of a PDP baseplate prepared at Seoul National University by Tae-Ho Lee. b) shows the baseplate with the YSZ sputtered film and c) shows the improved base plate layer sequence with SiO_2 diffusion barrier layer.

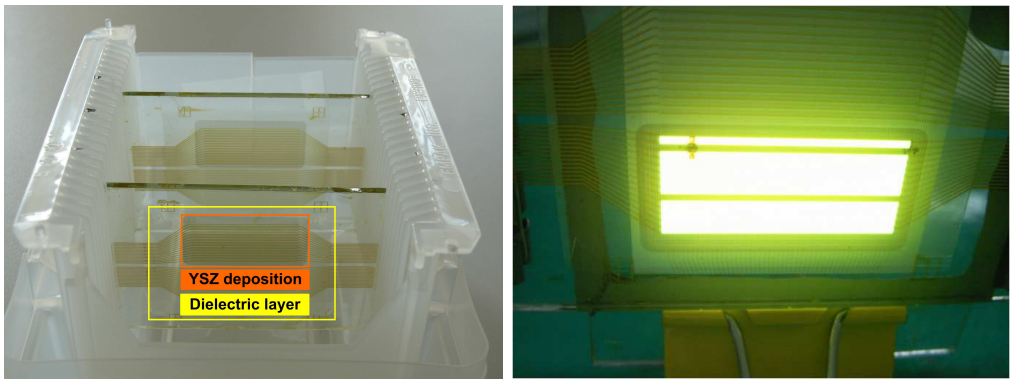

(a) (b)

Figure 5.7: The first two deposited YSZ films on a PDP base plate (prototype P01 and P02, see table 5.2) are shown in picture a). The YSZ films are slightly grey because an Al mask was used during the sputtering process. After exchanging the Al mask with a stainless steel mask new deposited films were transparent. Picture b) shows one of the prototype cells under discharge conditions. The dark lines are caused by dielectric breakdowns in the YSZ film.

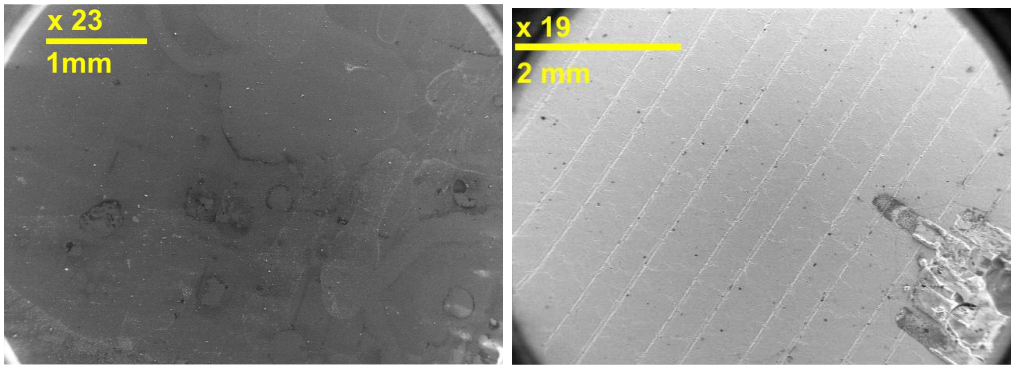

(a) (b)

Figure 5.8: SEM overview of MgO coating, figure 5.8(a), and YSZ coating, figure 5.8(b). The lines seen in figure 5.8(b) are cracks in the YSZ film which are not present in the MgO film. In the lower right part of the YSZ coated prototype PDP cell an electrical breakdown can also be seen.

Set No.	film No.	PDP sample	ignition voltage/V	sustain voltage/V	returned to Gießen	ToF-SIMS analysis
1	55	P01	Prototype		Yes	
1	55	P02	Prototype		Yes	
1	55	P03	Reference			
2	56	P21	300-340	220-210	Yes	Yes
2	67	P04	370-410	250-230	Yes	Yes
2	67	P05	310-380	260-220	Yes	
2	67	P06	defect	defect	Yes	
2	69	P15	330-390	270-230	Yes	
2	69	P18	320-390	260-210	Yes	
2	71	P09	310-350	250-210	Yes	Yes
2	78	P10	330-360	250-210	Yes	
2	78	P11	320-350	240-220	Yes	
2	78	P12	300-350	240-220	Yes	
2	78	P17	300-360	250-200	Yes	
3	67	K672	280-350	240-210	Yes	Yes
3	71	K673	300-360	270-230	Yes	
3	71	K711	n.n.	n.n.	Yes	Yes
3	71	K712	n.n.	n.n.	Yes	
3	78	K782	n.n.	n.n.	Yes	
3	78	K783	n.n.	n.n.	Yes	
3	78	K784	290-340	260-220	Yes	Yes

Table 5.2: List of all with YSZ coated PDP base plates investigated by Tae Ho Lee. Base plates broken during deposition process or PDP cell assembly are not listed here. All high temperature YSZ film depositions from set 3 showed bad layer condition after arrival and were not analyzed. Samples are firstly sorted by set number and secondly by conditions during film deposition. The prototype PDP cells and the reference cell from set 1 were deposited with a RF power of 180 W instead of 160 W.

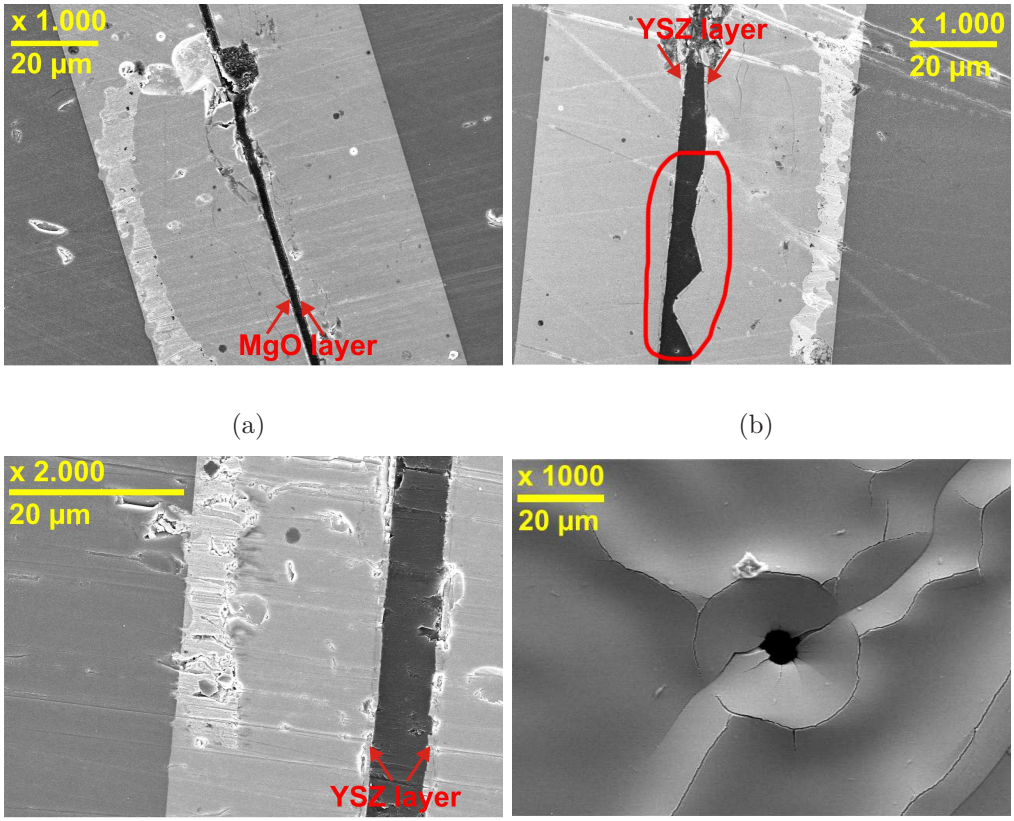

Figure 5.9: SEM images of prepared cross sections (as described in the text) from YSZ coated prototype P01 and the references P03, see table 5.2. Figure 5.9(a) shows a MgO coated part and figure 5.9(b) the YSZ coated part after discharge experiments. The red circle marks a place of layer destruction of the YSZ film and dielectric layer. This kind of destruction was not detected after film deposition and annealing of reference P03 as shown in figure 5.9(c). Figure 5.9(d) shows a closer look to a crack region where also a pore in the YSZ film can be seen.

the resulting cross section polished. Starting with a 30 µm diamond coated polishing paper the cross sections were polished down to 0.1 µm in several polishing steps. The overview SEM images of the P01 prototype depositions of MgO and YSZ in figure 5.8 show already that the YSZ film interacted during discharge experiments with the dielectric material. The prototype PDP cells from set 1 showed that interaction between dielectric material and coating layer occurred as can be seen in figure 5.9. Figure 5.9(d) shows cracks and pores in the film.

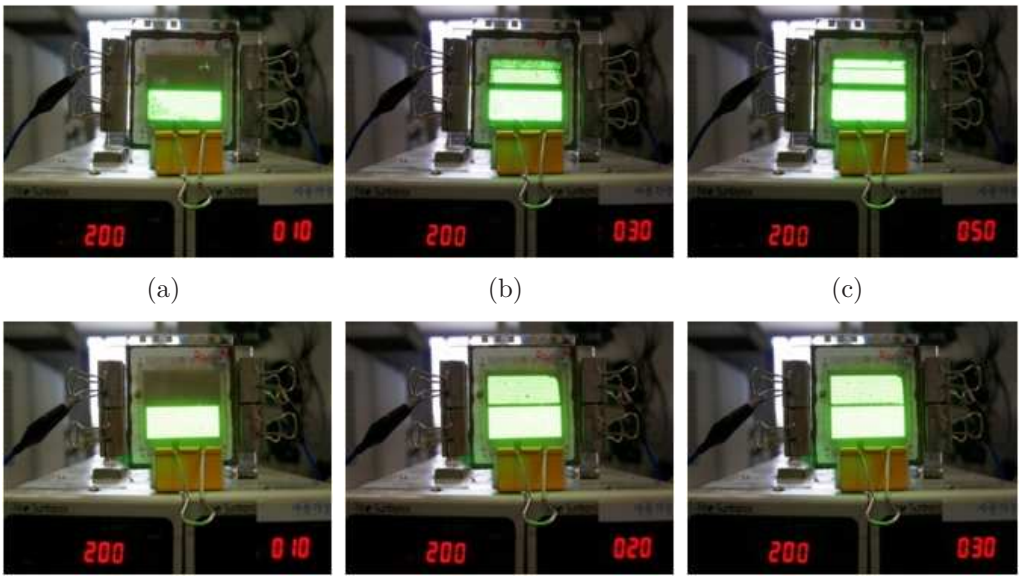

(a) (b) (c)

(d) (e) (f)

Figure 5.10: Determination of sustain voltages at SNU by Tae-Ho Lee from PDP sample P09 a) 210 V, b) 230 V, c) 250 V and from PDP sample P21 d) 210 V, e) 220 V, f) 230 V. The YSZ film is always located in the upper half of the PDP test cell. A smaller range of sustain voltage for the whole film (as for P21) indicates a well deposited film with constant thickness over the complete deposition area. The sum of the red numbers gives the applied voltage in each picture.

The reference base plate P03 was heated to 300°C to test whether the cracks in the film occur only at higher temperatures. After 48 h of tempering no cracks were observed. After the prototype tests the dielectric material was exchanged and the deposition parameters of layers varied to evaluate different deposited YSZ films. In set 2 the stability of YSZ coated PDP cells could be improved. According to the measured ignition and sustain voltages some film deposition parameters could be discarded. Figure 5.10 shows exemplary two

PDP test cells during determination of the sustain voltages (Pictures taken at SNU). The sum of the numbers visible in the pictures give the applied voltage.

In the third set of prepared PDP for first time SiO_2 diffusion barrier coated base plates were investigated. The main experimental focus of set 3 was the ex-situ layer analysis via ToF-SIMS and the comparison between base plates with and without SiO_2 diffusion barrier layer. The determined ignition and sustain voltages at SNU are also given in table 5.2. Exemplary ToF-SIMS data is shown in figure 5.11. Layer stability was again enhanced according to set 2 YSZ-PDP cells. The introduction of a diffusion barrier solved a lot of dielectric breakdown problems that occurred in previous used PDP test cells.

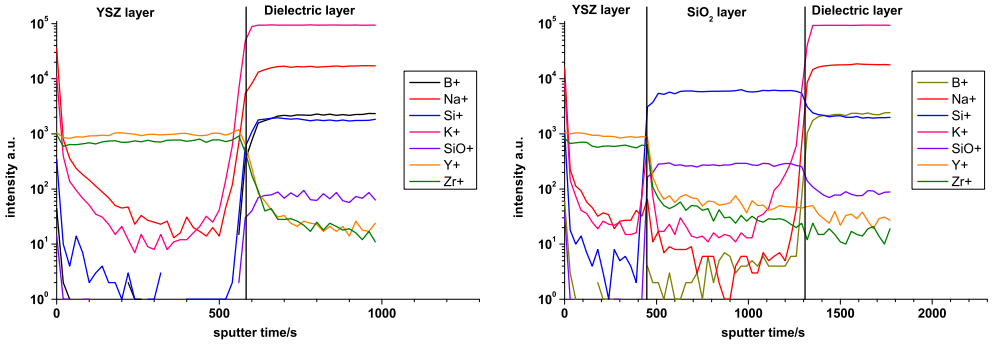

(a) (b)

Figure 5.11: ToF-SIMS results for YSZ coated PDP base plates figure 5.11(a) without and figure 5.11(b) with SiO_2 diffusion barrier layer. In both cases depth profile analysis was performed with 2 kV cesium sputter ion gun (current 164 nA) and for secondary ion analysis a bismuth LMIG (Bi^+, 25 kV) was used. A diffusion of elements from the dielectric layer into the YSZ layer could not be detected with a SiO_2 diffusion barrier layer.

5.3 Selection of Dielectric Material

The examinations described in section 5.2 helped to choose the deposition parameters for the YSZ film deposition. In addition the experiments showed that a dense and homogeneously thick YSZ film across the complete deposition area is much more stable during DBD ignition than rough and inhomogeneous layers. Especially for the DBD electrochemical experiments in this work this aspect is of greater interest.

The PDP base plates from SNU were not perfectly flat due to the production process. The conducting paths (several µm high) were prepared by a screen printing process on a float glass substrate and afterwards the dielectric (several tenth of µm high) is put about them. The dielectric has finally a structured surface with hills and valleys which sets the gap distance of the PDP test cell if the top base plate is put on the dielectric to a constant distance over the complete PDP test cell. The thickness of the YSZ layer ontop of the dielectric was about 500 nm. The interaction of the YSZ layer and the dielectric during discharge ignition led to the problem of dielectric breakdowns observed in set 1 and 2. Due to the float glass substrate it also was not possible to exceed operating temperatures above 450 °C over long times.

A flat and high temperature stable dielectric system therefore was much more suited for electrochemical experiments. An improvement of the YSZ-PDP cell with SiO_2 diffusion barrier layer could be observed and in addition the variation of deposition parameters in [87] were performed on float glass substrates and for high temperatures on fused silica substrates.

From these results respectively experimental conditions it was reasonable to chose a simple dielectric system witch does not really interact with the conducting paths (or electrode) and the YSZ functional layer. The Korean base plates therefore were due their complexity of materials used and their surface structure discarded for use in the electrochemical experiments.

The dielectric material used should be an electric insulator and stable at higher temperatures. A small thermal expansion coefficient was also a necessary basic condition. To avoid diffusion problems of dielectric material and YSZ layer, YSZ itself was checked for its thermal expansion coefficient and dielectric properties. Thermal expansion data for different doped YSZ materials can be found in [118]. The dielectric constant of YSZ ceramic material varies according to temperature, frequency, and doping amount as can be found in literature [56, 119, 120, 121, 122].

According to literature often fused silica with a dielectric constant of about $\varepsilon_r = 3.8$ [57] is used as dielectric material in DBD applications. Comparing both materials the YSZ thermal expansion coefficient is comparable according to the absolute value of the fused silica values. The dielectric constant of YSZ is about one magnitude higher at room temperature than the fused silica dielectric constant. Depending on the size of the catalytically involved YSZ deposition area a complete homogeneous heating cannot be guaranteed.

In addition a direct contact of the catalytic active material YSZ to metal parts or other catalytic active materials should be avoided. With this considerations a fused silica dielectric with a deposited YSZ layer seemed the best

choice. That YSZ deposition on fused silica could be well performed, was known due to the work of B. Pachner [87]. With a homogeneously deposited YSZ film a DBD arrangement like described in section 3.1.1 and especially shown in sub figure c) (double sided planar reactor type) of figure 3.1. For such a kind of reactor the preparation of metallic electrodes was necessary. The material selection and electrode preparation is described in the next section 5.4.

5.4 Deposition of Metallic Electrodes

Carbon monoxide and oxygen had to be used in the catalytic experiments, thus both reducing and oxidizing cases are present in the experimental chamber. Another boundary condition is the thermal stability of the electrode material over several hours or even days at elevated temperatures of up to 500 °C.

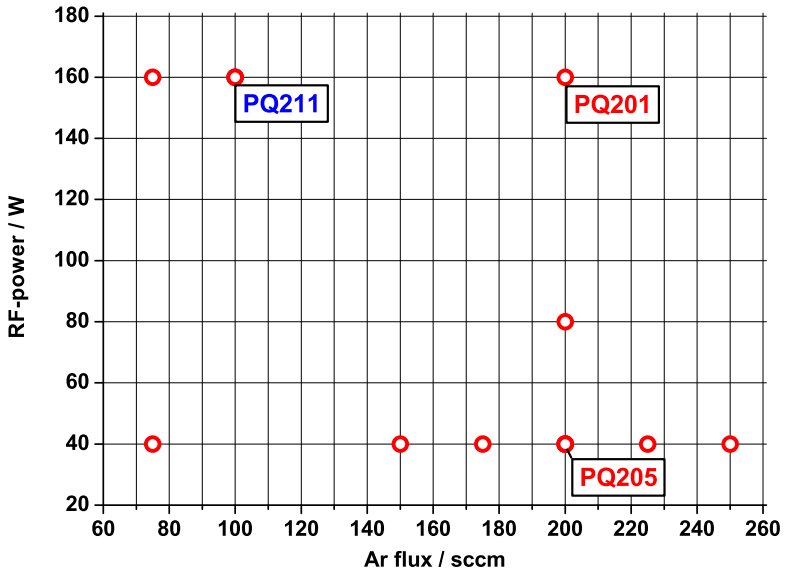

Figure 5.12: Overview of platinum electrodes prepared by sputtering at room temperature. Samples are shown according to Argon gas flux and RF-power. Deposition parameters are indicated by ○. The boxes show the sample names which are discussed in this work. Colors for the sample numbers are chosen according to the used films conditions of sample deposition (without or with YSZ buffer layer on fused silica).

Copper and palladium were tried as electrode material but both were not stable at 500 °C in an oxygen atmosphere. The use of a noble metal such as

gold or platinum was necessary. Because of the possibility to use the sputtering machine in the I. Institute of Physics of the Justus-Liebig-University Gießen platinum was chosen as electrode material. A three-inch-diameter platinum target was used (Platinum target purity 99.99 %, manufactured by Kurt J. Lesker Company Ltd Hastings, United Kingdom) for electrode deposition.

The platinum films should be temperature stable up to 700 °C to show no dewetting of the electrode at the operating temperatures of up to 500 °C. Dewetting of platinum electrodes is a known phenomenon described in literature on YSZ films [123, 124]. To achieve the best deposition parameters several conditions were tested. Figure 5.12 shows the different deposition parameters that were tested. XRD measurements and ToF-SIMS analysis showed that a polycrystalline platinum film deposited on fused silica with multiple grain orientations was more stable than a mainly single crystalline oriented film. The different influence of temperature on the platinum film depositions tested can be seen in figure 5.13. Best film conditions could be achieved with the parameter setting PQ205 (RF-power: 40 W, 200 sccm Ar flux).

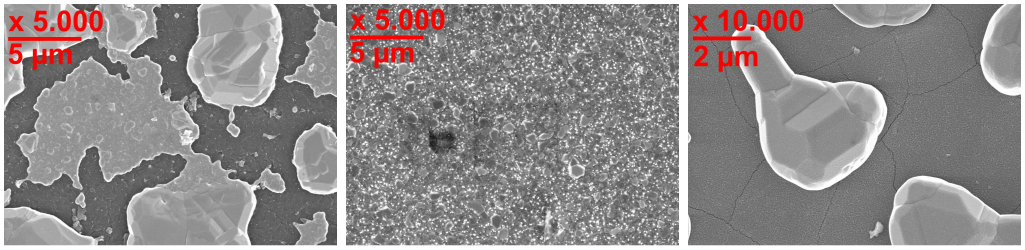

(a) (b) (c)

Figure 5.13: SEM images of platinum films after annealing for 48 hours consecutively at 500 °C, 700 °C and 900 °C. Subfigure 5.13(a) shows platinum film deposited under condition PQ201 and subfigure 5.13(a) under conditions PQ205. For deposition conditions PQ211 which are shown in subfigure 5.13(c) a YSZ buffer layer between the fused silica substrate and platinum layer was introduced. Figures a) and c) show dewetting of the platinum film. Best stable platinum films were prepared with sputter parameters of deposition conditions PQ205.

5.5 Experimental Setup

Direct Barrier discharges (DBD) are presently used in several applications. Possible usages were mentioned before in section 3.1.3. To combine a PDP device with an electrochemical experiment some preparations have to be made for the DBD generation itself (building a generator for discharge ignition), the design of an electrochemical plasma cell and the sample preparation itself. The sample preparation with functional layer, platinum electrode deposition, and the choice of the dielectric material was already discussed.

This section describes now the complete experimental setup with the assembly of the alternating current generator (section 5.5.1), the final dielectric plate system used in this work (section 5.5.2), and the completion of the electrochemical flow through DBD reactor (section 5.5.3). In addition the furnace calibration for high temperature measurements is also shown here (section 5.5.4). Afterwards the assembly of the quadrupol mass spectrometer (QMS) setup (setion 5.5.5) of the Prisma 200 used is described.

5.5.1 Assembly of a Self-Constructed Alternating Current (AC) Generator for the Electrochemical Catalysis Reactor

DBD discharges are usually ignited within the kHz frequency range. First tests were performed with a 45 kHZ generator type 3005SLR with a power of 1.7 kW (manufactured by Softal electronic GmbH). The measurements showed that this frequency was too high for the slower electrochemical processes in the gas phase inside of the discharge. Although the light intensity of the discharge increases with higher frequencies, electrochemical processes have significant reaction rates which are often in the range of ms. The accessible time at 40 kHz for chemical reactions is only 25 μs. To obtain greater time constants frequencies in the range from 1 kHz to 10 kHz were necessary. Additional pre-experiments showed that at least a current of about 30 mA has to be obtained to ignite and sustain the discharge. This led to the requirement of building an alternating current generator that succeeds both basic conditions which are mentioned here.

A schematic of the whole alternating current generator is shown in figure 5.14. As high voltage source a power supply of an old vacuum pump was used and modified for the requirements of these experiments. The alternating current was realized with four switches which were diagonally oppositely linked. The high voltage (HV) part was two times galvanically isolated from the rest of the generator.

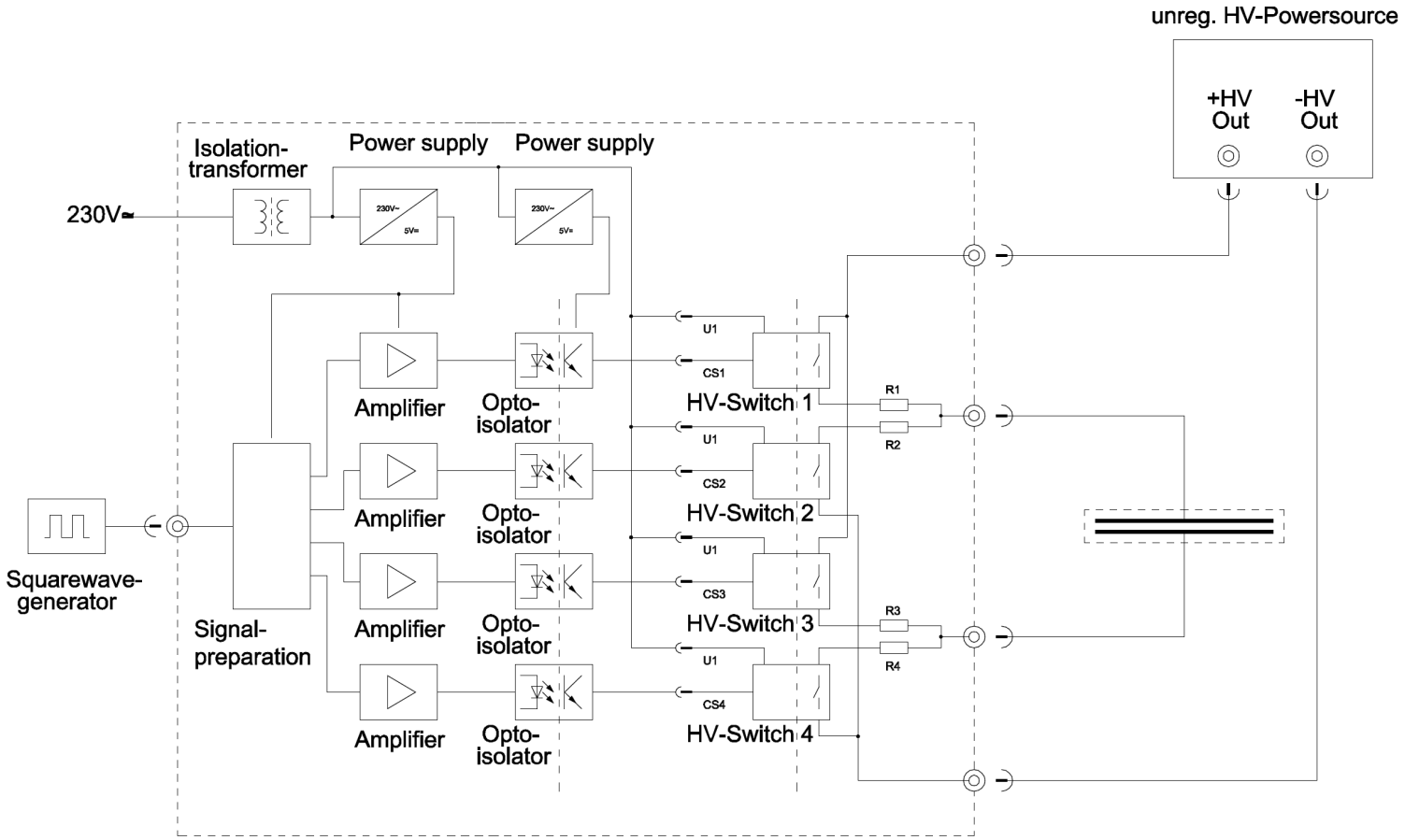

Figure 5.14: Schematic of the AC generator build for DBD discharge. Draft by H. Weigand.

(a) (b)

Figure 5.15: The square wave function generator a) and function analyzer b) used for the experiments.

Each HV switch was connected to an opto-isolator which again galvanically isolates the rest of the generator from the Square Wave Function Generator (SWFG) (Model 126 VCF/Sweep generator from Exact Electronics Inc., USA) as shown in figure 5.15(a). The frequency was measured with a Frequency Counter FC 7002 M (from ELV, Germany) as shown in figure 5.15(b). The assembled generator uses the rectangular signal from the SWFG to alternate the high voltage of the DBD.

Discharges with frequencies from 1000 Hz up to 10 kHz can be investigated with this setup. The adjustment of the HV was performed by an isolating transformer which can be manually adjusted from 0% to 100% power output. The HV followed a linear function of the adjusted value on the isolating transformer. A closer look on the frequency dependent HV output is later given in section 6.1.3

The discharge current is limited by 50 kΩ resistors as can be seen in the schematics of figure 5.14. The maximum of applied voltages can be up to 4 kV due to technical limitations. The resistors were equipped with a radiator for overheating protection. The detailed electronic map of the AC generator can be found in the appendix. Figure 5.16 shows the top view inside the reactor and the connecting wires between discharge and AC generator and power supply.

5.5.2 Design of Dielectric Base Plate System

As explained before (section 5.3) a new reactor concept was planned for electrochemical experiments. At the end a flow-through reactor with parallel arranged dielectric plates was designed. The possibility of heating the whole discharge area was planned and led to several limitations according to the experimental setup. In addition for a defined comparison of the experimental data the discharge volume and the catalytic surface involved should always be of the same size.

Taking all required conditions into account a fused silica plate with the

(a) (b)

Figure 5.16: Figure a) shows a top view inside of the AC generator assembled by H. Weigand (Institute of Physical Chemistry). Figure b) shows in the upper part the front view of the AC generator with simple schematics of the cable connections: red and blue high voltage input, A and B connection to the electrodes of the dielectric plates and on the left bottom function generator input. Below the AC generator the high voltage source (power supply of a vacuum pump) can be seen.

thickness of 1 mm and size of 9 cm times 7 cm (manufactured by Vogelsberger Quarzglastechnik, Germany) was the best choice. To have a flat surface for the deposition of the YSZ films one side of the fused silica plates was polished down to optical quality. The other side was frosted polished for better deposition conditions of the metal electrode.

For the deposition of the YSZ films onto the polished side a mask was prepared which arranged a 3.5 cm square over exactly the same position of every dielectric. For every experiment two plates with identical YSZ layers were prepared. Three densely deposited films with different grain sizes were chosen for the electrochemical surface catalysis experiments. Reference dielectric plates without YSZ film deposition were also selected. Table 5.3 shows the deposition parameters and the quantity of dielectric plates prepared.

For the DBD application an electrode had to be sputtered on the unpolished side of the dielectric plate opposite of the deposited YSZ films. The platinum electrode has the same size of 3.5 cm into square with an additional supply connection at the lower right corner of the electrode. It was sputtered onto the unpolished side of the fused silica. A deposition mask was prepared for the platinum electrode sputtering and the electrode exactly arranged on the opposite side of the YSZ deposition. This arrangement ensures that the discharge occurs over a well defined surface area respectively volume and exactly between the both YSZ films deposited on the fused silica dielectric plates. All dielectric plates were first deposited with the YSZ film and then

Film No.	Ar flux /sccm	O_2 flux /sccm	Substrate T /°C	Quantity
58	250	10	700	4 plates
67	50	0	RT	4 plates
71	45	5	RT	4 plates
Ref				8 plates

Table 5.3: Summary of YSZ deposition parameters used for the film preparation on the fused silica dielectrics with "58" high temperature deposition, "67" non-reactive room temperature deposition, and "71" reactive room temperature deposition.

with the platinum electrode. Figure 5.17 shows an exemplary picture of one deposited fused silica plate. After the deposition of a functional YSZ layer and electrode all dielectric samples were annealed in a furnace to achieve stable platinum electrodes and YSZ films. The annealing was a two-step heating procedure and is shown in figure 5.18.

(a) (b)

Figure 5.17: Fully prepared fused silica dielectric after annealing with a) YSZ non reactive sputtered room temperature deposition "67" (size 3.5 cm into square) and b) PQ205 platinum electrode (size 3.5 cm into square with supply connection in the lower right part).

5.5.3 Design of Electrochemical Flow Through DBD Reactor

For the electrochemical experiments several boundary conditions have to be taken into account. A steady state experiment seems not reasonable at first due to pressure changes according to the volume loss in the carbon

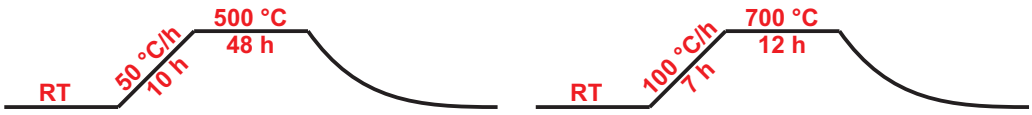

Figure 5.18: Schematic drawing for the two step annealing route of all fused silica dielectric plates starting at room temperature (RT).

monoxide oxidation and leakage occurrence in the vacuum system. Although for some special experiments a Batch Experiment (BE) seems to be the first choice. QMS (see section 4.1) and OES (see section 4.2) measurements offer a fast access to the experimental data of a Flow Through Experiment (FTE). OES is an in-situ technique and shows directly the composition of ions and existed atoms respectively molecules in a discharge. Additionally the QMS with a capillary mounted directly behind the discharge gives a near in-situ composition of the gas phase in the discharge. Time delay of the measurement signal here is only given by the capillary used for gas transfer from the reactor into the QMS vacuum system. Details of the Assembly of the QMS wil be found later in section 5.5.5.

Finally both techniques are sensitive to small changes in gas composition inside of the discharge zone, which makes them the perfect choice for the discharge analysis of a FTE system. Advantages and Disadvantages of a BE and a FTE experiment are discussed with real measurement data later in this work, see section 6.1.4.

For an investigation of plasma catalytic effects it is necessary to avoid other catalytic materials near the discharge zone. This led to the use of the fused silica plates as described in the last section 5.5.2 with the smaller area of the discharge zone according to the size of the dielectric plate. Additionally the extraction of the gas via a capillary (for detailed description see section 5.5.5) should take place as near as possible at the discharge zone. Dielectric plates had also to be oriented precisely inside the DBD reactor to obtain best gas flux conditions.

Lastly it has to be possible to heat the whole discharge area to temperatures of at least 300 °C where the oxygen ion conductivity of the YSZ is sufficiently high. The different behavior of YSZ at room temperature and at temperatures when ionic conductivity takes place is a key aspect of this work.

Taking these basic conditions into account two parallel-orientated dielectric plates were used. The plates are orientated in gas flux direction so that the discharge zone is perpendicular to the gas flux. Each dielectric plate is placed into a brass holder which is mounted into a brass chamber used as DBD reactor. At the beginning of the experiments one of the holders

was hold in position by being directly mounted on the bottom of the brass chamber and the second was adjustable for different gap distances. This was used to find out best discharge conditions according to different gap distances of the dielectric plates. Later the movable holder was also mounted to the bottom of the brass chamber to ensure having the same gap distance in every experiment. Each holder was equipped with a heater which can heat the discharge zone up to about 450 °C, which was sufficient for the designated temperature inside the discharge mentioned before. The calibration of the heaters is shown later in this work (section 5.5.4). An top view of the described DBD reactor is shown in figure 5.19.

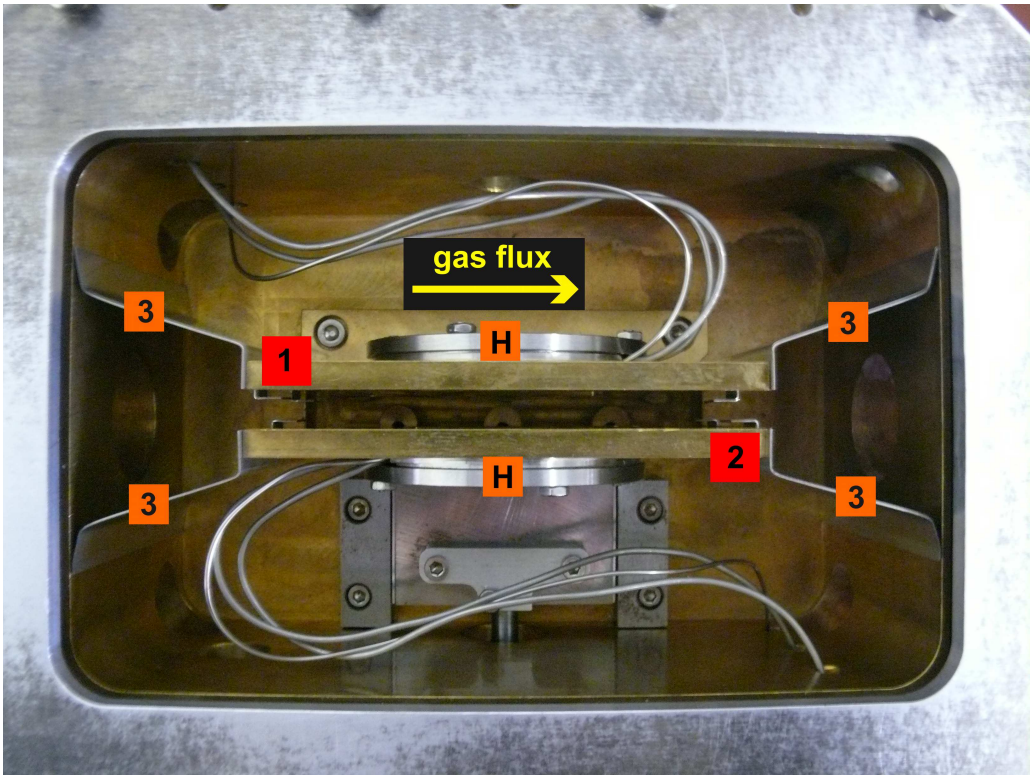

Figure 5.19: Top view inside of the first assembly of the DBD reactor. The gas flux between the dielectric plates (not installed in this image) is represented by the arrow. The fixed holder is marked with 1 and the adjustable holder with 2. Shielding plates which were installed to channel the gas flux directly between the dielectric plates are marked with 3. H stands for the heaters.

A detailed view of the holders used for the first experiments can be seen in figure 5.20(a). After the first experiments it became clear that additional

isolation was needed due to high voltage breakdowns to the brass holders via the gas phase. For this purpose the recess clearance in the holder above the electrode was extended and filled with a ceramic plate consisting of Al_2O_3. In addition to avoid short circuits two plates of mica (thickness 0.5 mm) were placed between the dielectric plate and brass holder respectively Al_2O_3 plate (manufactured by Friatec GmbH).

A second place for short circuits was the electric connection hole inside the holder. To prevent electrical breakdowns a Al_2O_3 husk (manufactured by Friatec GmbH) was placed as a shielding piece for the high voltage supply. The isolating parts can be seen in figure 5.20(b) and the assembled isolated brass holder in figure 5.20(c). In this figure it can also be seen that the stainless steel shielding plates were exchanged with brass shielding plates. Figure 5.20(d) shows the view from the dielectric plate side with the isolation of the platinum electrode and the supply connection visible against the brass holder.

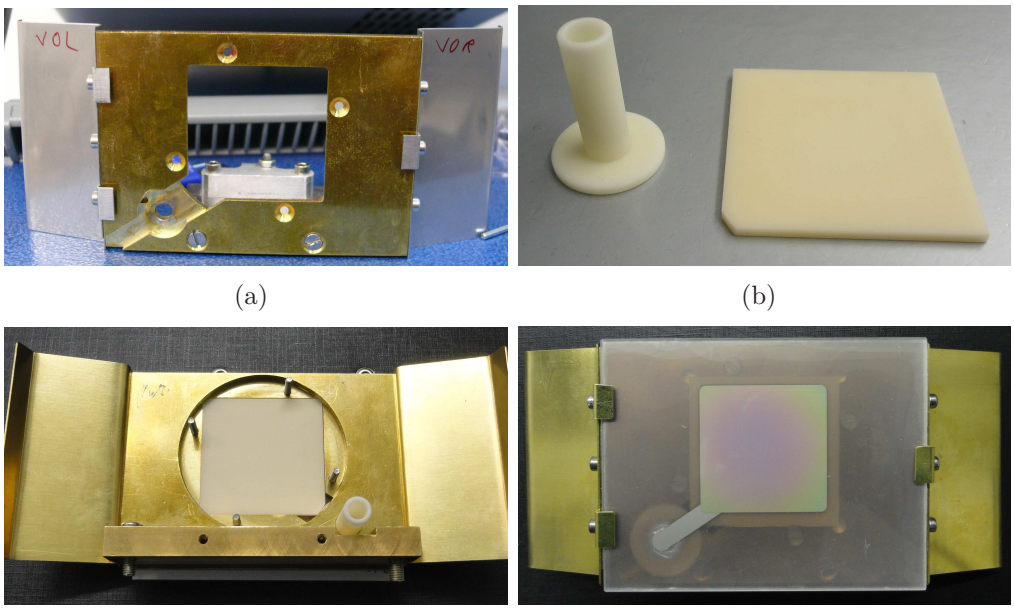

(a) (b)

(c) (d)

Figure 5.20: Figures show a) brass holder with stainless steel shielding plates as first manufactured, b) ceramic isolation pieces which were added after short circuits inside the reactor chamber, c) brass holder with shielding plates consisting of brass instead stainless steel and installed isolating parts and d) front view of holder with equipped dielectric plate. The isolating parts can be seen through the fused silica.

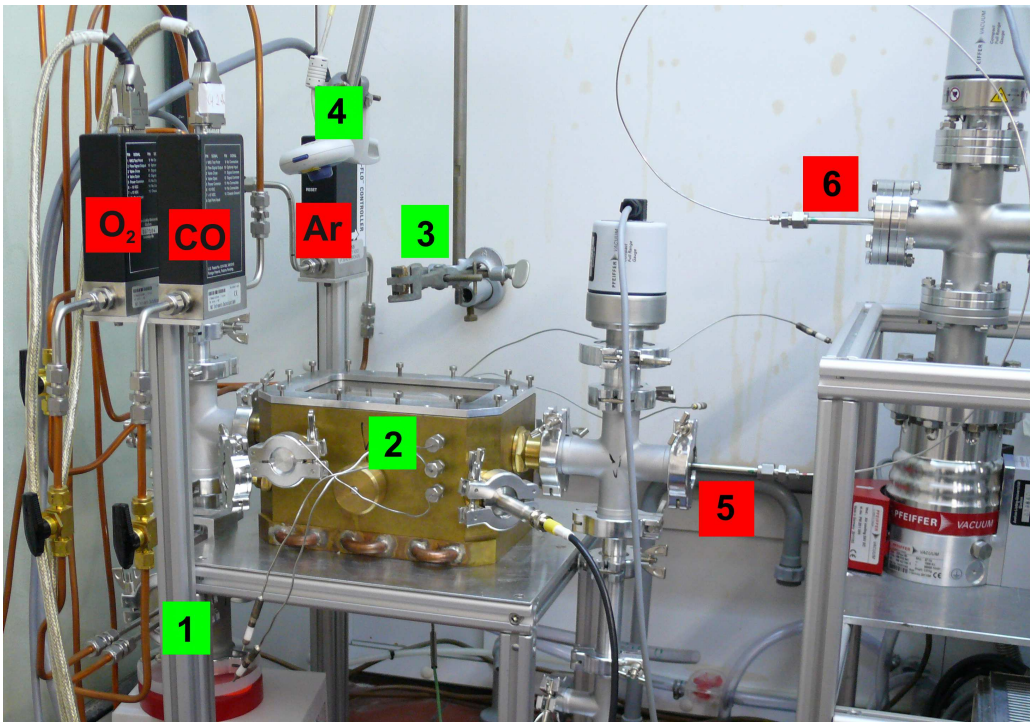

Figure 5.21: Experimental setup of the DBD electrochemical reactor: 1) gas inlet, 2) reactor chamber, 3) holder for OES fibre glass detector, 4) webcam for direct visual control of discharge, 5) capillary flange DBD reactor side, 6) capillary flange QMS side, the mass flow controllers are marked with the gases used: O_2, CO and Ar. The Baratron is not visible in the image due to its place between the mass flow controllers. One high-voltage-lead-through can be seen on the right corner in the front of the reactor chamber, the second is diagonally arranged on the left corner of the backside (not visible).

The brass chamber is sealed on top with a 4 mm thick both-side-polished fused silica plate and is evacuated with a DUOLINE 10 rotary vane pump from Pfeiffer Vacuum (end pressure 1.0E-3 mbar). The pressure was measured before the gas entry into the brass chamber with a Baratron manometer type 626B13MDE (measurement range from 1000 mbar to 0.1 mbar, from MKS instruments Germany GmbH).

Each gas flux was controlled by a mass flow controller (20 sccm for O_2 and CO, 50 sccm for Ar, all from MKS instruments Germany GmbH). Mass flow controllers and Baratron manometer were connected to a MKS control unit 647B during all experiments.

Both furnaces were controlled with an Eurotherm 2416 heating control unit and connected to a PC for adjustment and programming. The temperature was measured with two type K thermocouples. During the heating the brass chamber walls were water cooled. A second cooling loop in the base plate of the brass chamber was installed but not used due to sufficient cooling from the cooling loop inside the walls of the experimental chamber. Temperature below the bottom of the brass chamber and on top of it was measured with a Keithley 2700 multimeter to ensure constant cooling conditions during measurements. The HV lead through is diagonally arranged in the corners of the reactor chamber. Figure 5.21 shows the DBD electrochemical reactor and the parts discussed.

The electrochemical reactor was connected with a capillary to the Quadrupol Mass Spectrometer (QMS). A detailed description of this connection is given in section 5.5.5.

5.5.4 Temperature Behavior of the Self-Constructed Furnaces with Built-In Dielectric Base Plate System.

To ensure that the designated temperature T of 300 °C can be achieved between the dielectric base plates the temperatures of furnace and between the base plates inside the discharge zone were measured according to the power level of the furnaces. The data is shown in figure 5.22. The designated temperature of 300 °C is gained with heater temperatures of 435 °C.

To compare the room and high temperature measurements the brass holders with furnace and base plates were adjusted so, that at furnace temperature of 435 °C a constant gap distance of about 1.5 mm was preset between the dielectric material.

In the case of temperature-dependent measurements under discharge conditions this led to the effect that the gap distance between the dielectric

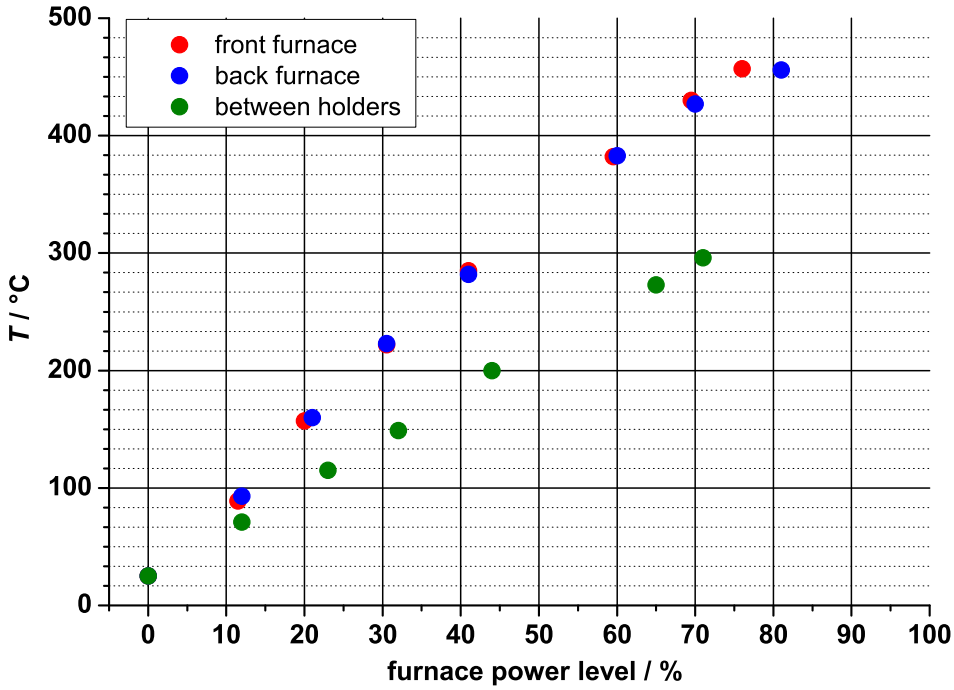

Figure 5.22: The correlation between the power level of the furnaces and the temperature reached between the dielectric plates without an ignited discharge is shown in the figure. The calibration was performed under a gas flux of 4 sccm oxygen and 11 sccm argon at a pressure of 152.4 mbar. This experimental conditions reflect in good agreement all gas setups used in experiments at elevated temperatures. For the measurement of the temperature between the dielectric plates one of the furnace thermocouples was temporarily used. A measurement of the temperature with ignited discharge is not possible. At a heating temperature of about 435 °C a temperature of 300 °C was achieved inside the flow through reactor.

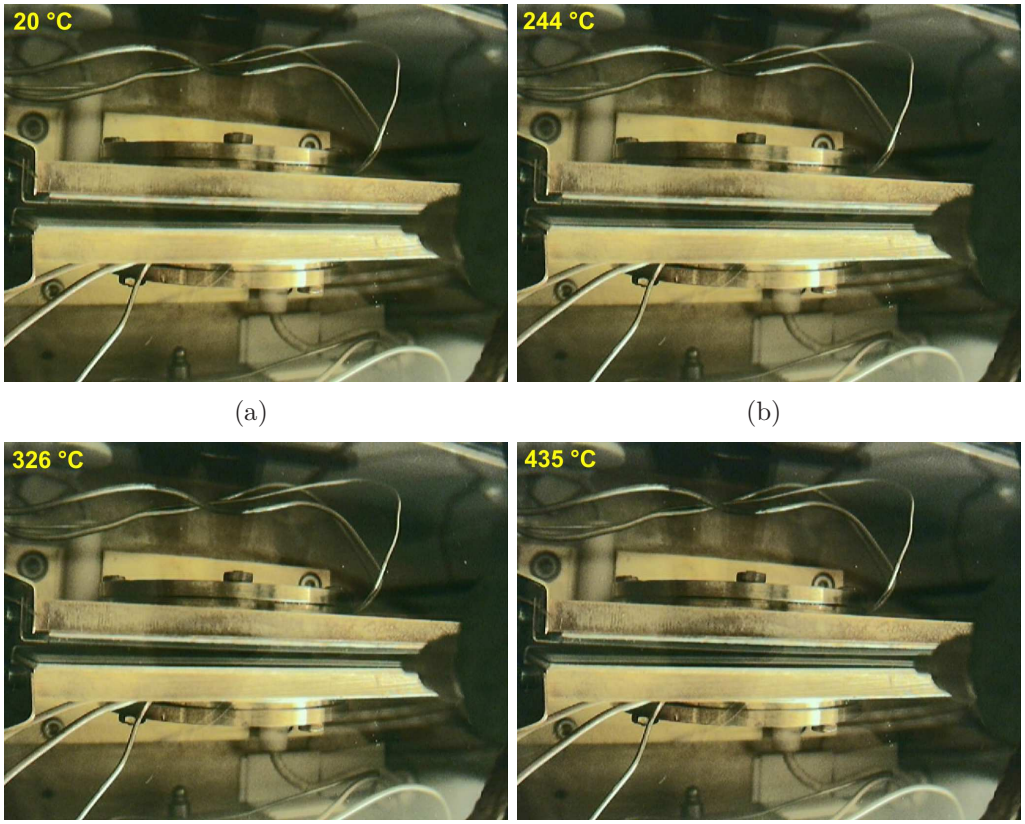

(a) (b)

(c) (d)

Figure 5.23: The figures show the gap distance between the dielectric plates at the given furnace temperatures. The difference of room temperature and elevated temperatures can be easily seen.

material increased to about 3 mm at room temperature (25°C). Figure 5.23 shows this temperature behavior of the dielectric base plates. The different gap distances can be clearly seen.

5.5.5 Assembly of Quadrupol Mass Spectrometer (QMS)

For the investigation of the gas composition a Quadrupol Mass Spectrometer (QMS) Prisma 200 (Pfeiffer Vacuum, Germany) was used. The prevacuum was generated with a DUOLINE 5 rotary vane pump (Pfeiffer Vacuum, Germany, end pressure 10^{-3} mbar). Vacuum was measured with a full range gauge PKR 251 (Active Pirani Cold Cathode Transmitter from Pfeiffer Vacuum). The prisma QMS could be switched off automatically due to vacuum breakdown detected by the PKR 251 unit which was connected directly to the Prisma. The ultra-high vacuum was established in the range of 10^{-8} mbar (or less) with a HiPace 80 turbo pump from Pfeiffer Vacuum. Figure 5.24 shows a picture of the setup of the whole QMS. The QMS was connected to a stainless steel (SS316) capillary (from Jasco Labor- & Datentechnik GmbH Deutschland) with an inner diameter of 1.3 mm and outer diameter of 1/16 inch. The capillary was connected with two vacuum-sealed fittings (from Swagelok GmbH) to a 6 mm stainless steel tube, which is welded on a stainless steel CF flange on the QMS side, and a KF flange on the electrochemical DBD reactor side.

DBD discharges can be ignited up to atmospheric pressures, therefore, as an additional assumption, the QMS should be capable to work even at normal pressures. The capillary was compressed about 1.5 cm after the end of the capillary inside the DBD reactor with a pair of tongs to reduce the gas flux trough the capillary. In this case a pressure around 10^{-6} mbar can be easily adjusted inside the QMS vacuum system and the QMS is operable at atmospheric pressures. Another possibility to increase pressure in the QMS vacuum chamber is to decrease the speed of the HiPace 80 turbo pump below the maximum speed of 1500 Hz. For optimal analysis conditions the capillary was held in a central position with a modified copper seal about 5 cm in front of the QMS analyzer.

The ionization probability of the QMS Secondary Electron Multiplier (QSEM) and Faraday Analyzer of the Prisma follows a linear behavior in the pressure range between 10^{-7} mbar till 10^{-5} mbar. Measurements were always performed within this range. The QSEM Analyzer can be adjusted by software calibration for a magnification of a factor of 2000 of the detected signals measured with a Faraday detector. This shortened the measurement time by a factor of around 10 and the detection limit was improved. The whole QMS setup was due to the capillary solution transportable and the

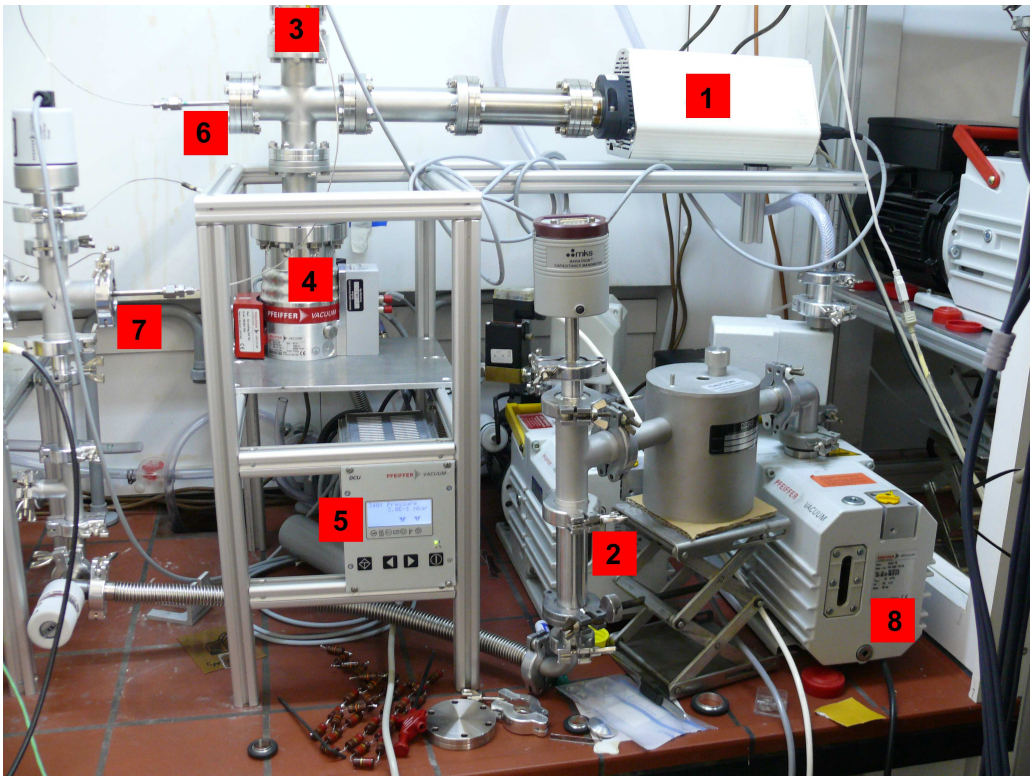

Figure 5.24: Experimental setup of the Quadrupol Mass Spectrometer: 1) Prisma QMS, 2) DUOLINE 5 rotary vane pump (in the back), 3) Full range gauge PKR 251, 4) HiPace 80 turbo pump, 5) HiPace 80 control unit, 6) capillary flange QMS side, 7) capillary flange DBD reactor side and 8) DUOLINE 10 rotary vane pump from DBD reactor.

capillary could be exchanged for other applications if necessary.

5.6 Investigation of Contamination on Dielectric Base Plates.

The kinetics of a chemical reaction can be altered by the use of a catalyst. In this work the YSZ layers work as a heterogeneous catalyst for a gas phase reaction. The key aspect of a catalyst is that it is a part of the reaction cycle but at the end it is unaffected by the reaction and in the same condition as before the chemical reaction, see section 3.2. At reducing atmospheres it can be possible that with greater carbon monoxide flux than oxygen flux a partial decomposition of carbon monoxide happens.

$$2\mathrm{CO} \leftrightharpoons \mathrm{CO_2} + \mathrm{C} \tag{5.1}$$

This so called Boudouard equilibrium normally takes place only at elevated temperatures when CO_2 decomposes over hot carbon into CO. Within a DBD electrons, excited atoms and molecules are present and with a higher partial pressure of CO the back reaction might be possible because of cracked CO_2 molecules. With this in mind the deposition of carbon on the YSZ film might be possible.

During experiments with non-reactive sputtered YSZ films (71) (see section 6.2) some dark contamination occurred at the edge of the deposited YSZ film. Figure 5.25(a) shows one of the dielectric base plates used in the experiments. To clarify whether the dark regions were a contamination of material on the surface YSZ layer or to find out whether the YSZ film is reduced as reported in [125] where blackening of YSZ was investigated a discharge experiment with a 100% carbon monoxide atmosphere at a pressure of 100.4 mbar was performed. A deposition of material based on the Mond process found by Ludwig Mond in the late 19^{th} century [126] should be enhanced in such an experiment.

After the experiment the reactor was opened and the YSZ coated base plates were examined. Figure 5.25(b) shows the front base plate and figure 5.25(c) the rear base plate with a black respectively dark brown YSZ surface. These experimental results showed that a closer look on possible contamination of the catalytic-active YSZ film and, in addition, the whole base plate was necessary.

The YSZ (71) base plates from figure 5.25 were investigated with ToF-SIMS depth profiling to gather information of deposited material. The ToF-SIMS technique was used because of the low detection limits of the different

(a)

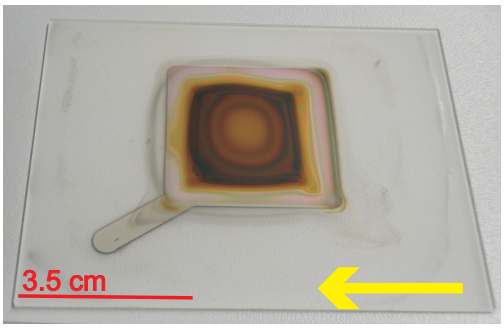

(b)

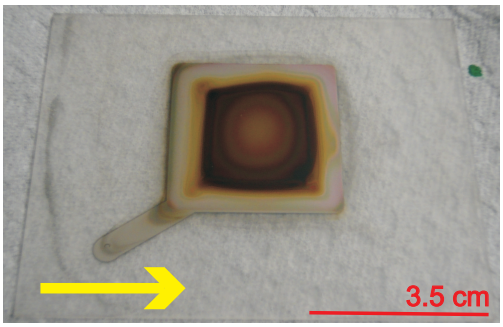

(c)

Figure 5.25: Figure a) shows the YSZ reactive sputtered room temperature coating (71) with size 3.5 cm times 3.5 cm on one of the dielectric plates used which has dark contaminations along the edges of the film coating. Figures b) and c) show the base plates after 100% carbon monoxide atmosphere experiment at 100.4 mbar pressure. The YSZ coating shows black, respectively, dark brown discoloration and contamination on the fused silica plate around the YSZ deposition area. The yellow arrows show the gas flux direction of the experiments.

elements. With the depth profiling also the thickness of a deposited layer can be measured and the distribution of different materials is detected. Figure 5.26 shows the measured depth profile of one of the YSZ 71 base plates. The depth scale is composed of two different measurements: One to obtain the complete depth profile and a second one to get the sputtering rate of the surface layer which was much faster then the sputtering of the YSZ layer. The fused silica has a similar sputtering rate as the YSZ ceramic.

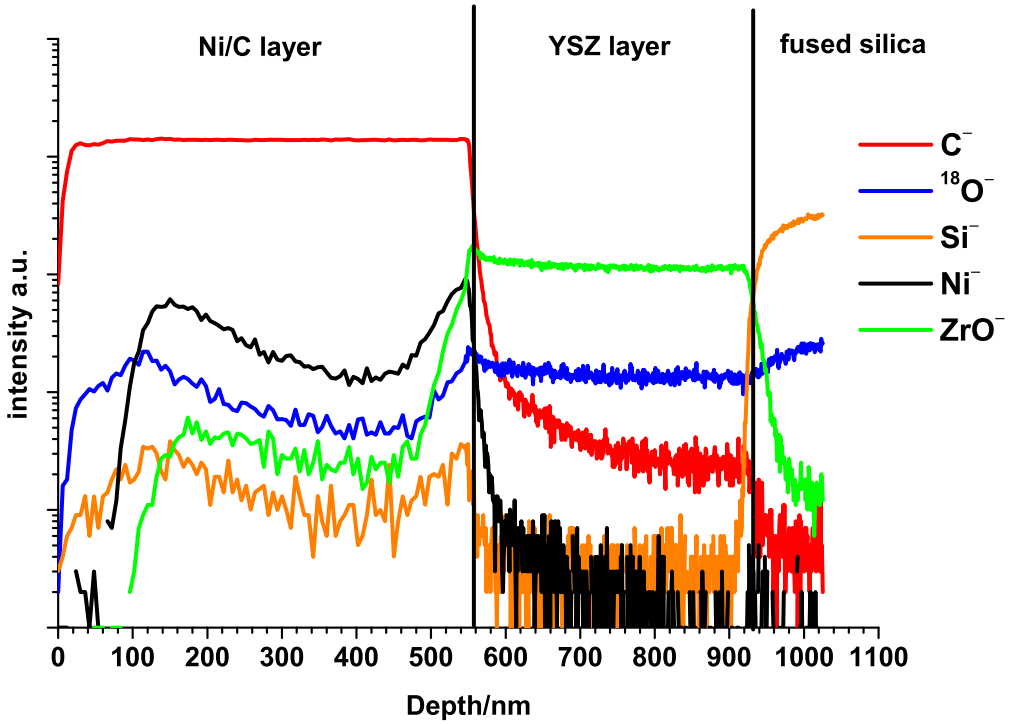

Figure 5.26: The figure shows the ToF-SIMS depth profile of the center of one of the YSZ surface film (reactive sputtering at room temperature, 71) from figure 5.25. A 2 kV cesium ion sputter beam was used for material removal and a bismuth LMIG (Bi^+, 25 kV) for analysis. A surface layer consisting of carbon and nickel covers the still intact YSZ layer. The fused silica base plate can be seen in the right part of the figure where the Si signal intensity rises at the end of the measurement.

The results proved indeed that surface contamination of carbon with nickel which were also observed by Mond et. al. in [126] when a carbon monoxide gas flux was passed over metallic nickel at elevated temperatures occur on the deposited YSZ films. Mond observed that the relation of carbon and nickel deposited varies according to the temperatures of the gas and

the duration of the experiment. The source of the nickel indeed could not be verified with this analysis. To exclude one possible origin of the nickel contamination all stainless steel pieces inside the flow through reactor were substituted by brass pieces. For further verification whether another source of nickel is still present in the experimental setup the sample preparation process of the dielectric plates was monitored with ToF-SIMS investigations.

For this purpose the dielectric base plates were investigated right after YSZ film deposition, after annealing, and after discharge experiments. It was found that during this preparation processes two main contaminations could be detected: chromium and nickel. Figure 5.27 shows an overlay of the main isotopes of chromium and nickel from the three recorded ToF-SIMS spectra. It can be seen that the chromium signal occurred after annealing and additionally the nickel signal can be detected after discharge experiments. The isotopic pattern of chromium and nickel was checked and the isotopes are correctly distributed. After discharge the intensity of the chromium surface signal decreased because of the additional nickel coverage of the surface.

It was found that the chromium is a surface contamination which is caused either by the heater element of the furnace or the annealing holder of the base plates during annealing procedure. The annealing route for all base plates was the same and could not be altered. The chromium contamination therefore was accepted as a preparation impurity of all dielectric plates. The mass spectra taken after discharge experiments shows signals of nickel. The origin of this contamination was still not clear, but of some interest because nickel is often used as a catalyst in chemical reactions.

As the nickel occurs only after discharge experiments the contamination comes from the experimental setup itself or the used gases. One possible explanation is the so called Mond process; a chemical transport reaction which was named after Ludwig Mond who investigated the interaction of carbon monoxide with nickel metal [126]. Because of the toxicology of the metal complex and its use in refining nickel metal many studies were performed [127]. The transport reaction mechanism can be described as

$$4\mathrm{CO} + \mathrm{Ni} \rightleftharpoons \mathrm{Ni(CO)_4} \tag{5.2}$$

Carbon monoxide reacts with nickel to nickel tetra carbonyl at temperatures of about 50°C and decomposes again to nickel and carbon monoxide at temperatures above 180°C to 200°C. Problems occur at elevated temperatures if a nickel contamination is deposited on a sample surface and further carbon monoxide decomposition takes places [126] to form a Ni/C surface layer. For the dielectric barrier discharge pure nickel depositions are another problem which influence the discharge stability and seemed to cause the flick-

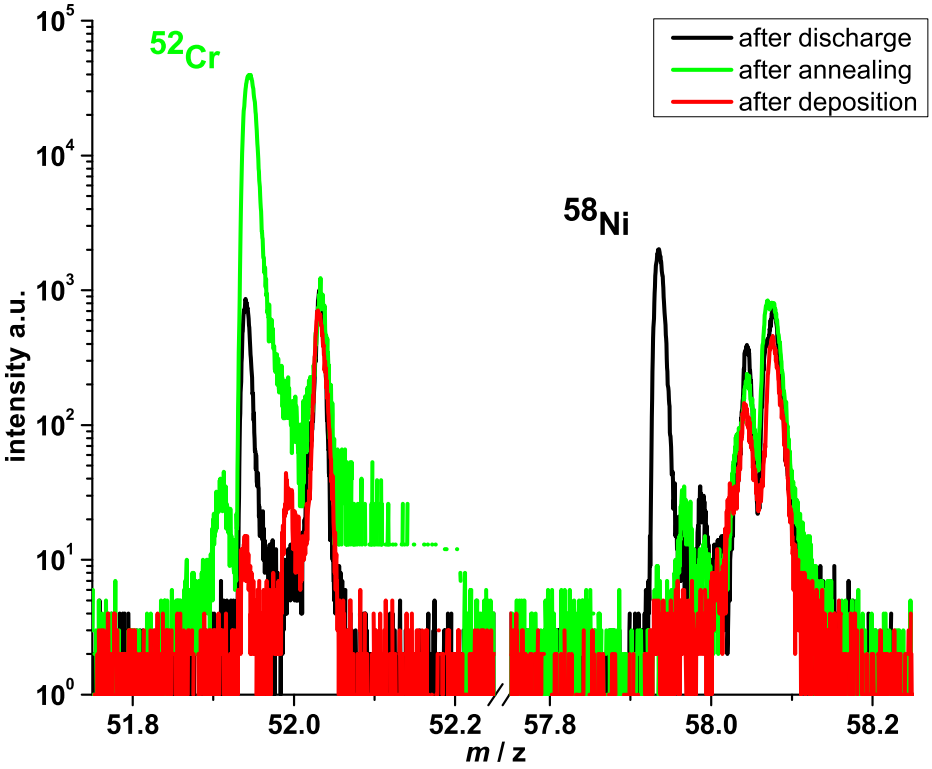

Figure 5.27: Detailed view of the main isotope masses of chromium (m/z = 52) and nickel (m/z = 58) from a overlay of ToF-SIMS spectra recorded during the preparation steps and after discharge investigations. After annealing procedure Cr signals appear and after discharge experiments Ni signals are detected. The Cr signal is decreased after discharge due to the nickel coverage of the sample surface.

ering discharges which were observed with the YSZ reactive sputtered room temperature deposition (71, see table 5.3) coated dielectric base plates.

Each deposition of metal inside the discharge zone can work as another electrode for the discharge. This might cause stability problems or even short circuits to other metallic parts of the flow through reactor. The stability of the discharges and the influence of the Ni contamination were further investigated with the non-reactive sputtered room temperature YSZ depositions (67, see table 5.3) coated base plates. The stability experiments were performed with a gas flux of 1 sccm oxygen, 1 sccm carbon monoxide and 13 sccm argon gas flux. The pressure of the experiments was increased to about 150 mbar due to stability issues of the discharge.

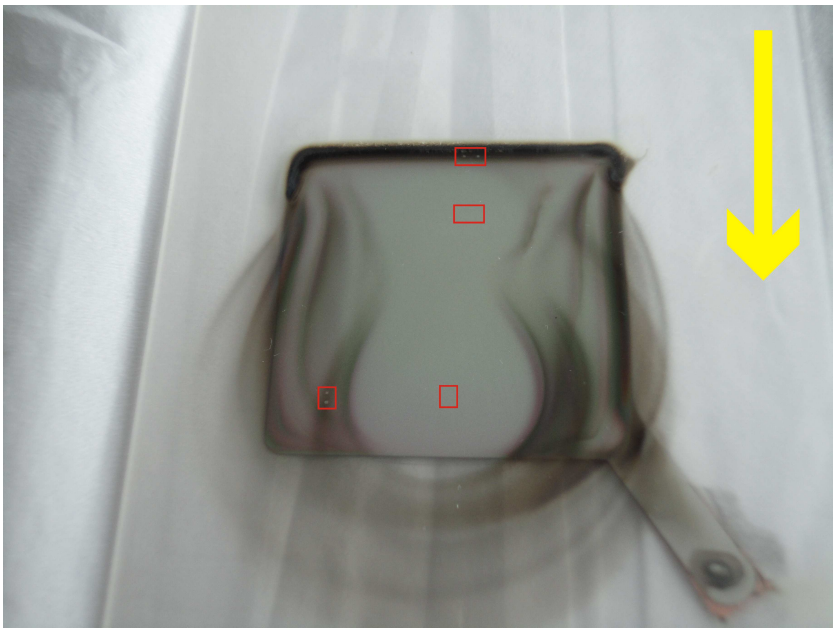

Figure 5.28: One of the YSZ coated base plates (film conditions 67) mentioned in the text is shown in the picture. The area of ToF-SIMS spectra and depth profiling are marked with red rectangles. The yellow arrow indicates the gas flux in the experiments. ToF-SIMS analysis showed similar profile data as already presented in figure 5.26. The Ni contamination in the uncovered middle film areas were negligible.

The stability of a DBD discharge also depends on the gap distance between electrodes respectively dielectrics, therefore the gap distance was investigated for stability issues. It was found that a distance of about 1.5 mm between the fused silica plates was the best gap distance for the DBD investigations. Discharge stability could be enhanced with this gap distance. The

reproducibility of measurements was increased and the nickel contaminations decreased.

After these experiments a reactor malfunction which was not explainable caused a contamination of the dielectric base plates. Therefore they were taken out of the reactor and examined with ToF-SIMS. Figure 5.28 shows a photograph of a base plate with non-reactive sputtered room temperature YSZ deposition (67) which shows dark contamination on the YSZ film and the fused silica plate itself. The area of ToF-SIMS investigations are marked with red rectangles in the image. The results were similar to the result from figure 5.26 and showed a Ni/C surface film at the contaminated area, therefore this result is not shown here. The nickel contamination in the uncovered middle of the YSZ coating was negligible.

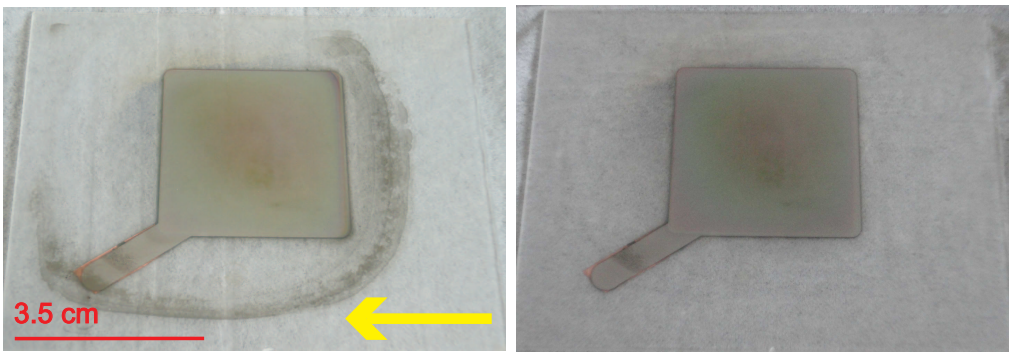

(a) (b)

Figure 5.29: The left picture shows a base plate with a 3.5 cm times 3.5 cm high temperature YSZ deposition (58, see table 5.3 with a nickel containing half ring (proved with ToF-SIMS and EDX) around the YSZ film deposition area. The yellow arrow gives the gas flow in the experiments. The half ring was deposited after constitution of a "hot zone" (as described in the text) at the gas inlet of CO, O_2 and Ar which was thought to avoid Ni contamination in the discharge zone. The right picture shows the same base plate cleaned with 13% nitric acid. The deposited contamination is completely removed.

Another possibility to hinder the nickel tetra carbonyl transport reaction is the establishment of a hot zone were the complex is destroyed and the nickel deposited on a metal surface were the contamination does not influence the discharge characteristics. For this purpose copper swarf were put right behind the inlet of the CO feed line and heated with an external heating band to temperatures of upto 180°C on the outer surface of one tube of the used KF system alumina cross (see figure 5.21 bottom left side marked with gas inlet). Figure 5.29(a) shows one of the used high temperature YSZ

deposition base plates with a nickel half ring which was deposited during the hot zone experiments.

The deposited nickel worked as trapping zone for further nickel metal deposition and destruction of the tetra carbonyl process. Even with the hot zone in the gas inlet it was not possible to avoid nickel deposition completely in the discharge area or near the discharge area at room temperature without greater reconfiguration of the experimental setup. Because the nickel tetra carbonyl contamination could also be in the gas bottle itself a cleaning route for the base plates was established. Nickel dissolves in diluted nitric acid which does not affect fused silica or YSZ films. 100 ml of a 65% concentrated nitric acid were diluted with 400 ml demineralized water to gain a 13% nitric acid for the cleaning process. Figure 5.29 shows one base plate with nickel contamination before and after nitric acid cleaning.

Chapter 6

Results and Discussion

In this chapter the main experiments are presented. Experimental conditions are laid out (for example gas composition) and the samples used introduced (section 6.1). The different experiments are discussed and their results presented. Several experiments were performed to examine the catalytic behavior of the functional YSZ thin film, but in addition the impact of different gas compositions according to ignition voltages and oxidation rates of carbon monoxide was also examined. Measurements were started at different frequencies and the frequency's impact on the discharge behavior was studied. The influence of the heating of the functional layer with the whole DBD system was investigated.

6.1 Experimental Settings

DBD experiments were performed with different film coatings and experimental settings. An overview of the prepared samples is given in section 6.1.1. The discharge conditions according to the gas flux of the different used gases is discussed in section 6.1.2. The influence of frequency is mentioned in section 6.1.3. Last, as already discussed earlier in section 5.5.3 the comparison of both possible experiment conditions (BE or FTE) is performed with measurement data and the consequences for the experimental work are discussed in 6.1.4.

6.1.1 Dielectric Plates for DBD Experiments

In section 5.3 the dielectric material used was discussed. In table 5.3 an overview of the number of samples prepared was presented. For the experiments always a pair of identically deposited dielectric plates was used. For a

better overview of the pairs of dielectric plates used table 6.1 shows the deposition parameters of YSZ films, the samples which are used in this chapter, and the measurements performed with this pair of dielectric plates.

Measurement which were performed with all dielectric base plates like ignition voltages determination and OES are not mentioned here. Some measurements were performed due to analytical questions which occurred during the experiments, so they are only performed with one pair of samples. At the beginning of the investigations first experiments were used to define the experimental parameters and to learn the influences on the discharge of different gas composition, applied high voltage and frequency. If preliminary measurements were performed with dielectric base plates this is also mentioned.

6.1.2 Gas Compositions

For the experiments performed in this work the sum of all gas fluxes of oxygen, carbon monoxide and argon was held constant at 15 sccm. The flux of the carrier gas argon was reduced when the gas flux of oxygen or carbon monoxide was increased. The influences of increased oxygen or carbon monoxide fluxes on the CO_2 generation were investigated. Another aspect has to be considered for the discharge characteristics. The oxidation of carbon monoxide with oxygen to carbon dioxide follows the reaction:

$$1O_2 + 2CO \leftharpoons 2CO_2 \tag{6.1}$$

which shows clearly that a higher CO oxidation rate should be consistent with a reduced pressure inside the discharge chamber due to the volume loss according to equation 6.1. This has an direct impact on the discharge characteristic which depends on the pressure and the composition of the gas inside the DBD reactor.

To study the behavior of the discharge first experiments were performed with a large variety of gas compositions. Eventually only a few of them were chosen for the plasma catalytic measurements. Table 6.2 gives an overview of all gas compositions tested within this work. The deposited films used with each gas compositions are presented. Detailed descriptions of the experiments are given in the next sections of this chapter.

6.1.3 Frequency-Dependent Measurements

The setup of the AC generator used in this work provides some boundary conditions for the charging and discharging of the dielectric plates, which

YSZ film	Sample number	Average film thickness	Measurements in section	Preliminary work in section / remarks
67	67-1	256 nm	6.3	5.6
67	67-2	312 nm	6.3	5.6
71	71-1	292 nm	6.2, 6.3	5.6
71	71-2	393 nm	6.2, 6.3	5.6
58	58-1	277 nm	6.2, 6.3, 6.5	5.6
58	58-2	309 nm	6.2, 6.3, 6.5	5.6
67	67-3	880 nm	6.2, 6.4, 6.5	5.6
67	67-4	897 nm	6.2, 6.4, 6.5	
71	71-3	750 nm	6.2, 6.4, 6.5	
71	71-4	860 nm	6.2, 6.4, 6.5	
58	58-3	637 nm	6.2, 6.4, 6.5	
58	58-4	406 nm	6.2, 6.4, 6.5	
	Pt-1	0 nm	6.1.4	fused silica broken
	Pt-2	0 nm	6.1.4	5.6
	Pt-3	0 nm	6.1.4	substitution for Pt-1
	Pt-4	0 nm	6.2, 6.4, 6.5	substitution for Pt-8
	Pt-5	0 nm	6.2, 6.3	
	Pt-7	0 nm	6.2, 6.3	
	Pt-6	0 nm	6.2, 6.4, 6.5	
	Pt-8	0 nm		relieved Pt film

Table 6.1: Dielectric plates prepared with and without YSZ coating. The YSZ coatings are given with the deposition numbers for non-reactive (67) room temperature, reactive (71) room temperature, and high temperature (58) sputtered films (see section 5.1). The average film thickness was calculated by averaging the thickness measurements at the middle of all four edges of the YSZ deposition area. The film thickness at the center of each deposition area will be higher than the averaged value. For the third (-3) and fourth (-4) YSZ deposition the sputter time was doubled for thicker films. Fused silica base plates without YSZ film coating are labeled Pt-X, with X being the sample number. The pairs of dielectric plates used are separated by hyphens.

gas mixture	YSZ deposition	O_2 /sccm	CO /sccm	Ar /sccm	Σ /sccm
0/0/15	UC	0	0	15	15
1/1/13	ALL	1	1	13	15
1/2/12	UC	1	2	12	15
2/1/12	ALL	2	1	12	15
2/2/11	58, 71, UC	2	2	11	15
4/1/10	ALL	4	1	10	15
2/4/ 9	71	2	4	9	15
4/2/ 9	58, 71, UC	4	2	9	15
4/4/ 7	71	4	4	7	15

Table 6.2: Summary of gas mixtures used in discharge experiments. The deposited films used with each gas mixture are quoted with the deposition numbers: For the non- reactive room temperature deposition (67), for the reactive room temperature deposition (71), for the high temperature deposition (58), and for the uncoated fused silica dielectric (UC). If a gas mixture was used in experiments with all dielectric base plate systems this is denoted with (ALL).

leads to a direct correlation of the high voltage output and the used frequency in the experiments. Theoretical considerations to this topic were given earlier in section 3.1.4. The applied high voltage on the discharge was measured right before the DBD at the connection cable input, which can be seen in the right side of figure 5.14. The high voltage applied to the discharge at a constant value Z of the isolating transformer was measured for different frequencies. According to the construction of the self-constructed alternating current generator a frequency-dependent behavior was expected.

Figure 6.1 shows the measurement data and linear approximations. The linear functions deduced from this measurement data are given in table 6.3. The high voltage U calculated from the functions is the amplitude of the square wave function used. The whole potential difference from amplitude to amplitude is the double of the high voltage calculated according to the linear fits.

Two effects are responsible for the different linear functions shown in table 6.3. Firstly the dissipation factor of the AC generator leads to thermal power loss at higher frequencies. This is a side effect of the mode of operation of the switches used in the generator setup, see figure 5.14 in section 5.5.1. For higher frequencies it is not possible with the self constructed alternating current generator to give a correct square wave function profile. The applied potential looks than more like a triangle wave function profile which follows

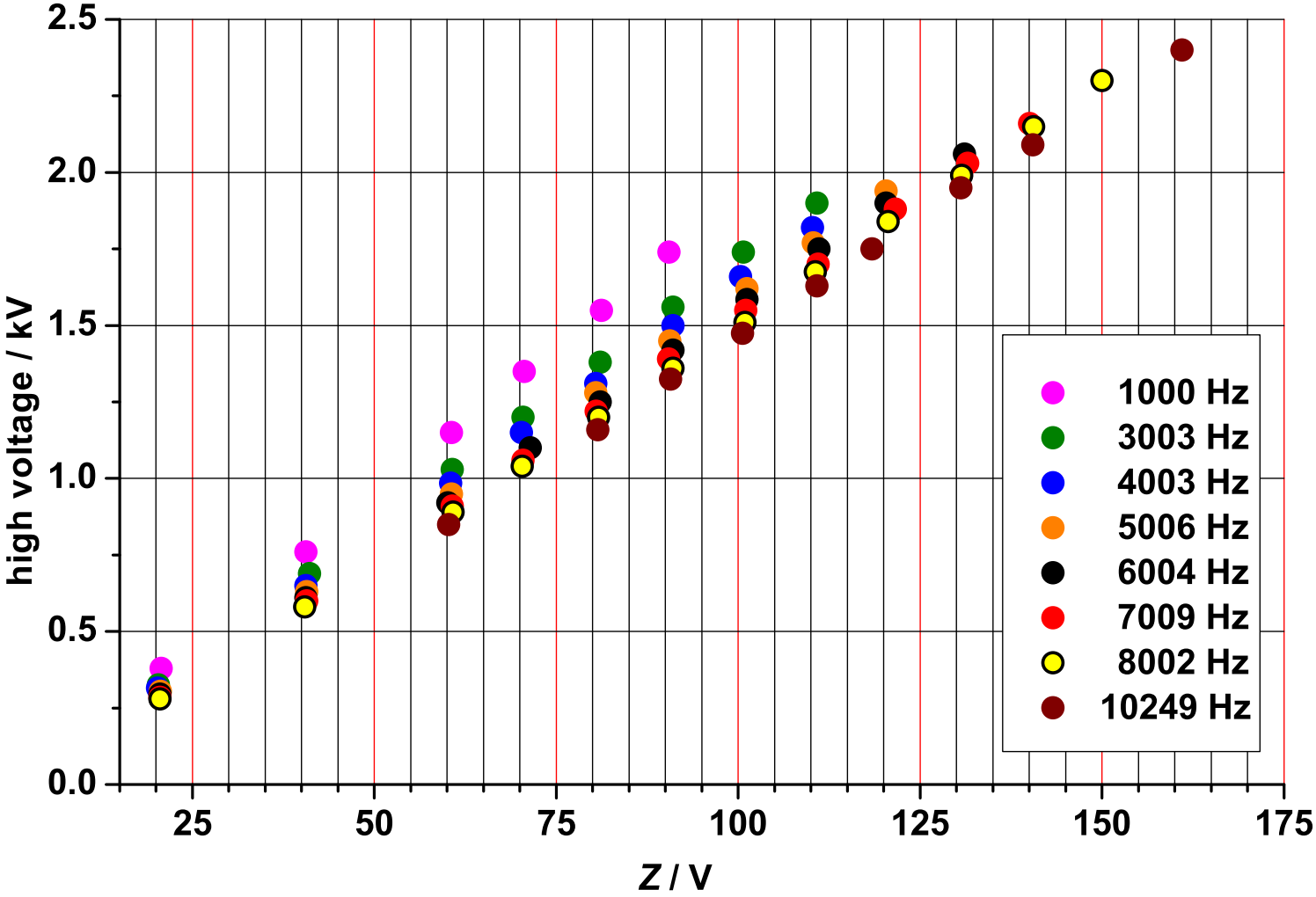

Figure 6.1: High voltage amplitude of the square wave function generator measured according to isolating transformer voltage Z at different frequencies. The linear best fit functions of the shown data are given in table 6.3.

Frequency/ Hz	High voltage U/V linear function fits according to isolating transformer voltage used Z/V
1000 ($\pm$5)	$U = 19.471 \cdot Z - 26.866$
3003 ($\pm$5)	$U = 17.466 \cdot Z - 29.411$
4003 ($\pm$5)	$U = 16.770 \cdot Z - 28.274$
5006 ($\pm$5)	$U = 16.395 \cdot Z - 37.123$
6004 ($\pm$5)	$U = 16.016 \cdot Z - 36.729$
7009 ($\pm$5)	$U = 15.713 \cdot Z - 38.778$
8002 ($\pm$5)	$U = 15.650 \cdot Z - 55.788$
10249 ($\pm$5)	$U = 15.448 \cdot Z - 79.677$

Table 6.3: Functions of the lines of best fit for the given frequencies. Applied high voltage in all experiments is calculated with this fits.

the function of equation 3.11. Secondly the power coupled into the discharge also depends on the loading of the dielectric plate DBD system.

The theoretical expectations from figure 3.2(b) were confirmed within the experiments. DBD discharges at 1000 Hz were very dark at a low power level and showed in measurements with an oscilloscope that the charging of the capacitor system is complete and after full charge of the dieletric system no further current was detectable. Discharges ignited at frequencies higher than 7000 Hz were bright with a continuous flow of current and a not fully loaded capacitor system. The input voltages in correlation to lower frequencies were up to 20% higher than the maximum voltage applied at the dielectric system at lower frequencies. Best experimental conditions could be achieved in the frequency range from 3000 Hz to 7000 Hz. These frequencies were chosen to be used in the main experiments.

Another frequency dependent effect should be also observable. The frequency ν dependent energy E coupled into the discharge should follow the equation

$$E = h \cdot \nu \tag{6.2}$$

where h is the Planck's constant. A linear increase of the energy input at higher frequencies should be visible in a higher CO_2 generation. This increase has to be taken into account if the absolute value of the catalytic enhancement by a YSZ film coating is investigated.

6.1.4 Experimental Setup: Batch or Flow-Through Reactor?

The different equilibrium constants of the main experiments are determined as introduced before in section 4.1, see figure 4.1. For the measurement of the rate enhancement two possible modes are conceivable. A reasonable choice is (as explained in section 5.5.3) the use of a flow-through reactor because gas leakage and volume loss due to the oxidation reaction are here negligible. This method has it's limitations when very small increasing signal intensities of the CO_2 signal occur. Then it might be possible that the error is in the range of the measured value itself. Therefore a comparison of the two possible experiment setups with measurement data will be here presented.

At the beginning of the investigations of the different gas compositions, with the first 45 kHZ generator used from Softal electronic GmbH, the difference between flow-through (FTE) and batch experiments (BE) were tested with uncoated dielectric base plates. For the BE the leakage rate was determined to be $2.0 \cdot 10^{-4}$ mbar $\cdot$ s^{-1}. With this leakage rate an increase of 1 mbar of pressure inside the reactor cell is reached within 1 hour and 23 minutes. The leakage gas is air and therefore mostly nitrogen, which can be seen in BE due to the increasing QMS signals of mass 14 (N^+) and mass 28 (N_2^+). Taking the elemental distribution of air into account the amount of detected ^{38}Ar in the QMS is increased by $5.6 \cdot 10^{-6}$ mbar if the reactor pressure increases by 1 mbar. Therefore ^{38}Ar was chosen as a constant signal to norm the measured signals of CO and CO_2. The increase θ of the mass signals according to the starting values I_0 was calculated as follows (with Z = 1 or 2)

$$\theta = \frac{\frac{I\ \mathrm{CO_Z}}{I\ ^{38}\mathrm{Ar}}}{\frac{I_0\ \mathrm{CO_Z}}{I_0\ ^{38}\mathrm{Ar}}} = \frac{I\ \mathrm{CO_Z} \cdot I_0\ ^{38}\mathrm{Ar}}{I\ ^{38}\mathrm{Ar} \cdot I_0\ \mathrm{CO_Z}} \tag{6.3}$$

Figure 6.2 shows the change of CO_2 and CO during a BE in relation to the starting values over a time of 8 hours for three different gas fluxes. The CO_2 signal increased as expected and at first the CO also decreased before at times over 6 h but due to the leakage of Nitrogen the mass 28 signal increased again. This effect is especially seen in the (1/2/13) and (4/2/9) gas setup.

For comparison with the BE the FTE data measured for two different gas fluxes is given in figure 6.3. In summary the batch reactor experiments are, due to leakage occurrence and long duration time, not useful for determination of the rate enhancement factor of the CO_2 generation. Therefore all experiments in the DBD reactor to obtain rate enhancement factors were performed in the flow-through mode.

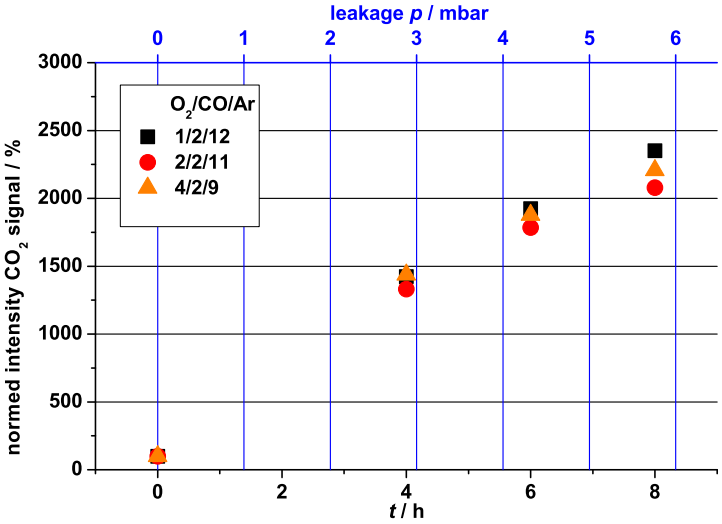

(a)

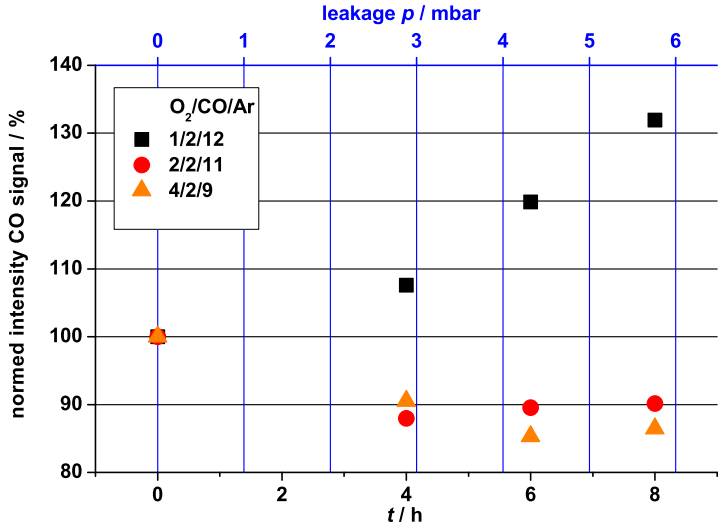

(b)

Figure 6.2: Both figures show the data measured from closed reactor experiments with O_2/CO/Ar gas flux (in sccm) of (1/2/12), (2/2/11), and (4/2/9). Figure a) gives the normed CO_2 and figure b) the normed CO intensities according to equation 6.3. The CO_2 signals show that small differences due to the gas setup occur. The CO normed intensities show for the (1/2/12) gas setup the influence of the leakage for low contents of reaction gases. The (2/2/11) and (4/2/9) gas setup with higher contents of O_2 and CO show the effect of the volume loss as discussed in section 6.1.2.

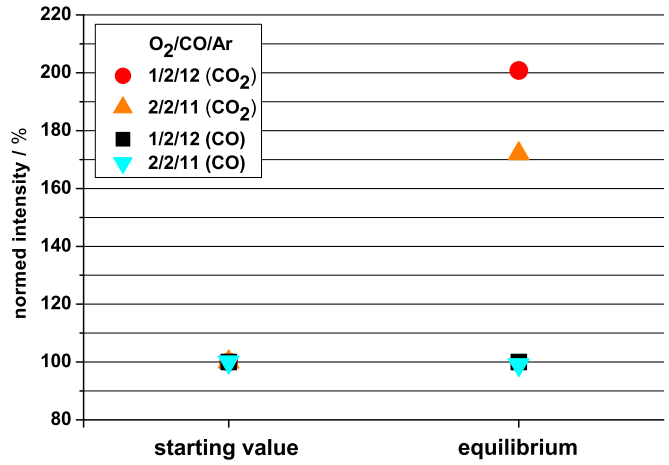

(a)

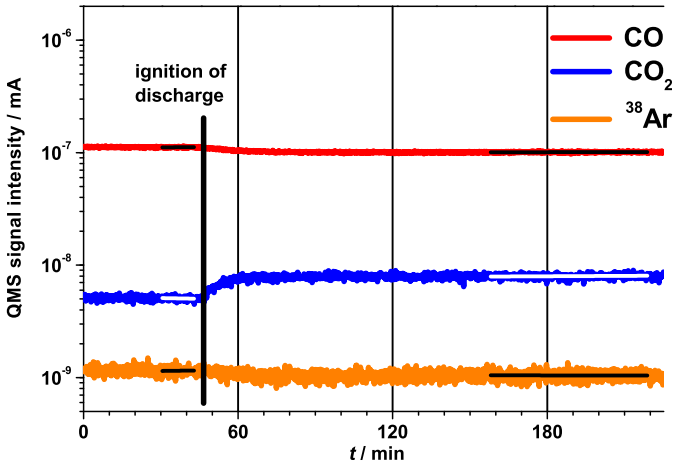

(b)

Figure 6.3: The figures show the obtained data of flow through reactor measurements. In figure a) the change of CO_2 respectively CO signal is given and in figure b) the recorded QMS data of the (2/2/11) gas setup with the fits for starting value (left side) and equilibrium (right side). In the flow through measurement the equilibrium rate is reached within 60 minutes and the leakage contamination is small enough that it is not detectable during measurements. In comparison to figure 6.2 the normed intensities of CO_2 and CO are reduced by factor 10 according to the 8 hour data. The access to the equilibrium rate nevertheless is also faster by a factor of 10.

6.2 Different Gas Composition Measurements.

As discussed before (section 6.1.2) the discharge can be ignited under gas mixtures with different fluxes of oxygen and carbon monoxide. The amount of the carrier gas argon was consecutively reduced and oxygen and carbon monoxide fluxes adapted. The flow-through rate of the gases was adjusted with a needle valve before the rotary vane pump to achieve constant pressure of 100.5($\pm$ 1.5) mbar for each gas mixture during the experiments. As a first experiment the ignition voltages of the different gas mixtures with uncoated fused silica dielectrics (Pt-X, with sample number X) were studied in respect to their frequency dependence.

For this purpose the voltage of the isolating transformer was slowly, manually increased until the OES signal of the discharge showed Ar lines in the spectra. With the isolating transformer voltages measured and the functions from table 6.3 the ignition voltages were calculated. The whole potential shift is the double of the amplitude. For easier comparison of the following data only the high voltage amplitude is compared. Figure 6.4(a) shows the measured ignition voltages of the different gas mixtures. It can be seen that the most influencing factor is the Ar flux. Additional fluxes of CO or O_2 increase the ignition voltages in a similar way as the (2/4/9) sccm and (4/2/9) sccm mixtures show.

The charging behavior of the AC generator for the dielectric plate system (as discussed in section 3.2) is also visible. Within these experiments no information could be obtained which gas mixtures cause problems in long term experiments. The ignition voltages were also determined for the reactive sputtered room temperature (71) YSZ coated dielectric base plates. In general the ignition voltages were higher in comparison to the measurements with uncoated dielectric plates, but the reproducibility of the measurements was bad. After several minutes of ignited discharge the ignition voltages were measured again and were up to 100 V lower then in the measurement with "cold" dielectric plates.

The dielectric constant of YSZ varies with increasing temperature [56, 122] and may be responsible for the reduced ignition voltages. Another possible explanation is that the YSZ surface is cleaned by plasma etching and therefore the ignition voltages are different. This effect is only observed with YSZ coated dielectric base plates. Figure 6.4(b) shows the ignition voltages of the "cold" YSZ coated dielectric plates (71) as measured.

With the data from the first ignition voltage experiments the 1000 Hz and 9000 Hz measurements were discarded and further rate enhancement coefficients obtained only in the range from 3000 Hz to 7000 Hz. First the uncoated base plates were investigated to measure the influence of the discharge at dif-

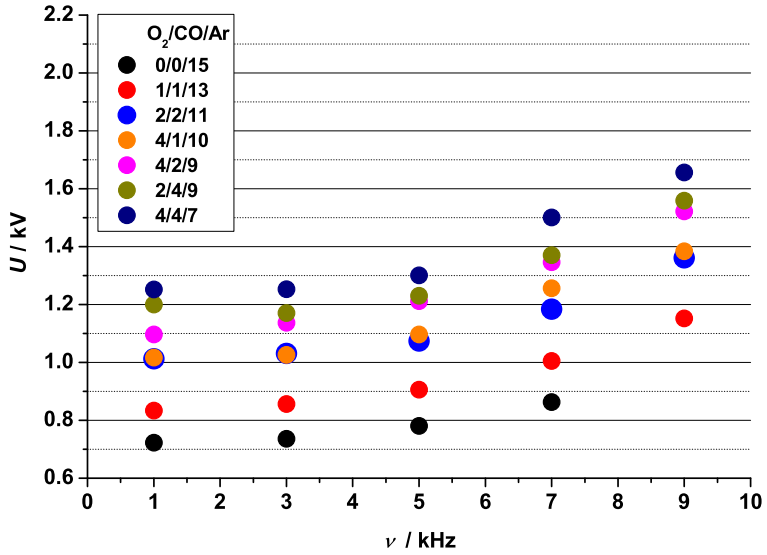

(a)

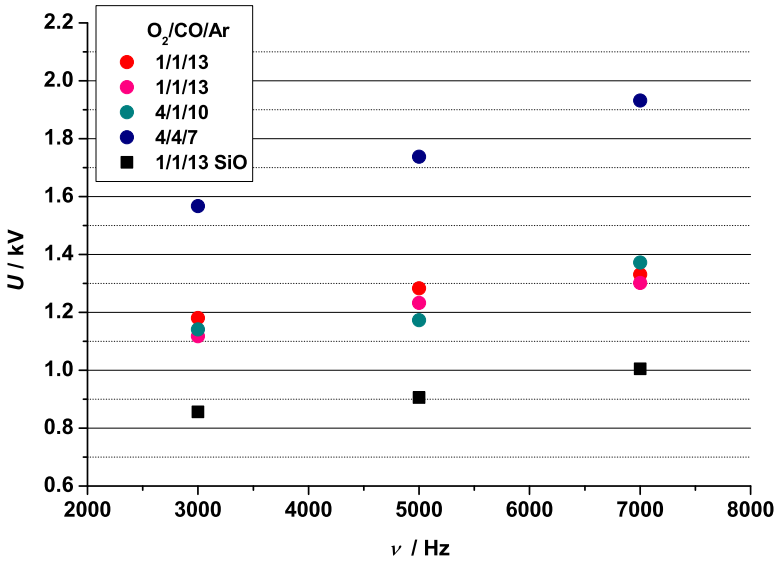

(b)

Figure 6.4: Both figures show ignition voltages of different gas mixtures used according to the frequencies ν used. All ignition voltages were measured at a pressure of 100.8($\pm$ 1.0) mbar. Figure a) shows the ignition voltages of uncoated base plates. The pure argon measurements were only performed till 7000 Hz. Figure b) shows ignition voltages of a few gas mixtures obtained with "cold" YSZ (71) coated dielectric plates. The ignition voltages are higher compared to the uncoated plates.

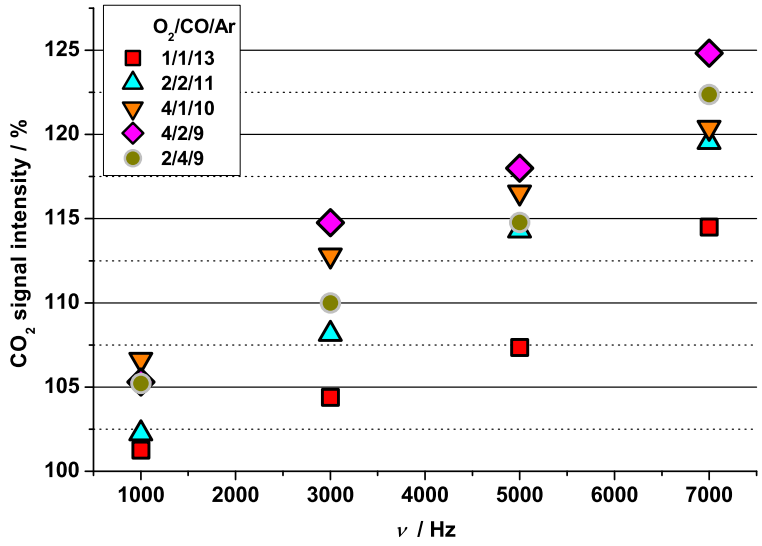

(a)

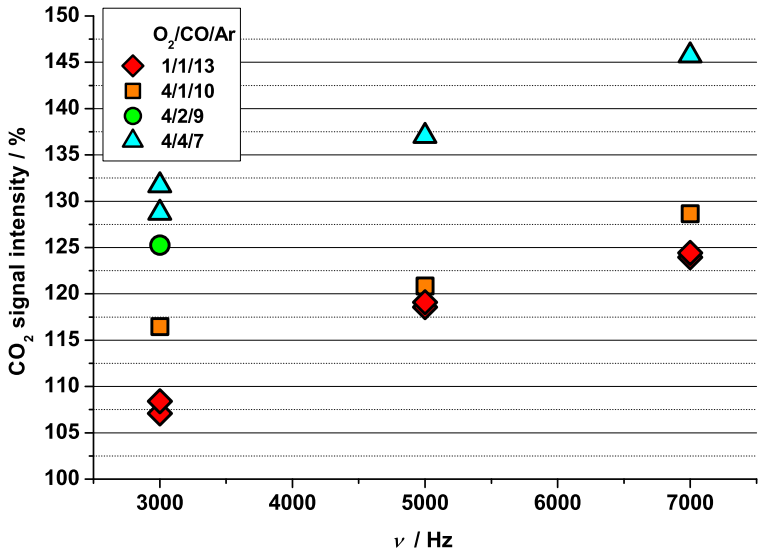

(b)

Figure 6.5: In figure a) the percentage increase of the CO_2 signal intensity can be seen that was measured after reaching the maximum rate enhancement during discharge ignition in correlation to the starting value. The data shown is from uncoated dielectric plates. Figure b) shows the percentage increase of the reactive room temperature sputtered YSZ coated dielectric plates (71) for several gas mixtures. The data is not normalized to the data from figure a).

ferent frequencies. The pressure in the flow through experiments was again adjusted with the needle valve and in the range of 100.8(± 1.0) mbar. Figure 6.5(a) shows the measured data of the CO_2 increase during the discharge from the equilibrium value at 100%.

It can be seen that a higher oxygen flux increases the CO_2 generation during discharge ignition and that higher frequencies lead to higher CO_2 generation rates as expected from Planck's equation. The same measurement with YSZ coated dielectric plates (71) is shown for several gas mixtures in figure 6.5(b). The nominal values of the CO_2 signal intensity increase are higher with the coated dielectric plates. The shown YSZ data is not normalized to the measurements from figure 6.5(a).

During the (4/2/9) measurement with the YSZ coating (71) the discharge began to flicker and the continuous glow discharge was no more present. After shutting down the discharge and opening the reactor a change of the coatings was observed. Investigations of the contamination were discussed earlier in this work in section 5.6. The results of the YSZ (71) base plates from figure 5.25 were that carbon and nickel contamination occurred on top of the deposited YSZ layer. As the 100% carbon monoxide discharge experiment showed higher contents of carbon monoxide in the gas mixture promote the deposition of carbon-nickel-films. Therefore in further experiments carbon monoxide fluxes greater than 2 sccm were not used. In the high temperature measurements the carbon monoxide flux used were therefore not greater than 1 sccm due to the increased deposition rate of contaminations at elevated temperatures.

In addition the base pressure for all experiments was increased to about 150 mbar to enhance the stability of the discharge and to reduce the free mean path of the molecules. The ignition voltages for uncoated base plates and YSZ high temperature deposition (58) were measured to compare with the data of the 100 mbar measurements. The 150 mbar data is shown in figure 6.6. Room temperature and high temperature measurements (discharge temperature of about 300 °C) are given in the graphics.

During the HT experiments all different YSZ films were investigated for the ignition voltages. Figure 6.7 shows the measured values for the three different (58 with □, 67 with ○ , 71 with △) deposited YSZ films at a discharge temperature of 300 °C.

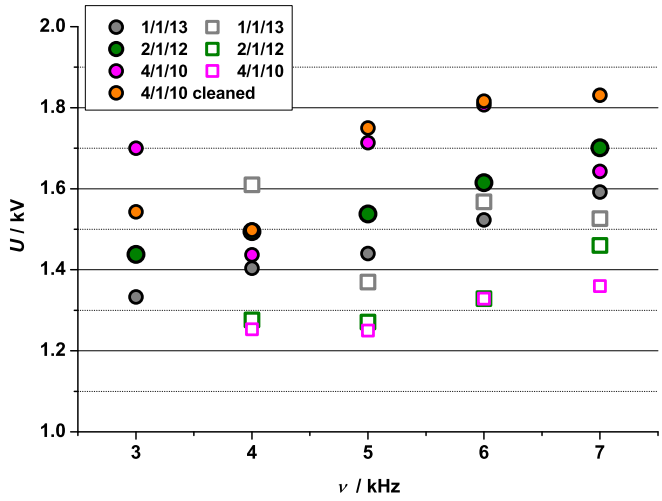

(a)

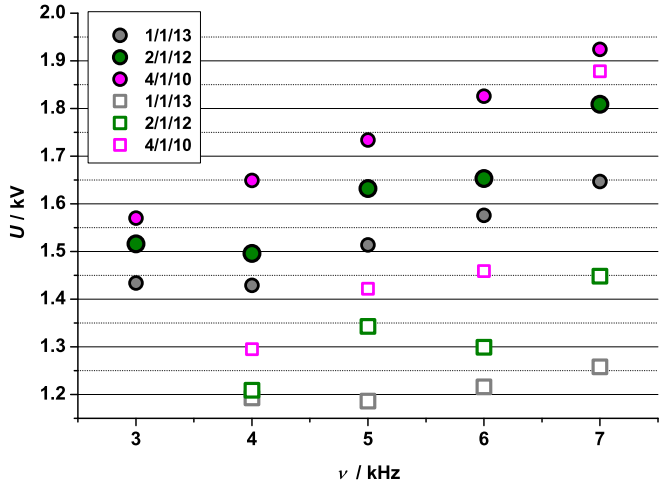

(b)

Figure 6.6: Figure a) shows the uncoated base plate ignition voltages for three different gas mixtures at room temperature (RT, presented by ○) and increased furnace temperature of 435 °C (HT, presented by □) which corresponds to a discharge temperature of about 300 °C. Additionally the difference for a new nitric acid cleaned base plate is shown by the example of the (4/1/10) gas flux setting. All measurements at RT were performed at a pressure of 151.5(± 1.5) mbar. The HT measurements were performed at a pressure of 155.0(± 0.6) mbar. Figure b) shows the ignition voltage determined for base plates coated with a high temperature YSZ film (58). The pressure in all measurements with YSZ coating was 153.0(± 2.5) mbar. (RT and HT marked as in figure a).

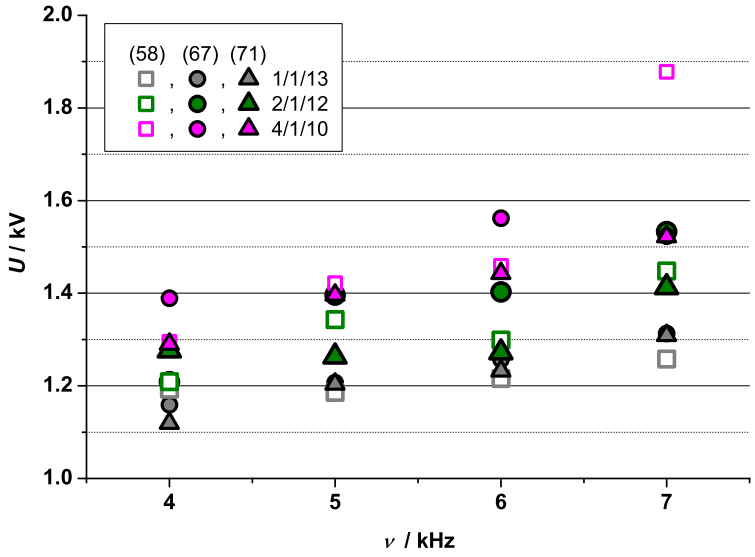

Figure 6.7: Measured ignition voltages for all deposited YSZ films (58, 67, 71) at a discharge temperature of 300 °C. Three different gas fluxes of O_2/CO/Ar were investigated: (1/1/13), (2/1/12), and (4/1/10) sccm. The ignition voltages are reduced according to the values recorded at room temperature with the deposited YSZ film (58).

6.3 CO_2 Measurements at Room Temperature

For the room temperature measurements the high temperature deposited YSZ coated (58) and purely fused silica base plates for reference purposes were used. Measurements were performed at pressures of about 150 mbar. Both dielectric systems (coated and uncoated) were tested with gas fluxes of O_2/CO/Ar of (1/1/13), (2/1/12) and (4/1/10) sccm. In addition the YSZ coated dielectric base plates were examined with (4/2/9) and (2/2/11) sccm gas fluxes. This two gas setups were discarded for the purely fused silica measurements due to the increased instability caused by higher Ni contamination because of the higher CO gas flux.

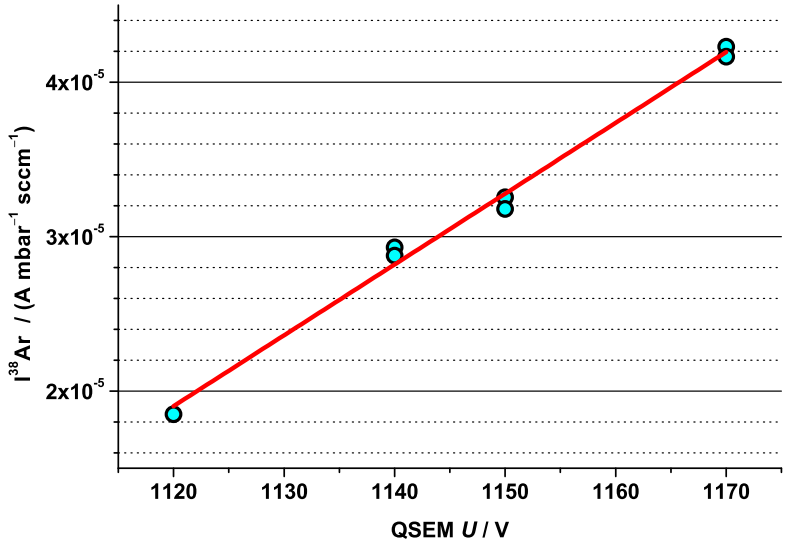

Figure 6.8: The figure shows the linear best fit function for the normalizing procedure of the QMS signals for the room temperature measurements. The linear function is given in equation 6.4.

The ^{38}Ar signal intensities per sccm for the investigated gas fluxes were plotted against the QMS Secondary Electron Multiplier (QSEM) adjusted voltages which gives a linear fit function to normalize the different measurements for better comparison. Figure 6.8 shows the measured data points and the best linear fit function which is given by the following numerical-value equation

$$I(^{38}\mathrm{Ar}) \cdot \frac{mbar \cdot sccm}{A} = 4.9 \cdot 10^{-4} \cdot U/V + 45.9 \cdot 10^{-4} \qquad (6.4)$$

with the adjusted QSEM voltage U in V the signal intensity of the normalized ^{38}Ar signal was calculated. The intensity increase per 10 V of QSEM voltage was calculated and the original data is multiplied with the amplification factor gained. All measured data was then compared to a QSEM voltage of 1170 V which was the highest through all measurements.

In the next subsections the normalized absolute values of different measurements are presented (6.3.1 and 6.3.2) and the catalytic (6.3.3) and the kinetic (6.3.5) behavior of the room temperature investigations shown.

6.3.1 (Reference) Measurements of Uncoated Fused Silica Base Plates

For the analysis of the catalytic activity of the YSZ films a reference has to be measured. In this work the purely fused silica dielectric base plates were taken as a reference. An ignited barrier discharge will lead to an increase of the CO_2 signal intensity even without a catalytic thin film coating. The increase of reaction rates in a plasma environment was discussed earlier in section 3. The influence of the discharge itself on the CO_2 generation was measured with different gas flux setups of (O_2/CO/Ar). Comparing the discharges of pure and coated dielectrics should eliminate the rate enhancement effect of the discharge and therefore give the real catalytic increase of the YSZ film.

Figure 6.9 shows the recorded data for all purely fused silica measurements performed. The gas setups tested (1/1/13), (2/1/12), and (4/1/10) showed higher absolute CO_2 generation at higher frequencies and higher oxygen gas fluxes. The greatest increase was measured with the (4/1/10) gas flux setup at 7 kHz. During the first (4/1/10) measurement discharge instabilities occurred. The dielectric base plates were then cleaned as mentioned earlier in section 5.6. After cleaning the (4/1/10) experiments were repeated and showed for the 3 kHz and 4 kHz measurement the same absolute CO_2 signal increase as the first measurement. Starting with 5 kHz all higher frequencies showed higher values of CO_2 than the first measurements before cleaning.

To investigate whether this was a measurement error or an indication for a discharge surface interaction which leads to a higher CO_2 conversion rate the 3 kHz and 4 kHz experiment were repeated. The recorded data was higher than the first measurement with the cleaned fused silica base plates. The signal increase of both measurements lay at about 10% to 13% which is also the same percentage increase as with the cleaned plates and the first (4/1/10) measurement. As mentioned before a Ni contamination might influence the catalytic properties of a YSZ coated dielectric but also a small contamination

of pure fused silica plates can be imagined to have an influence on the CO_2 generation rate. This might be the explanation for the higher CO_2 values after cleaning during the measurement. The continuous use of the dielectrics during the (1/1/13), (2/1/12), and (4/1/10) experiments might lead to a Ni contamination which is too high to have a good catalytic influence, and therefore the reduced intensities in the first (4/1/10) measurements can be explained. A final explanation of this behavior needs further research on this special effect observed.

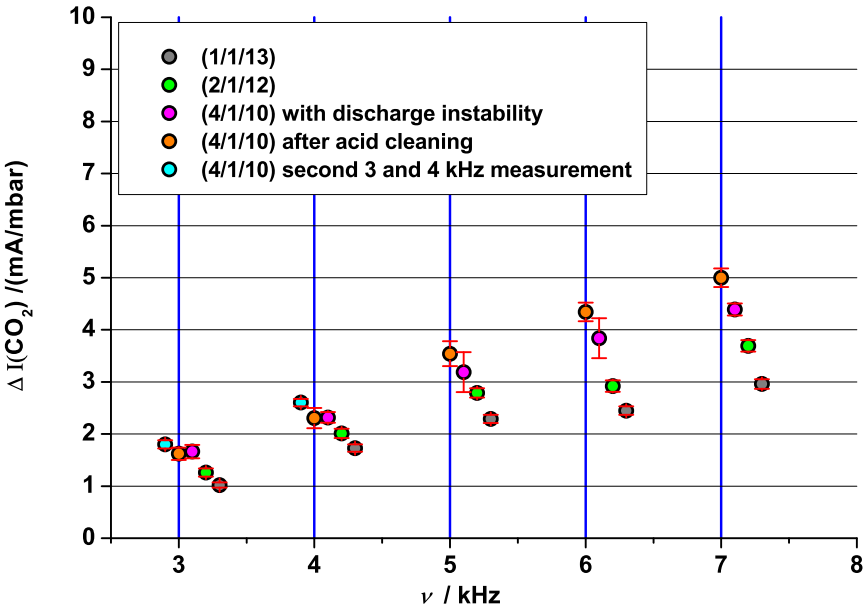

Figure 6.9: The figure shows the measured data of purely fused silica dielectric plates. Three different gas fluxes of (O_2/CO/Ar) were chosen for experimental investigation ((1/1/13), (2/1/12) and (4/1/10) in this order). For better comparison the different gas fluxes were shifted in the x scale. The frequencies used in the discharge experiments are marked with blue lines. During the (4/1/10) measurement (marked with magenta) discharge instabilities occurred. After this measurements the base plates were cleaned with nitric acid and then repeated. The recorded data is marked with orange. After the 7 kHz measurement the 3 kHz and 4 kHz experiment were repeated. This data is marked with blue.

6.3.2 Measurements of Fused Silica Base Plates Coated with YSZ Film

For the determination of the catalytic activity the experiments described in the previous section 6.3.1 were repeated (gas setups of ((1/1/13), (2/1/12), and (4/1/10)) with the coated dielectrics. In addition two additional gas mixtures (4/2/9) and (2/2/11) were investigated. The YSZ film used in this experiments was the high temperature YSZ deposition (58). Figure 6.10 shows the absolute values of the CO_2 signal intensity increase.

All recorded data showed higher absolute values at higher frequencies. The absolute signal increase was higher than that seen with the purely fused silica base plates. Similar absolute values were measured for the (1/1/13) and the (2/1/12) gas fluxes which is not fully understood, yet. The other gas mixtures showed higher absolute values than the (1/1/13) gas mixture, therefore the discharge investigations of the (2/1/12) gas flux setup seemed to be systematically too low.

A possible explanation might be a higher Ni surface contamination as during the other experiments which caused a less active YSZ surface area. After the 7 kHz measurement of the (1/1/13) and (2/1/12) gas mixtures the 3 kHz measurement was repeated. In both cases higher absolute values were measured. In the case of the (1/1/13) gas setup it seems that a kind of YSZ film activation has happened. The recorded 5 kHZ data showed a greater increase in the absolute value as should be expected from the previous measurements at lower frequencies.

The higher CO_2 intensity of the second 3 kHz measurement fits well in this theory. This can even better be seen in figure 6.11 of the catalytic rate enhancement. The second 3 kHz experiment with the (2/1/12) gas mixture showed only an increase in the range of the statistical error of the first measurement and therefore in all other gas mixture the 3 kHz experiment was not repeated. Figure 6.11 on the other hand indicates that there might also be some kind of surface activation during the experimental series of the (2/1/12) gas flux experiments.

6.3.3 Catalytic Rate Enhancement of YSZ Film Coating at Room Temperature

The experiments with the dielectric base plates with a YSZ coating sputtered at room temperature (non-reactive (67) and reactive (71)) helped to determine the experimental settings for the high temperature YSZ film deposited base plates (58). Measurements were performed within the frequency range from 3000 Hz to 7000 Hz. Starting with a (O_2/CO/Ar) gas flux setting of

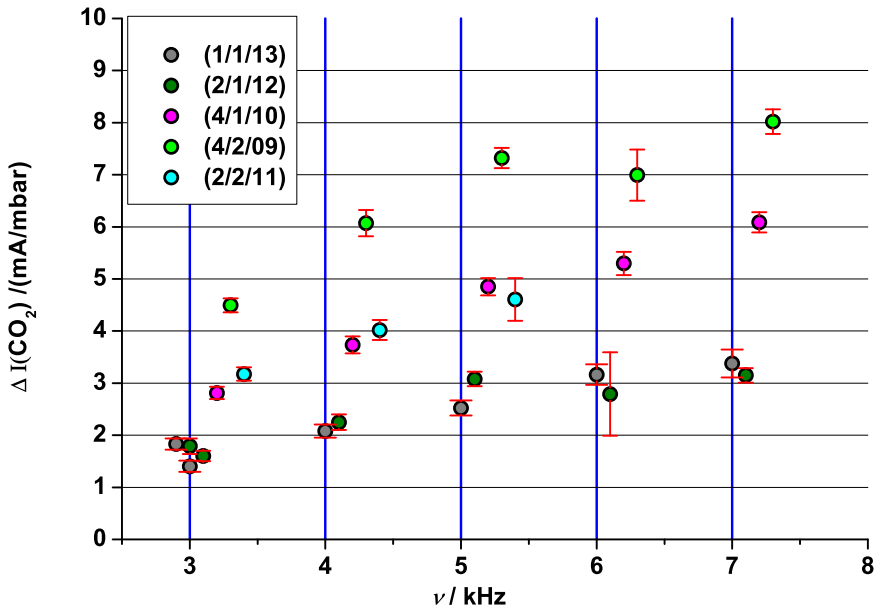

Figure 6.10: The figure shows the measured data of YSZ coated purely fused silica dielectric plates. The investigated thin film coating used in these experiments was the high temperature YSZ film deposition (58). Five different gas fluxes of (O_2/CO/Ar) were investigated ((1/1/13), (2/1/12), (4/1/10), (4/2/09), and (2/2/11) in this order). For better comparison the different gas fluxes were shifted in the x scale. The frequencies used are marked with blue lines. During the (2/2/11) measurements (marked with blue) discharge instabilities occurred, therefore the 6 kHz and 7 kHz measurements were discarded. After the 7 kHz measurement of the (1/1/13) and (2/1/12) gas flux setups the 3 kHz measurements were repeated.

(1/1/13) sccm the oxygen flux was increased to 2 sccm and 4 sccm with a respectively decreased ar gas flux. The CO gas flux was hold constant at 1 sccm. Reducing atmospheres with higher carbon monoxide gas fluxes were discarded as mentioned before.

For the catalytic rate enhancement analysis it was necessary to subtract the effect of the discharge itself for the investigation of the catalytic behavior of the YSZ thin film. This can be easily performed by dividing the measured values of the coated dielectric by those of the purely fused silica dielectric. The result is a rate enhancement factor R in % as described in section 4.1. The calculated values are shown in figure 6.11 for the gas fluxes of (1/1/13), (2/1/12), and (4/1/10) (the last gas flux setup after cleaning series) for all frequencies examined between 3 kHz and 7 kHz. The rate enhancement factor is for all investigated gas fluxes higher at lower frequencies. The repeated 3 kHz measurement (after the 7 kHz measurement) off all gas fluxes and the second 4 kHz measurement of the (4/1/10) gas setup showed higher rate enhancement factors than the first investigations.

It seems that during the discharge an activation of the film surface happened which leads to higher CO_2 conversion rates. The rates of the (2/1/12) gas flux mixture seemed to be systematically to low. The possibility of intense Ni contamination on the YSZ surface film which was mentioned already in the case of the lower CO_2 signal intensities of the (4/1/10) measurements and the occurring instability of the discharge (see figure 6.9) might be responsible for the observed behavior. Before the (2/1/12) measurement no additional cleaning of the base plates was performed therefore This might be responsible for the lower catalytic rate enhancement activity that was recorded. Only the 6 kHz and the 7 kHz measurements of the (2/1/12) gas flux setting have a value of R below 100%.

6.3.4 Influences of Different Frequencies

As mentioned before in section 6.1.3 the power input of the discharge and therefore the energy accessible for the oxidation reaction should follow Planck's law (equation 6.2). The frequency dependent conversion rate should be of the same value in uncoated and coated dielectric base plate systems. As an example figure 6.12 shows by the (4/1/10) gas flux experiment gained data for both discharge systems (SiO_2 and YSZ) the absolute values of the CO_2 signal increase and the linear fits of the measured data.

For the YSZ data set the 5 kHz measurement point was neglected for the linear fit calculation. Both linear fits give a slope of $(8.19(\pm 0.19)\cdot 10^{-7})$. The both other investigated gas flux setups (2/1/12) and (1/1/13) showed a similar behavior, nevertheless the slopes of the different experimental systems

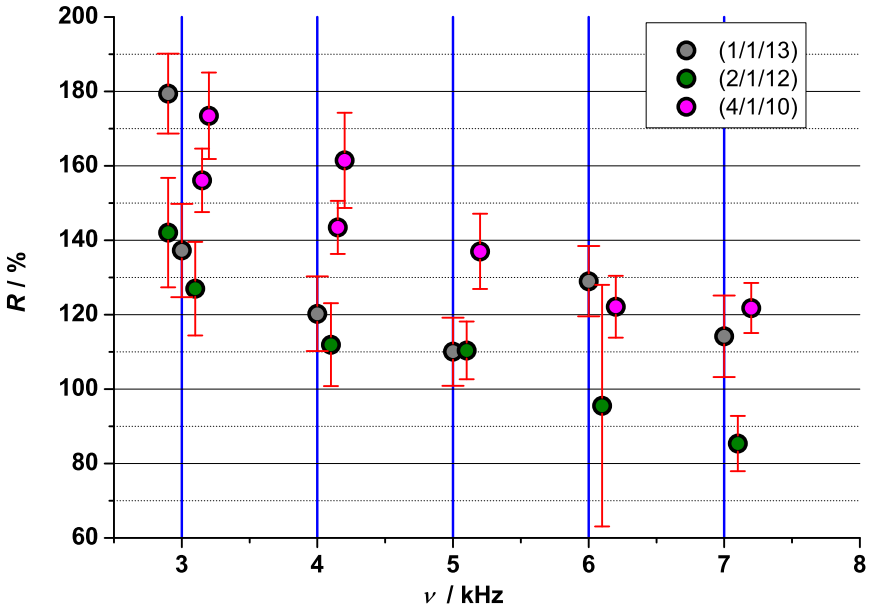

Figure 6.11: The figure shows the calculated values for R for three different gas fluxes. All gas mixtures show higher catalytic activity at lower frequencies and catalytic rate enhancements greater than 100% except of the last two frequencies of the (2/1/12) gas flux measurements. As mentioned in the text the higher values of R correspond to measurements of lower frequencies after the 7 kHz experiments. A value of R of 100 % means that the increase of the CO_2 signal is the same with uncoated fused silica base plates and with YSZ coated dielectrics. For better comparison the different gas fluxes were shifted in the x scale. The frequencies used are marked with blue lines.

were not as close as the ones of the (4/1/10), but within the range of the error. The data of all fits with the accordant errors of the slopes is given in table 6.4. The data show that the slope is higher for discharges with higher amount of oxygen.

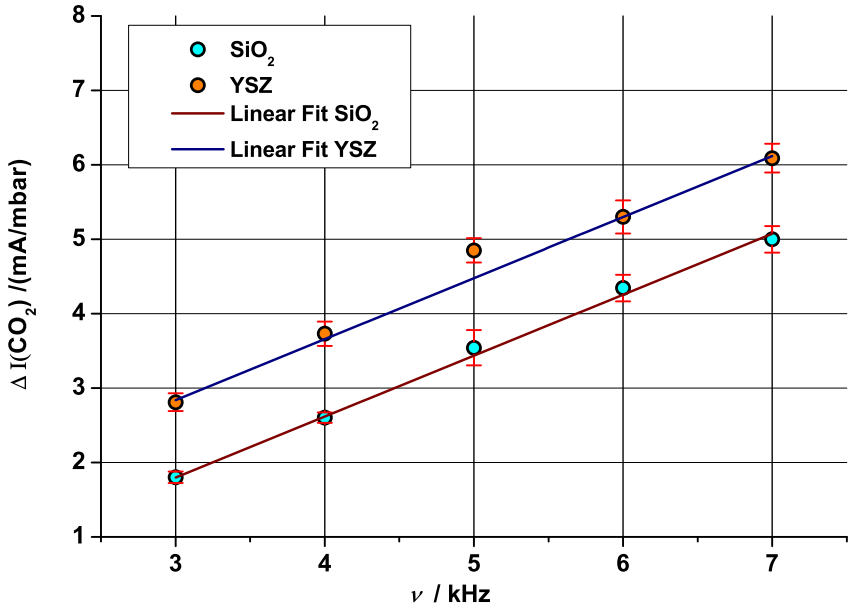

Figure 6.12: The figure shows for the (4/1/10) gas flux experiments with both discharge systems (SiO_2 and YSZ) the linear fits of the measured data for the frequency dependent factor calculation. The slope of both fits can be determined as $8.19(\pm 0.19)\cdot 10^{-7}$.

6.3.5 Kinetic Behavior at Room Temperature

For heterogeneous catalysis different kinetic models exist which differ in the reaction route of the gas molecules or atoms. In the so called Langmuir-Hinshelwood-Mechanism both reactants are adsorbed at the catalyst surface and trough surface diffusion the reaction finally starts and in the end the desorption of the product follows. In the Eley-Rideal-Mechanism only one of the precursor adsorbs at the surface. The second precursor reacts with the adsorbed first precursor to the product. After the reaction the desorption of the product takes place. Another possible mechanism in the case of YSZ is the Mars-van-Krevelen-Mechanism. Here the first precursor adsorbs at the surface of the catalyst and then it is oxidized by a lattice oxygen. After this

gas flux setting	system	slope $/10^{-7}$	error $/10^{-7}$
(1/1/13)	YSZ (58)	4.06	($\pm$0.42)
(1/1/13)	SiO_2	3.87	($\pm$0.54)
(2/1/12)	YSZ (58)	6.49	($\pm$1.04)
(2/1/12)	SiO_2	5.92	($\pm$0.64)
(4/1/10)	YSZ (58)	8.19	($\pm$0.19)
(4/1/10)	SiO_2	8.19	($\pm$0.19)

Table 6.4: Obtained values of the slopes of all linear fits of the YSZ high temperature deposition coating (58) and the uncoated SiO_2 dielectric base plates for the frequency dependent influence of the discharge at room temperature. The values of the slopes increase with increasing content of oxygen in the discharge.

the desorption of the product leads to an oxygen vacancy which is afterwards again substituted with oxygen.

From the carbon monoxide oxidation at a platin catalyst it is known that this reaction follows the Langmuir-Hinshelwood-Mechanism. For the plasma assisted heterogeneous catalysis used in this work it is conceivable that a different mechanism is responsible for the CO oxidation due to the different experimental setup of the catalytic reactor. The different slopes of the linear fits obtained for the Planck energy coupling calculation performed in the last section 6.3.4 show that differences according to the partial pressures of oxygen inside the discharge occur. Therefore further analysis is needed. In addition also the change of the partial pressure of CO is investigated.

For the kinetic behavior in discharges investigated at room temperature the measurement data of the YSZ coated (high temperature deposition (58)) dielectric base plates was taken and an analysis of the concentrations of the precursors CO and O_2 in correlation to the absolute increase of the CO_2 signal intensity of the QMS measurements. Figure 6.13 shows the correlation between partial pressure of oxygen in the discharge and the increase of the CO_2 signal intensity in the QMS. The pressure of the CO gas was constant at about 10.3($\pm$0.1) mbar in all measurements.

As already presented in figure 6.10 the data of the (2/1/12) gas flux setting (which corresponds to the around 20 mbar values) showed very low intensity increases, especially the catalytic rate enhancement factors in figure 6.11 were below 100% which was not observed with any other gas flux setting in the case of coated dielectrics. Therefore a systematically error cannot be excluded. The best data in figure 6.13 is the 5 kHz discharge ignition data set, which shows a nearly linear increase with higher oxygen content. The

same analysis was performed for the partial pressure of CO in the discharge with the data of the (4/2/09) and (4/1/10) gas flux settings. The analysis is shown in figure 6.13. Here the partial oxygen pressure was constant at about 40.7($\pm$0.15) mbar in all measurements. For a good kinetic model the data base is too low to conclude a mechanism.

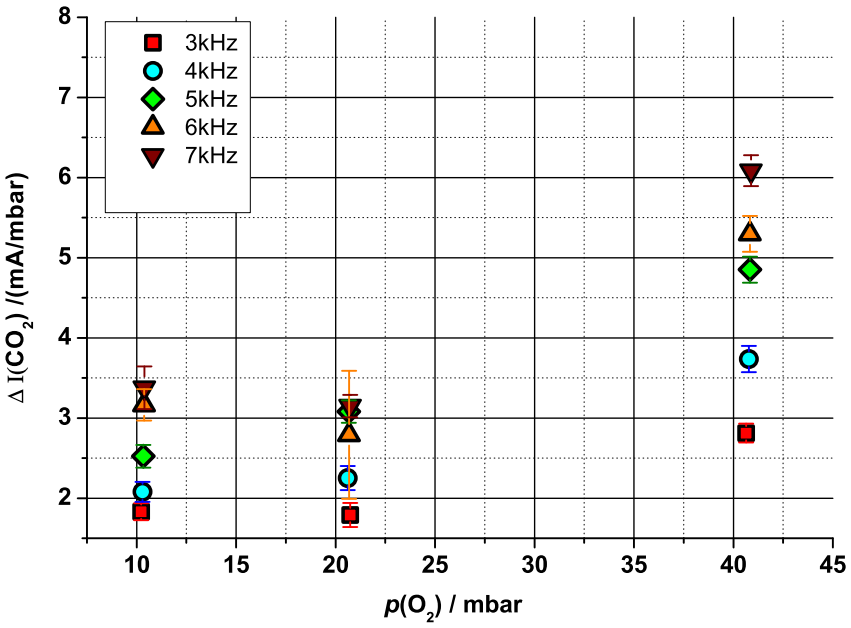

Figure 6.13: The graphics show the absolute increase of the CO_2 signal intensity correlated with the partial oxygen pressure of the discharge. The overview shows the data for all investigated frequencies. The best data is the one of the 5 kHz measurements. Here a nearly linear increase with higher oxygen content could be observed.

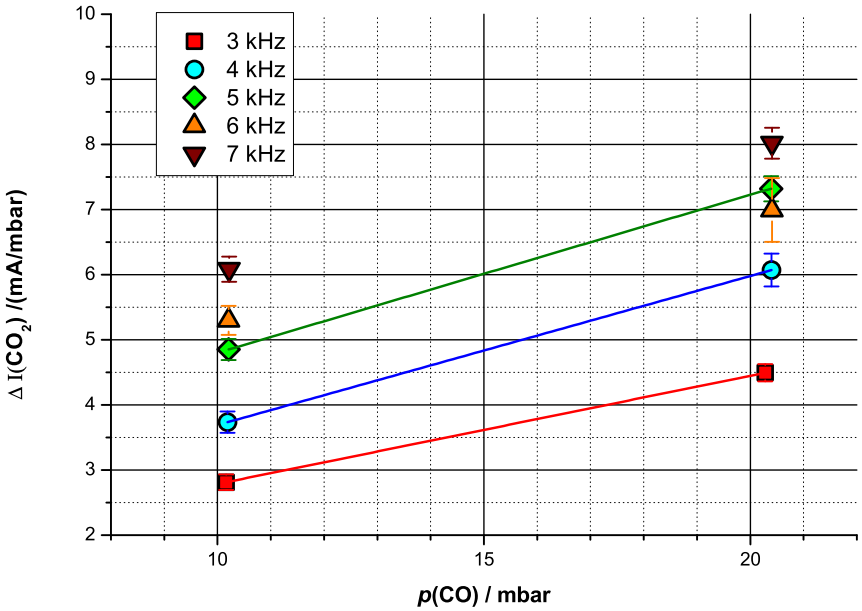

Figure 6.14: The graphics show the absolute increase of the CO_2 signal intensity correlated with the partial carbon monoxide pressure of the discharge. The overview shows the data for all investigated frequencies. Here the 6 kHz and 7 kHz data for the higher CO partial pressure has to be taken with care, because the recorded data of the (4/2/09) measurement seems to be statistically to low. The printed connection lines for the data of the lower frequencies show in good agreement similar increases if the partial pressure is doubled. Therefore this should be also suspected for the higher frequencies.

6.4 CO_2 Measurements at Elevated Temperature

The ionic conductivity of YSZ follows, as explained in section 3.4 an exponential law which is strongly correlated with the temperature of the ceramic material. As the oxygen conduction through the YSZ anion lattice is also a thermally activated process a minimum temperature for sufficient ionic conductivity is required. In the case of YSZ the ionic conductivity is at around 300 °C high enough for a large variety of applications. For the high temperature discharge experiments therefore a temperature of about 300 °C has to be achieved inside the furnace. As shown earlier in section 5.5.4 this aim was achieved with the heaters. In all FTE the heaters were set to 435 °C which corresponds to a temperature of 300 °C in the discharge zone.

6.4.1 (Reference) Measurements of Pure Fused Silica Base Plates

The room temperature measurements showed that the CO_2 signal intensity increase in the QMS is different according to the dielectric base plates used. For the high temperature measurements similar effects could be expected on basis of a theoretical expectation. For the high temperature measurements the experiments were performed with gas fluxes of (O_2/CO/Ar) of (4/1/10), (2/1/12), and (1/1/13). It was found during the experiments that it was better to start with greater oxygen gas flux due to the Ni contamination during the discharge experiments. Although much better discharge stability was observed at elevated temperatures the decomposition of the nickel tetra carbonyl lead to small surface contamination especially with the (1/1/13) gas flux setup.

Figure 6.15 shows the measured data of the uncoated fused silica base plates with the gas fluxes used. It can be seen that the increase of the CO_2 signal intensity is more than 1 magnitude lower than at room temperature. Additionally the increase of all gas fluxes seems to be in the same absolute magnitude. The data points shown are the average values of the recorded CO_2 signal. The error bars show that the QMS signal fluctuates around the average value.

The fused silica base plate values should be used as a reference data set, but, as it can be seen in the next section 6.4.2, the differences of the data recorded with the base plates with YSZ thin film coating were in the same order of magnitude, therefore a comparison to reference values was neglected. Taken the error of all measurements into account there is no significance of

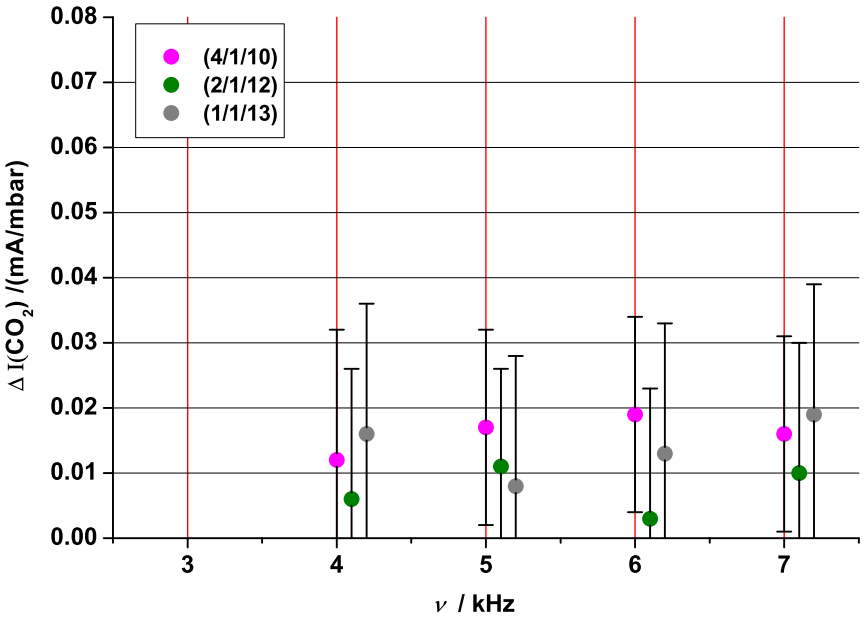

Figure 6.15: Measured data for all gas fluxes used with pure fused silica base plates ((4/1/10), (2/1/12), (1/1/13)) are shown in the graphics. The error bars indicate the fluctuations of the absolute values. The data points are the average absolute values of the measurements. It can be seen that all gas fluxes nearly have the same signal increase and that there is no frequency dependence. For better comparison the different gas fluxes were shifted in the x scale. All measurements were taken at the same frequencies as the (4/1/10) gas flux setup.

the comparison of this data.

6.4.2 Measurements with YSZ Thin Film Coated Fused Silica Base Plates

Three figures show the recorded data of the gas fluxes used. For direct comparison of all measurement data the absolute values of the fused silica base plates are also shown in each figure. First figure 6.16 shows that the low temperature deposited YSZ films (67) and (71) are catalytically more active and lead to higher absolute signal intensities increase. For this both film sets the error of the data is unfortunately higher than for the high temperature deposited YSZ film (58) or for the pure fused silica.

Similar behavior can be seen in figure 6.17 for the second gas flux setup. In both measurements the YSZ coated base plates seem to show a small frequency dependency. For the last measurement in figure 6.18 this behavior was not observed. The (1/1/13) gas flux setup showed for all dielectric systems nearly the same absolute values. This lead to the assumption that here a catalytic enhancement does not take place and the absolute CO_2 value increase is only depending on the discharge influence itself. To check whether this might be a closer look on the CO_2 signal intensity according to the furnace temperature is necessary. The correlated measurements are shown in the next section 6.4.3.

6.4.3 Temperature Dependent CO_2 Signal Intensity Measurements

Measurements were started at 435°C and then a temperature ramp of 1°C per minute was started, which led to a duration of 6:55 hours until room temperature (20°C) was reached. Then for at least 1:30 hours temperature was held constant at 20°C till the CO_2 signal intensity was at a constant value. After this the same temperature ramp with a duration of 6:55 hours was used to heat the whole system again to the starting value of 435°C.

Again it was waited until the CO_2 signal intensity was at equilibrium. This temperature profile was repeated without ignited discharge and with an applied voltage just below the ignition voltage of the discharge to find out whether there are influences of the alternating potentials even if no discharge is ignited. In some measurements the assigned voltage at elevated temperatures was not sufficient to sustain the discharge at room temperature with the wider gap distance, for description see section 5.5.4.

With a small adjustment of the applied voltage it was possible to ignite

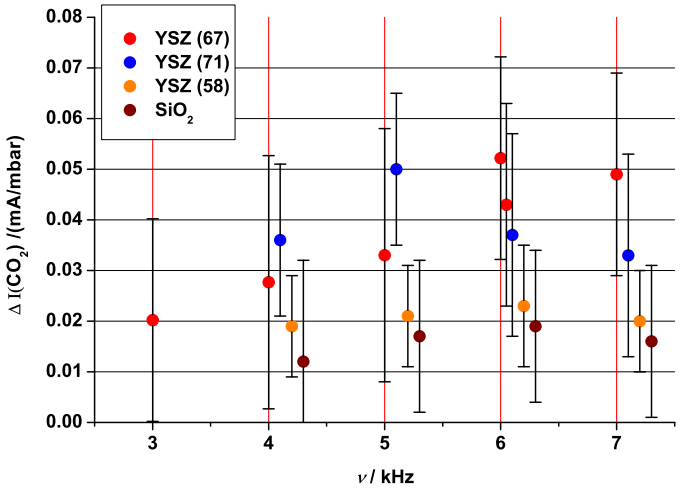

Figure 6.16: The figure shows the CO_2 signal increase measured at elevated discharge temperature of 300 °C with all deposited YSZ films (67), (71), and (58) in correlation with the purely fused silica base plates. Here the data for the (4/1/10) gas flux is given in the following figure 6.17 the (2/1/12) gas flux and in figure 6.18 the (1/1/13) gas flux data is shown. The absolute values of all measurements are in a small range compared to the room temperature measurements. The highest increases of the CO_2 signal can be found with the (4/1/10) gas flux. The high temperature deposited YSZ film "58" shows only small CO_2 increase in all gas compositions. For better comparison of the frequency-dependent data the values of different dielectric plates were shifted in the x-scale.

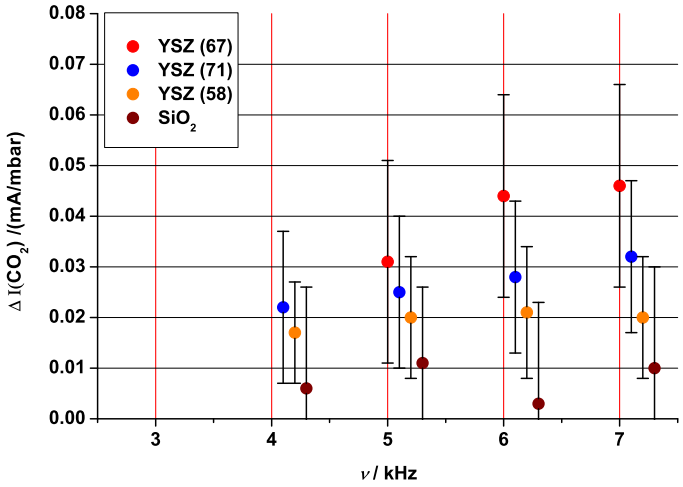

Figure 6.17: The figure shows the CO_2 signal increase measured at elevated discharge temperature of 300 °C with all deposited YSZ films (67), (71), and (58) in correlation with the purely fused silica base plates. Here the data for the (2/1/12) gas flux is given. The complete data was already interpreted in the caption of figure 6.16. For better comparison of the frequency-dependent data the values of different dielectric plates were shifted in the x-scale.

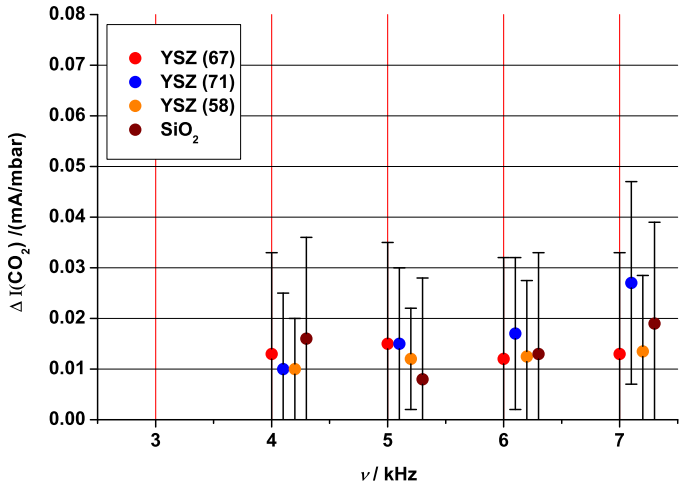

Figure 6.18: The figure shows the CO_2 signal increase measured at elevated discharge temperature of 300 °C with all deposited YSZ films (67), (71), and (58) in correlation with the purely fused silica base plates. Here the data for the (1/1/13) gas flux is given. The complete data was already interpreted in the caption of figure 6.16. For better comparison of the frequency-dependent data the values of different dielectric plates were shifted in the x-scale.

the discharge again. One exemplary measurement with the (1/1/13) sccm gas flux setup with YSZ deposited (reactive sputtered room temperature (71)) dielectric base plates is shown in figure 6.19. The figure shows an overlay of the three different measurements and the used furnace temperature profile. In addition the designated temperature profile of the temperature between the base plates was also calculated. The heat transfer should take some extra time even with the slow temperature ramp of 1°C per minute, therefore this profile is an estimation of the real values at a given furnace temperature.

Two black bars indicate the temperature of strongly increasing CO_2 conversion rate. This generates a temperature range between 180°C and 210°C when the decrease respectively increase of the CO_2 signal intensity takes place. The lower temperature is from the cooling down ramp which seems reasonable. Processes that work at higher temperatures can mostly sustain longer even at temperature that are to low for the normal process temperature. The higher temperature of the range is from the heating ramp, which seems also correct. A higher necessary ignition temperature of a process is often seen, because chemical activation energies first hinder the reaction before enough energy is available to start the process and overcome the activation energy value. For further discussion the point of increased conversion will be set to 200°C what should be a good estimated value. Investigations with the two other gas flux settings used for high temperature investigation showed the same kind of CO_2 signal progress during the temperature ramp experiments.

To clarify whether this strong increase is related to the YSZ coating of the dielectrics the same measurement was performed with uncoated fused silica dielectrics with the (1/1/13) gas flux setup. The data of this investigation is shown in figure 6.20 and compared to the already shown YSZ coated dielectrics. It can be seen that the general progress of the temperature profile seems to be very similar whatever dielectric base plates are used. Although the YSZ related temperature profile is higher at elevated temperatures a direct influence of the YSZ coating can only be seen at room temperature, where the YSZ coated dielectrics show a significant higher CO_2 signal intensity.

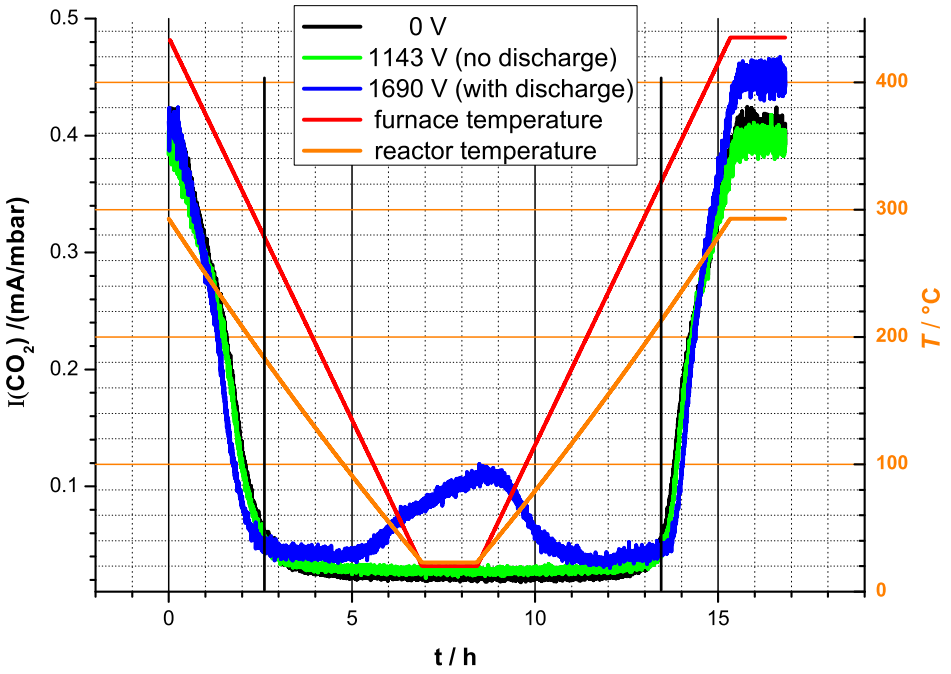

Figure 6.19: The figure shows the temperature profile of the (1/1/13) gas flux setup which was used with the different applied voltages as described in the text. In addition the calculated reactor temperature profile from the data of figure 5.22 is also shown in the graphics. Two black bars mark the temperature when the CO_2 signal intensity decreases respectively increases rapidly. In the cooling down cycle this corresponds with a reactor temperature of about 180°C and in the heating up cycle of about 210°C. At room temperature the measurement with discharge ignited showed increasing CO_2 intensity as it was expected from room temperature measurements. The minima at around 150°C reactor temperature of the CO_2 signal need to be further researched. A simple explanation for this behavior can actually not be given. An applied voltage below the ignition voltage seems to have no influence of the CO_2 signal intensity.

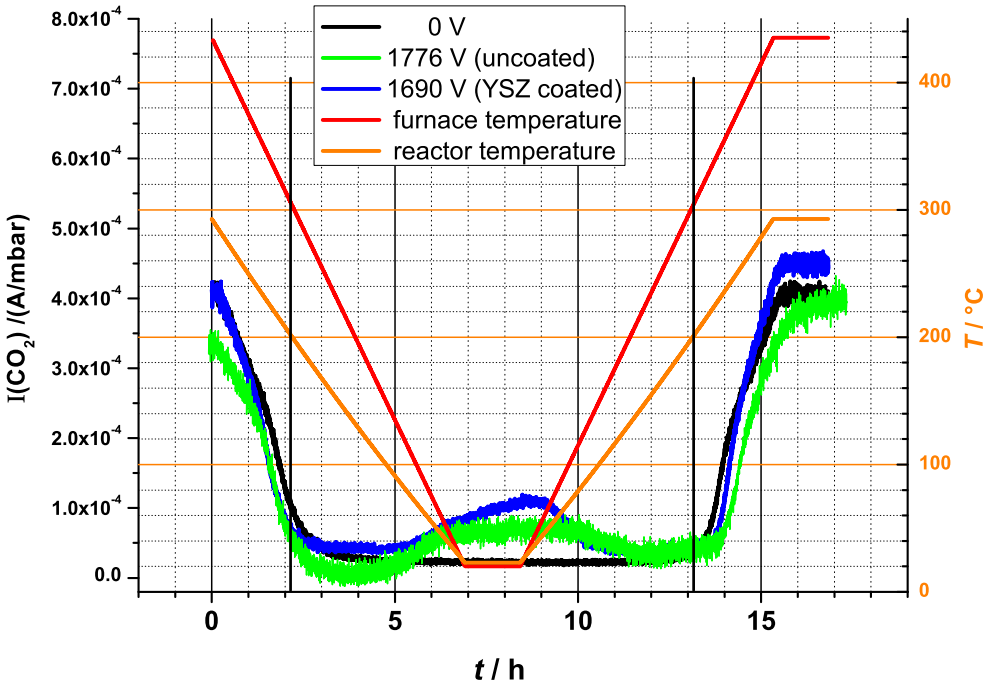

Figure 6.20: The figure shows the temperature profile of the YSZ coated dielectrics from figure 6.19 and the profile of uncoated fused silica dielectric as reference measurement. The reference discharge was investigated at a slightly higher applied voltage. The QMS data is normalized to the YSZ coated measurement and time profile. In addition again the furnace temperature and the calculated discharge temperature as already shown in figure 6.19 are plotted again. Two black bars indicate a discharge temperature of about 200°C.

6.5 Optical Emission Spectroscopy (OES) Measurements

As introduced before in section 3.6 OES is an in situ technique to monitor the excited and ionized molecules and ions in a gas discharge. OES has the drawback to detect only positively charged molecules and ions. The direct detection of the negatively charged oxygen ions O^- is not necessary as long the key focus lies on the reaction rate enhancement of the CO_2 generation. The reaction product carbon dioxide usually is positively charged.

OES here works as a monitoring tool right at the discharge area with the possibility to check whether the signal intensities in the quadrupol mass spectrometer (QMS) are real signals from the discharge or whether other influences for example from the capillary system caused an increase of the CO_2 signal. If the QMS data can be confirmed by the OES measurements a real signal increase and therefore real catalytic enhancement was detected.

For a correct assignment of the measured wavelengths the used SP2500i had to be calibrated according to the dispersion of the used grating. An easy way to get the dispersion is by experimental measurement and calculation of the dispersion with linear regression. To obtain the linear dispersion for all wavelengths different known emission lines had to be measured at different center wavelengths λ_C (which are the wavelengths that are assigned to the middle of the CCD chip) of the spectrograph. The CCD channels of each known emission line was recorded in correlation to the chosen λ_C, then a linear regression was performed to get the dispersion factor for each single emission line. From all dispersion factors of different wavelengths a linear regression gives the wavelength correlated dispersion, which was used to recalculate the measured OES signals into the correct wavelengths.

For the dispersion calculation in this work the following emission lines given in table 6.5 according to the named sources of light were taken.

light source	λ/nm	λ/nm	λ/nm	λ/nm	λ/nm
Hg neon light	404.66	435.83	546,07	576.96	579.07
Argon plasma	696.54	763.51	772.38	826.45	
Oxygen plasma	777.19	844.64			

Table 6.5: Emission lines used for the calculation of the wavelength dependent dispersion factor.

Taking the size of the CCD chip into account the wavelength dispersion can be calculated in nm/mm for a specific λ_C:

$$\frac{d\lambda}{dx} / \left(\frac{nm}{mm}\right) = \left(13,44(\pm 0,03) - 2,38(\pm 0,41) \cdot 10^{-4} \cdot \lambda_C\right) / \left(\frac{nm}{mm}\right) \quad (6.5)$$

A detailed description of the procedure to get the dispersion factors with experimental measurements was given earlier in [116]. All OES investigations performed were used to check the data measured by the QMS system for irregularities or systematical errors. Especially the parameters gas flux, frequency and temperature could be differentiated with the measured emission spectra. All spectra which are shown in the following sections were recorded at pressures around 150 mbar operating gas pressure. The influences of the different mentioned parameters are shown and discussed. The gas flux compositions are always given in the order of (O_2/CO/Ar).

6.5.1 OES at Room Temperature

Within the room temperature OES the differences of different frequencies and gas flux compositions were investigated. In general emission lines of excited atoms correspond to greater wavelengths due to the lower energy difference of the electron levels engaged. Ionic species can be found at shorter wavelengths below 650 nm. The intensity of the ionic emission lines is very low depending on the small ionization level of low temperature discharges. The emission lines above 650 nm were mostly 10 to 1000 times higher in intensity. Theses atomic emission lines are in the case of molecules present in the discharge often superposed by band spectra.

A spectra overview for different gas compositions at relatively high pressures around 500 mbar and high frequency of 44 kHZ were already presented in section 4.2 in figure 4.2. The main experiments were performed at a pressure of about 150 mbar. Lower pressures may cause different excitation processes in the discharge itself and therefore the OES of identical gas compositions at different pressures may be different, too.

In addition the energy input at different frequencies into the discharge might also draw a distinction. Therefore firstly an overview of the discharge spectra with YSZ coated dielectric base plates (high temperature deposition (58)) in the wavelength range from 225 nm till 875 nm at different frequencies from 3 kHZ to 7 kHZ is given in figure 6.21. All OES are from measurements of the (2/21/12) gas flux composition recorded right after discharge ignition. The ionic region between 225 nm and 575 nm is given in figure 6.21(a) and the region of mostly excited atoms is shown in figure 6.21(b).

It can be seen in figure 6.21 that the frequency influences the OES signal intensities. The signal intensity increases with higher discharge frequency.

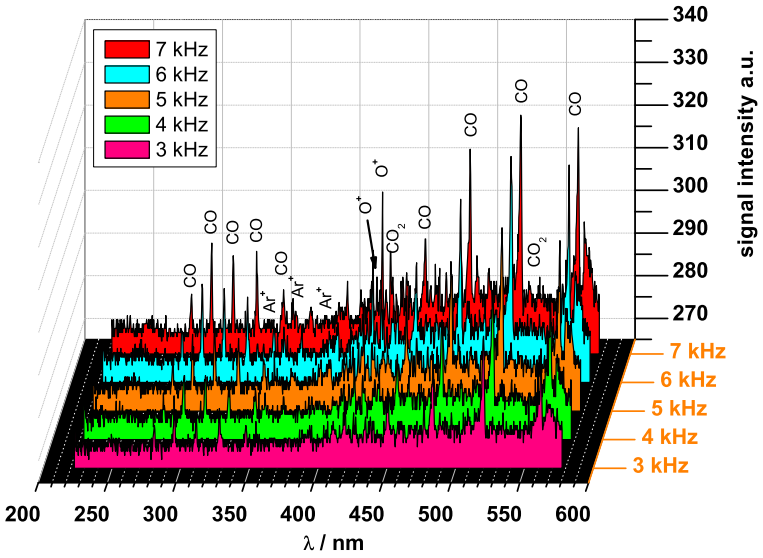

(a)

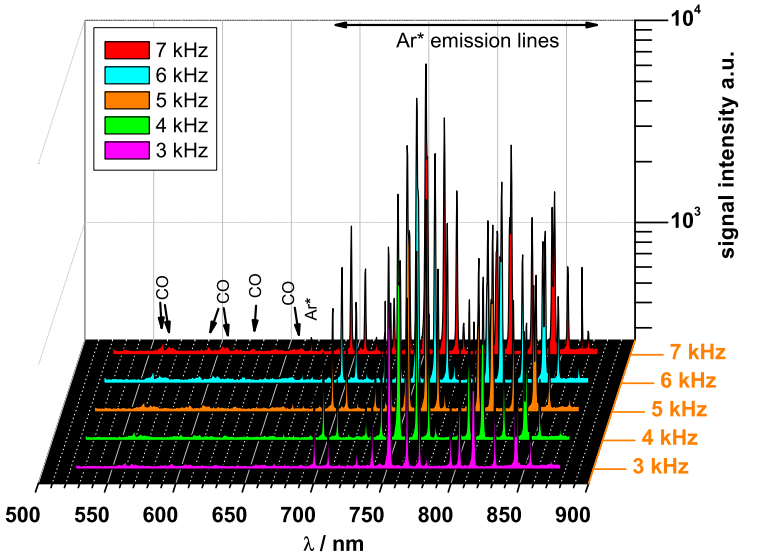

(b)

Figure 6.21: Optical emission spectra of a (2/1/12) sccm gas flux setting of a YSZ coated (high temperature deposition (58)) base plate system. Figure 6.21(a) shows the wavelength region between 225 nm and 575 nm were mostly ionic species and band systems can be found. Figure 6.21(b) shows the higher wavelength region between 525 nm and 875 nm were the spectra are mostly dominated by emission lines of excited Ar atoms. The difference of discharges ignited between 3 kHz and 7 kHz is presented in the figures. The OES were recorded right after discharge ignition in a flow through experiment.

This fits very well into the observation that the absolute CO_2 signal intensities increase linearly with higher frequencies as discussed earlier in section 6.3.4.

A difference in the line spectra cannot be detected, therefore, the assumption of a energy coupling according to Planck's equation into the discharge seems to be correct and only a increase of emission lines can be measured. Figure 6.21(b) shows also that the differences of the OES in the wavelength region between 700 nm and 875 nm are only small. This region of all spectra is dominated by excited argon emission lines . Therefore only the lower wavelength region is presented in the following data analysis because it gives a deeper inside of the concentration and distribution of the ionic species inside the discharge.

The measurements at room temperature showed for the reference system and the coated system similar OES data. The argon emission spectra which dominates the wavelength region above 700 nm has several carbon monoxide emission lines and molecular bands visible. Oxygen is especially represented by two larger emission lines at 415.32 nm respectively 415.65 nm (doublet line) and several possible transitions at 418.55 nm, 418.98 nm, 419.25 nm, 419.63, and 419.67 nm which can be assigned to ionized oxygen atoms [99]. The wavelength difference of some of this emission lines are less then the resolution limit of the used 150 lines grid, therefore an exact assignment is not possible.

The denoted wavelengths although are definitely oxygen emission line because they were found in a pure oxygen and in oxygen/argion spectra, see figure 4.2. Two areas at about 425.65 nm and about 527.55 nm could be correlated to carbon dioxide in an argon/carbon dioxide discharge. The most emission lines in the lower wavelength region correspond to band species or ions designated to carbon monoxide. These lines are proven all by own measurements of a argon/carbon monoxide discharge.

Figure 6.22 shows the spectra recorded for the reference system and the YSZ coated dielectrics. It can be seen that all discharge show a emission scheme that is strongly correlated to carbon monoxide. Here even a very low content of 1 sccm in the gas flux is enough to characterize the discharge as a carbon monoxide (/argon) discharge. Ar^+ emission lines are only a few to be found and at lower intensities as the other gases.

Both systems show that the general intensity of the emission lines is reduced with larger amounts of oxygen in the gas flux. Additionally the intensity of the mentioned O^+ emission lines is also reduced with higher oxygen concentration in the discharge system. The QMS measurements showed that with higher oxygen gas flux the CO_2 conversion rate is higher.

In investigations of carbon dioxide/argon spectra it was found that the

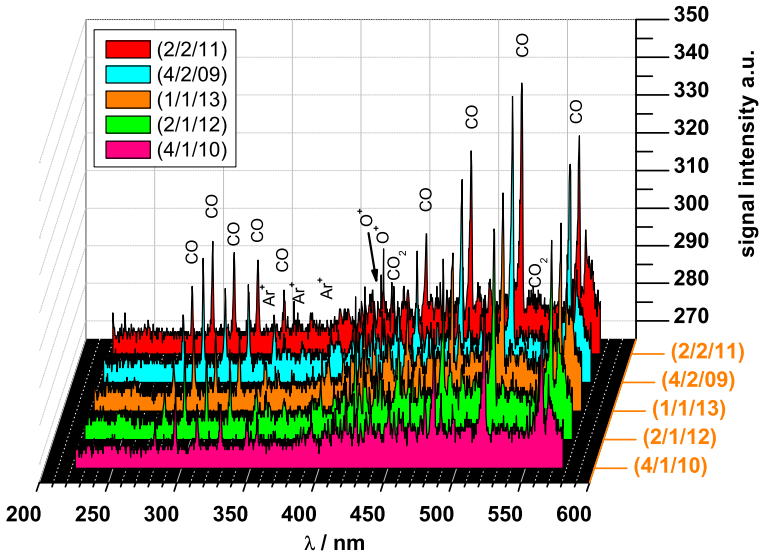

(a)

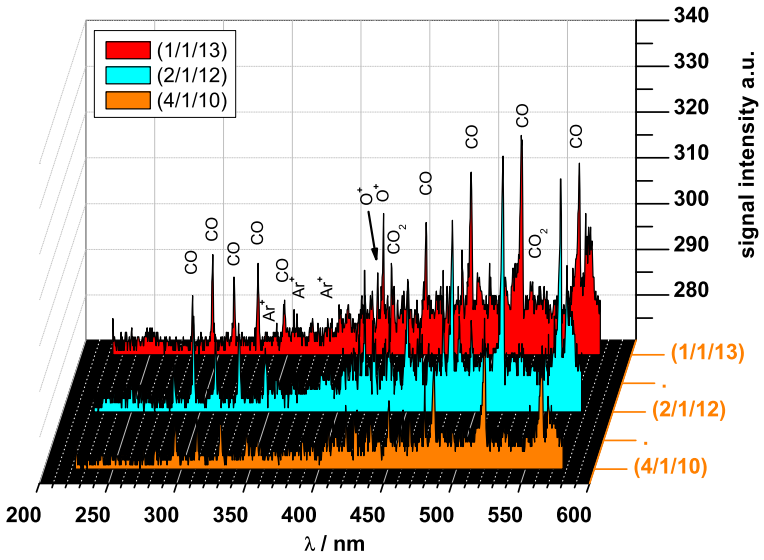

(b)

Figure 6.22: Optical emission spectra of all investigated gas fluxes discharges at room temperature and a frequency of 7 kHZ. Figure 6.22(a) shows the data from the YSZ coated (high temperature deposition(58)) dielectric base plates and figure 6.22(b) the pure fused silica dielectric base plates. All pressures in the flow trough experiments were around 150 mbar. The (4/2/9) measurement data of figure a) was taken at a frequency of 5 kHZ. After discharge stability problems with higher CO gas fluxes the carbon monoxide flux was reduced to 1 sccm in the reference measurements.

carbon dioxide gas reduces the intensity of other molecular and some atomic ions. An possible explanation could be that vibration and/or rotation bands of the molecule are excited. A similar loss of positive oxygen ions was measured in a DC discharge with ion conducting electrodes consisting of YSZ in [41]. Steinmüller et al. concluded that the loss of positive molecular and atomic oxygen ions has to come from an increased concentration of negative oxygen ions.

Taking into account that a lot of CO^+ can be detected in the discharge this leads to the assumption of a large number of free electrons in the discharge. With increasing oxygen gas flux the probability for electron attachment reactions of the electronegativ oxygen gas molecules increases and may therefore cause the loss of the positive oxygen ions. Electronegative gases often show electron attachment reactions [96, 97] and therefore a certain amount of negativly charged ions. The concentration of negative ions depends on the discharge characteristics and may vary according to the discharge ignition procedure.

QMS measurements showed as already presented schematically in figure 4.1 a fast increase after discharge ignition of the CO_2 signal intensity. This fast increase at the beginning of the experiments should be activated at least partially through the ignition itself. The energy coupling into the discharge depending on Planck's law was already discussed earlier in section 6.3.4. Especially in the case of the YSZ coated dielectrics QMS data showed a fast increase of signal intensity followed by a slow long time increase over 30 to 60 minutes.

The discharge bombards the functional YSZ layers with ions and electrons and heats therefore the surface area. This seems to have a positive effect on the carbon monoxide conversion rate. If this is a correct interpretation of the discharge situation then OES measurements should show that the greatest differences of the spectra recorded will be visible during the first minutes after ignition and afterwards the differences according to the slow signal increase should be lower.

Another point should also be visible, if the fast increase ist caused by the discharge itself the effect should be higher igniting the discharge with higher frequencies. This should be also visible in the OES data. Figure 6.23 shows for the (1/1/13) gas flux setting the OES recorded at a frequency of 3 kHz in the case of YSZ (high temperature coating (58)), figure 6.23(a) and at a frequency of 6 kHz for a fused silica dielectric system.

The analysis of the OES data confirmed the estimations from the QMS measurements. The greatest intensity loss of the spectra could be observed within the first 15 to 20 minutes of discharge ignition and the change of spectra intensities is greater within discharges operating at higher frequencies.

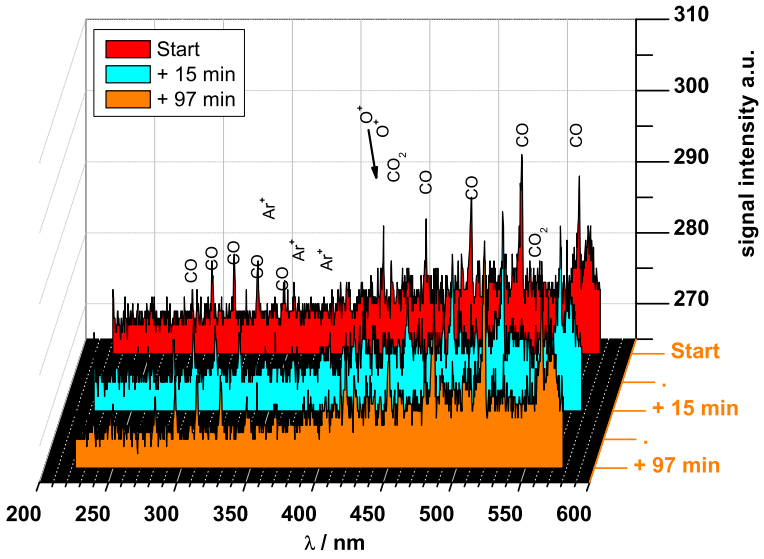

(a)

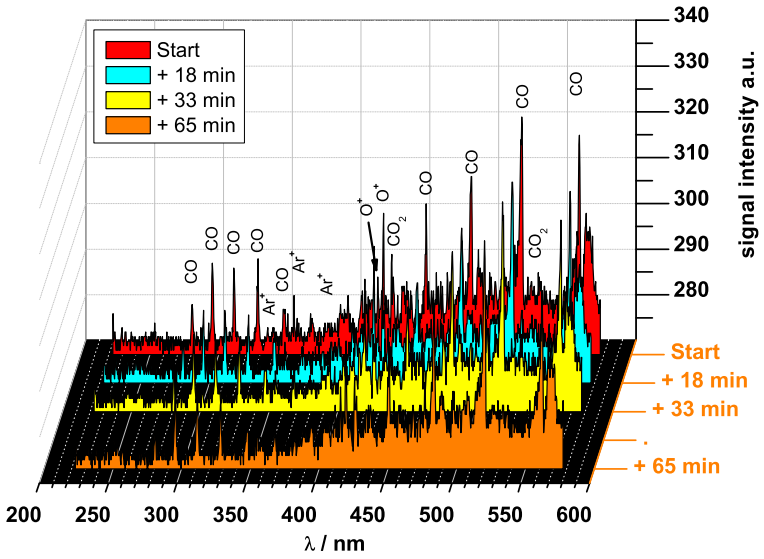

(b)

Figure 6.23: Optical emission spectra of the (1/1/13) gas flux settings for YSZ coated (high temperature coating (58)) dielectric base plates at a frequency of 3 kHZ and pure fused silica base plates at a frequency of 6 kHZ. It can be seen that the loss in intensity during one hour of discharge ignition is less at the lower frequency and that the greatest decrease of signals occurs within the first 15 to 20 minutes after discharge ignition.

6.5.2 OES at Elevated Temperatures

The temperature dependent measurements which were presented in section 6.4.3 were combined with OES spectra investigations. The strong signal increase in the QMS measurements of the carbon dioxide signal should be visible in the emission spectra. An overview of a spectra in the wavelength range from 225 nm to 875 nm of the (1/1/13) gas setup experiment is given in figure 6.24. Here the first subfigure shows the lower region from 225 nm to 575 nm and the second figure gives the region from 525 nm to 875 nm.

Although as discussed before, see figure 5.23, the gap distances of the dielectric plates are not the same at room and elevated temperatures therefore the OES of different temperatures have to be evaluated with care. Greater gap distances led to a larger discharge volume which usually should increase the signal intensities of the OES from a statistical view point. The low temperature gas discharge ionization value of about 10^{-6} is independent from the discharge temperature increase of about 270 K and therefore the change of discharge volume gives a proportional increase of ionic species in the discharge which should be visible in higher intensities at lower temperatures where the gap distance is larger.

The QMS data showed that at a certain temperature a strong increase (between 180 °C and 210 °C) of the carbon dioxide signal intensity takes places. Subfigure 5.23(b) shows that at a furnace temperature of 244 °C which corresponds about 160 °C discharge temperature already a little bit smaller gap distance than at room temperature can be seen. This temperature is still below the strong CO_2 signal increase interval.

From these considerations it was expected that the OES differ for different temperatures whereupon the observed lower intensities in CO_2 rich gas discharges as observed at room temperature should be recorded again. Figure 6.24 shows that the signal intensities of the complete spectra is more and more reduced with higher temperatures. From the OES data no evidence could be get why the QMS CO_2 signal shows a intensity minima between 100 °C and 180 °C. It was not possible to clarify this observed effect within the scope of this work.

With this data analysis another question arised. Is the conversion rate at elevated temperature of the carbon monoxide at a 100% rate? Because CO emission signals are still present in the OES a full conversion should not be expected. To clarify this point the comparison of a FTE and a BE was performed with YSZ coated (non-reactive room temperature deposition (67)) dielectric base plate during the (4/1/10) gas setup experiments. Here again like at room temperature the highest CO_2 signal increase could be detected and therefore the conversion rate should be the highest of all tested gas flux

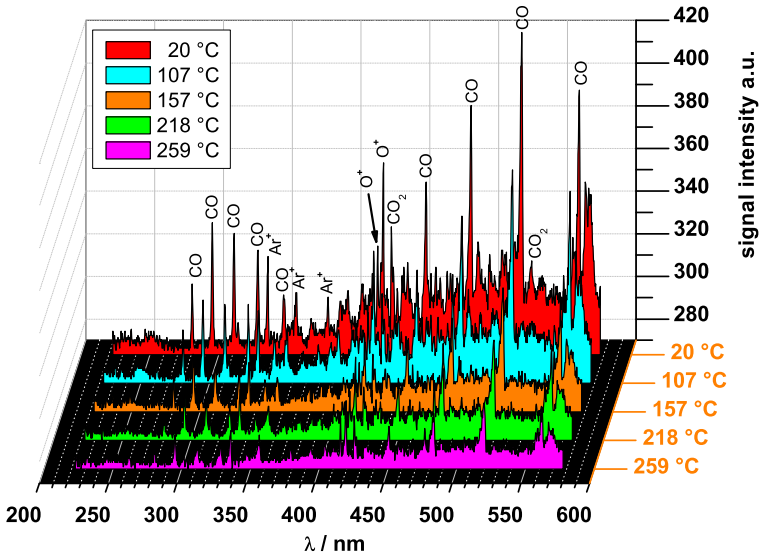

(a)

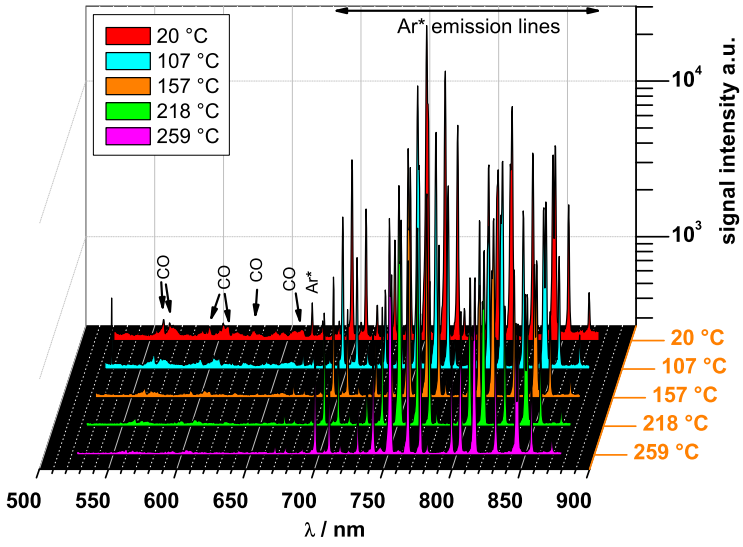

(b)

Figure 6.24: The figures show for five different discharge temperatures the recorded OES spectra for the YSZ coated (reactive sputtered room temperature (71)) during the (1/1/13) gas setup experiment from about 225 nm to 875 nm. The wavelength region from about 700 nm to 875 nm is dominated by excited argon emission lines. The ionic character of the discharge is presented especially by the wavelength region from 280 nm to about 660 nm.

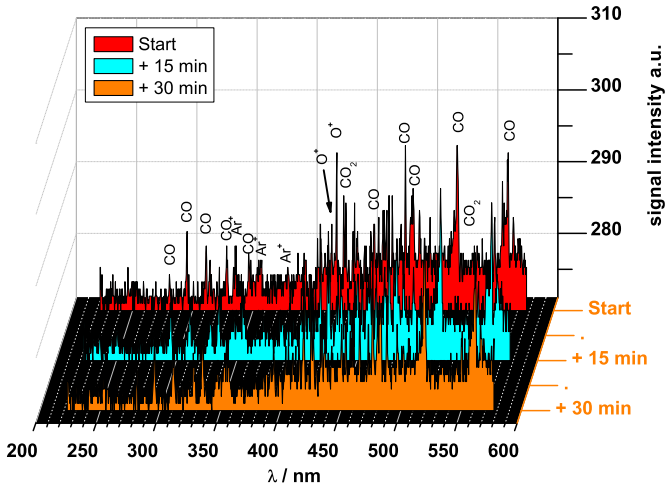

(a)

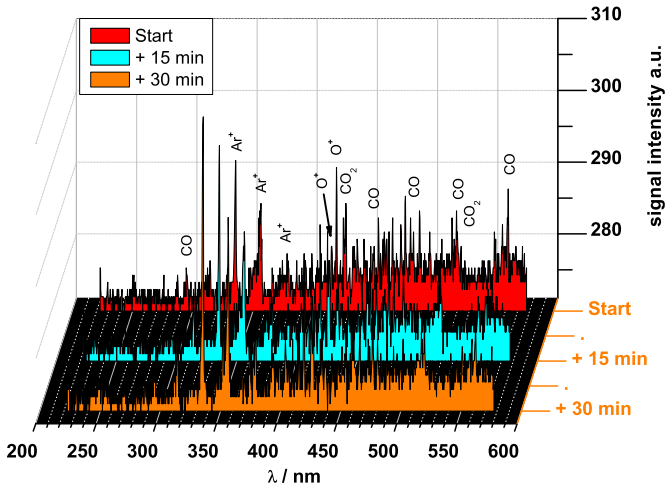

(b)

Figure 6.25: Optical emission spectra of YSZ coated (non-reactive room temperature deposition (67)) base plates during (4/1/10) gas flux setting. For direct interpretation of the CO to CO_2 conversion rate the data of a FTE was compared with a BE at elevated temperature. Figure 6.25(a) shows the change of spectra during ignited discharge of the FTE and figure 6.25(b) after sealing the reactor chamber and stopping the complete gas flux. In the BE the intensity of the CO emission lines is further decreased and especially the Ar^+ lines in the wavelength region between 330 nm and 370 nm increase during discharge ignition of 30 minutes. A full conversion of carbon monoxide is therefore not reached at discharge temperatures of about 293 °C.

setups. Figure 6.25 shows the comparison of FTE and BE Experiment at furnace temperature of 435 °C which corresponds to a discharge temperature of about 293 °C. OES after 15 and 30 minutes after discharge ignition are compared and analyzed.

The FTE Experiment shows slightly decreasing OES intensities which corresponds to the slightly increase of the signal intensity of CO_2 in the QMS. Both as the QMS data showed, that the change is very small. After sealing the reactor chamber and stopping of all gas fluxes a strong increase of the CO_2 signal intensity can be recorded and the pressure inside the reactor reduces due to the volume loss from the carbon monoxide oxidation , see equation 6.1. From the reduced pressure an increase of the general excitation processes inside the discharge is induced resulting in higher recorded intensities in the QMS.

The CO signal intensities in the OES decrease and due to the lower carbon monoxide content of the gas discharge the intensities of several Ar^+ signals increase during the 30 minutes of discharge ignition as can be seen in figure 6.25(b). These experimental results proved that the conversion rate of carbon monoxide to carbon dioxide is not complete at discharge temperatures of 292 °C.

With this in mind a closer look to the OES spectra of all investigated dielectric base plate systems is necessary to understand the origin of the strong CO_2 signal increase in the QMS. The general idea, that an increased discharge temperature of about 300°C should improve the oxidation rate of carbon monoxide by using YSZ coated dielectric base plates, has to be reconsidered because the intense CO_2 signal increase at about 200°C of discharge temperature occurs earlier than expected and an similar increase was observed by using only fused silica dielectric plates.

At elevated temperature the QMS data of all dielectric base plate systems with all YSZ depositions and the reference system without deposition showed only small increases after discharge ignition, see figures 6.16 and 6.17 or a constant increase for all different frequencies in the case of the (1/1/13) gas flux setting, see figure 6.18. The direct comparison of all gas fluxes investigated with the uncoated fused silica dielectrics in figure 6.15 showed also that the discharge ignition with uncoated dielectrics had nearly no effect on the CO_2 conversion rate.

For further analysis of the time dependent behavior after discharge ignition the (1/1/13) gas flux setup is skipped because the QMS data showed no differences after discharge ignition independent of the used dielectric base plates. Starting with the OES spectra of the reference system it should be no difference visible in the OES data. Figure 6.26 shows that this assumption is correct. The spectra of the (4/1/10) and (2/1/12) gas flux settings are only

slightly different. A greater change as recorded at room temperature could not be detected.

In direct comparison to the reference system the YSZ coated films sputtered at room temperature showed at both mentioned experimental conditions a slightly increase of the CO_2 signal intensity during the QMS measurements. Therefore a small decrease of the OES should be visible after discharge ignition, as it was observed at room temperature measurements. The data for the non-reactive YSZ film deposition at room temperature is shown in figure 6.27 and the data of the reactive film deposition at room temperature (71) is shown in figure 6.28. The assumption is proved with the recorded OES for both depositions.

From room temperature measurements, see figure 6.22, it is known that depending on the gas flux setting several observations according to the change of emission lines detected with OES in the different gas discharges. Therefore this comparison is repeated at elevated temperatures. Figure 6.29 shows a similar intensity behavior of the recorded OES according to the gas flux settings. Again as observed at room temperature the (1/1/13) gas flux setting shows the highest intensities.

In contradiction to the room temperature measurements at elevated temperature significant Ar^+ emission lines below 400 nm can be detected. It seems that the carbon monoxide character of the discharge is reduced due to the higher carbon monoxide oxidation rates detected in the QMS measurements. The other gas fluxes with higher oxygen contents show the same lower signal intensities already known from the room temperature measurements.

With this result figure 6.18 of the (1/1/13) gas flux experiments seems to fit very well into the experimental observations. As the discharge characteristics of an argon discharge are even by little amounts of other gases influenced (which was shown earlier in this work, see section 4.2, especially figure 4.2) the interpretation of the (1/1/13) data is more clear. The amount of carbon monoxide still present in the discharge seems to be that much reduced that the influences of the CO emission lines is onto the discharge characteristics is lowered. This fits very well into the strongly visible O^+ emission lines as already described within the room temperature measurements. If for example half of the CO concentration reacted to CO_2 only a quarter of the oxygen concentration has reacted and therefore the CO/Ar characteristics changed into O_2/Ar discharge characteristics, which would explain the recorded OES.

For a concluding analysis of the measurement data a comparison of all (1/1/13) OES of all base plate systems used in this work at elevated temperatures is given in figure 6.30. All measurements show the same strong argon and oxygen emission lines. This behavior is only observed at elevated temperatures with this gas flux setup at such an intense value. Both other

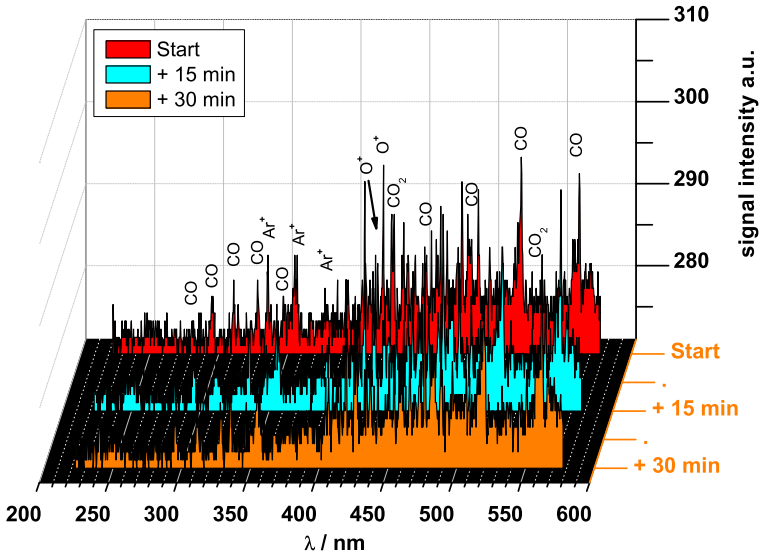

(a)

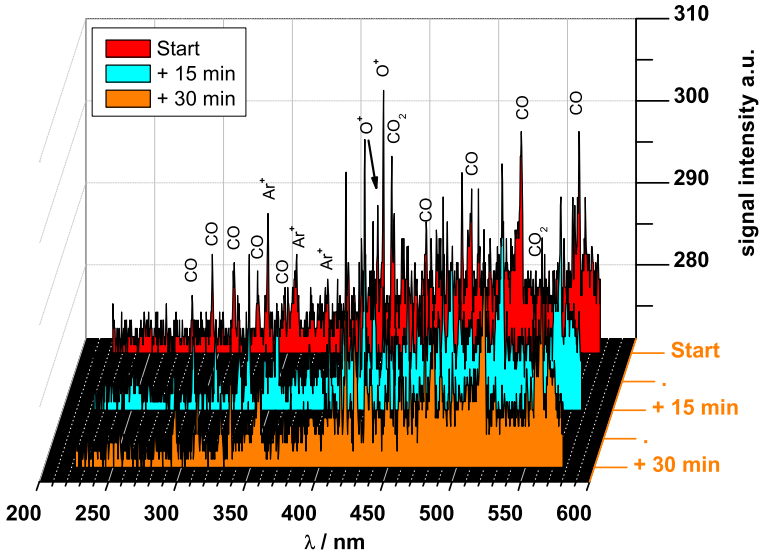

(b)

Figure 6.26: Optical emission spectra of uncoated fused silica dielectric base plates during ignited discharge under experimental conditions of (4/1/10) gas flux settings in figure 6.26(a) and (2/1/10) gas flux settings in figure 6.26(b). Even after 30 minutes of discharge ignition the OES has not changed as seen in the room temperature measurements.

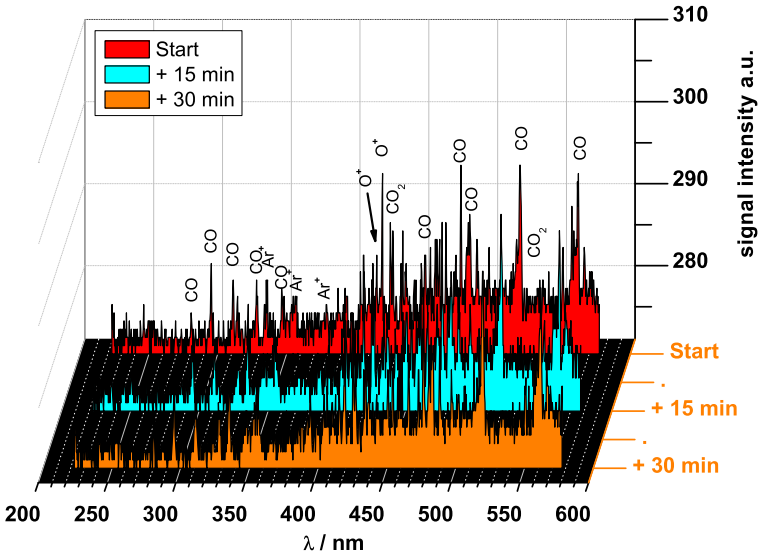

(a)

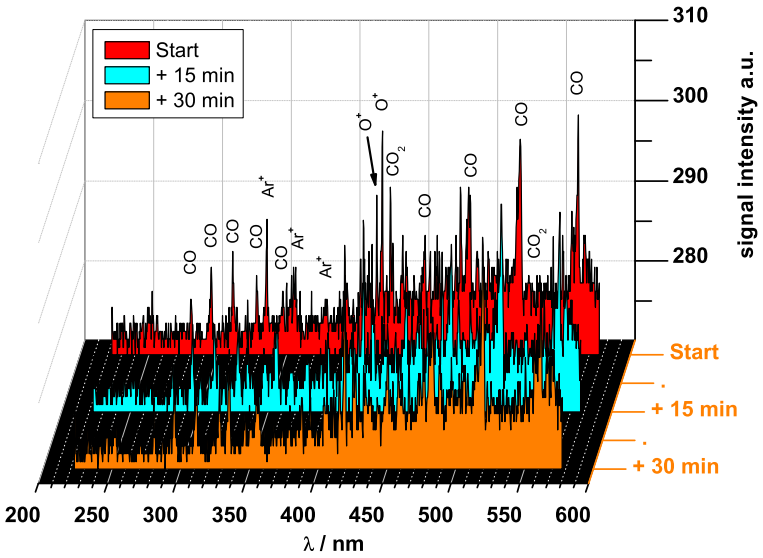

(b)

Figure 6.27: Optical emission spectra of YSZ coated dielectric base plates with non-reactive room temperature deposition (67). Comparison of the (4/1/10), figure 6.27(a) and the (2/1/12) gas flux settings, figure 6.27(b). Figure 6.27(a) is the same spectra as already shown in figure 6.25(a). After 30 minutes of discharge ignition the signal intensities of the OES are slightly decreased

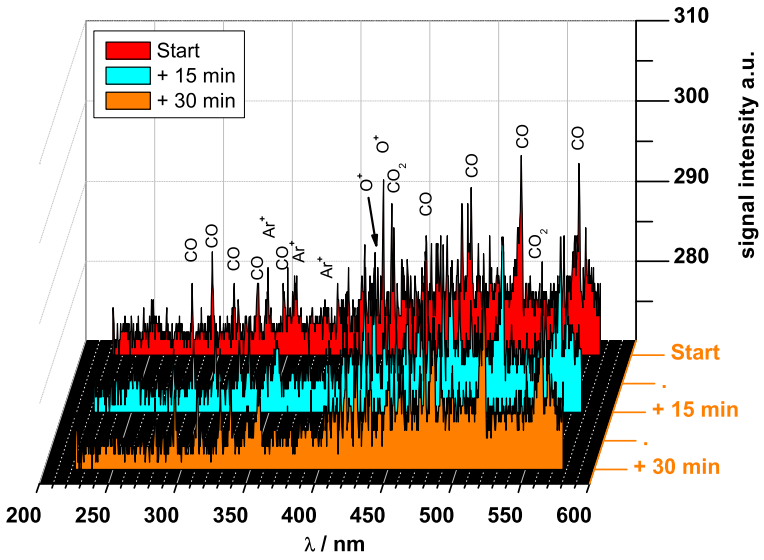

(a)

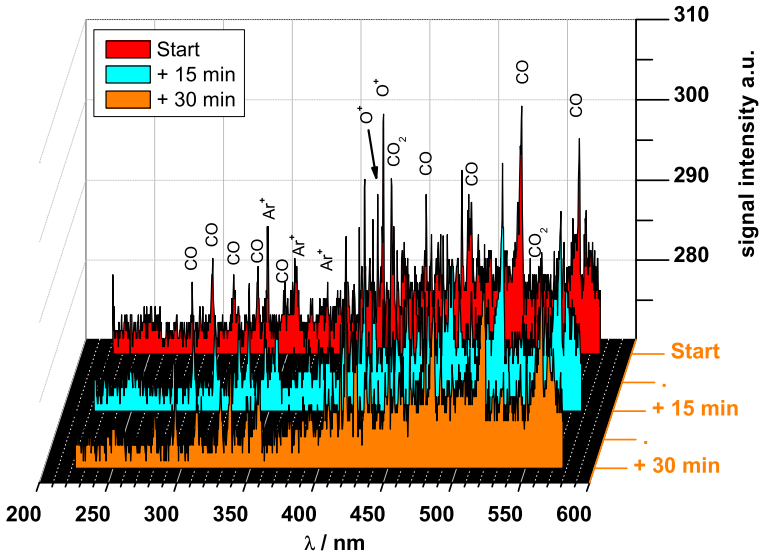

(b)

Figure 6.28: Optical emission spectra of YSZ coated dielectric base plates with reactive room temperature deposition (71). Comparison of the (4/1/10), figure 6.28(a) and the (2/1/12) gas flux settings, figure 6.28(b). After 30 minutes of discharge ignition the signal intensities of the OES are slightly decreased.

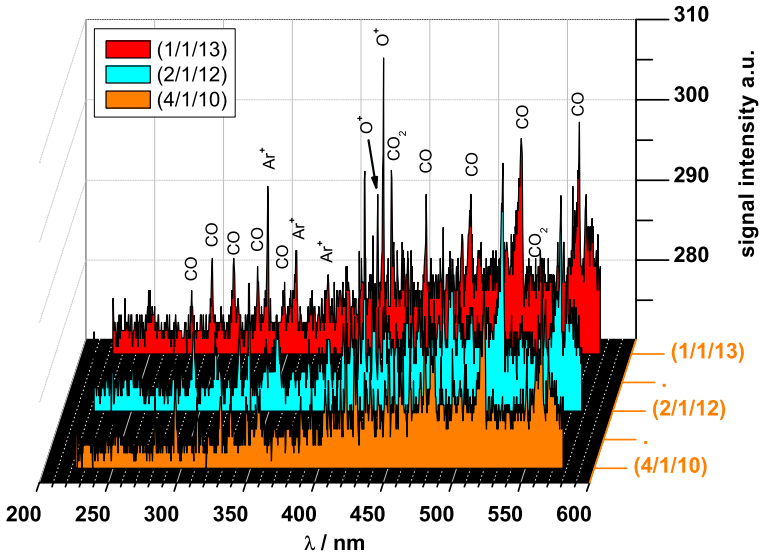

(a)

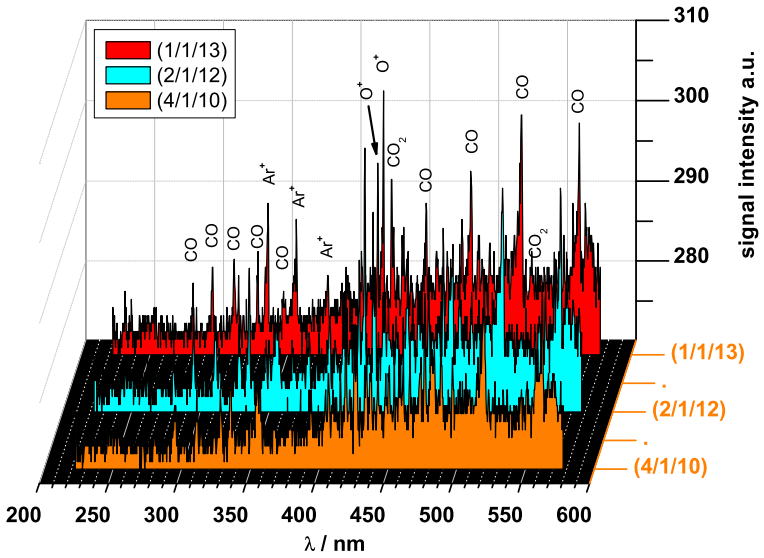

(b)

Figure 6.29: Optical Emission spectra of all investigated gas flux settings ((4/1/40), (2/1/12), and 1/1/13)) for the reactive sputtered room temperature YSZ deposition, figure 6.29(a) and the reference fused silica dielectric system, figure 6.29(b). The OES signal intensity decreases with higher oxygen contents as observed during room temperature measurements. Differences can be found in the data of the (1/1/13) experiments. Here several Ar^+ emission lines can be detected below 400 nm, which were not present in such an intensity at room temperature.

investigated gas flux settings show also higher oxygen emission lines, but the argon emission lines are at similar intensities as CO emission lines. This is still more intensive as recorded in the room temperature and therefore a confirmation of the increased carbon monoxide oxidation rate which was observed in the QMS measurements.

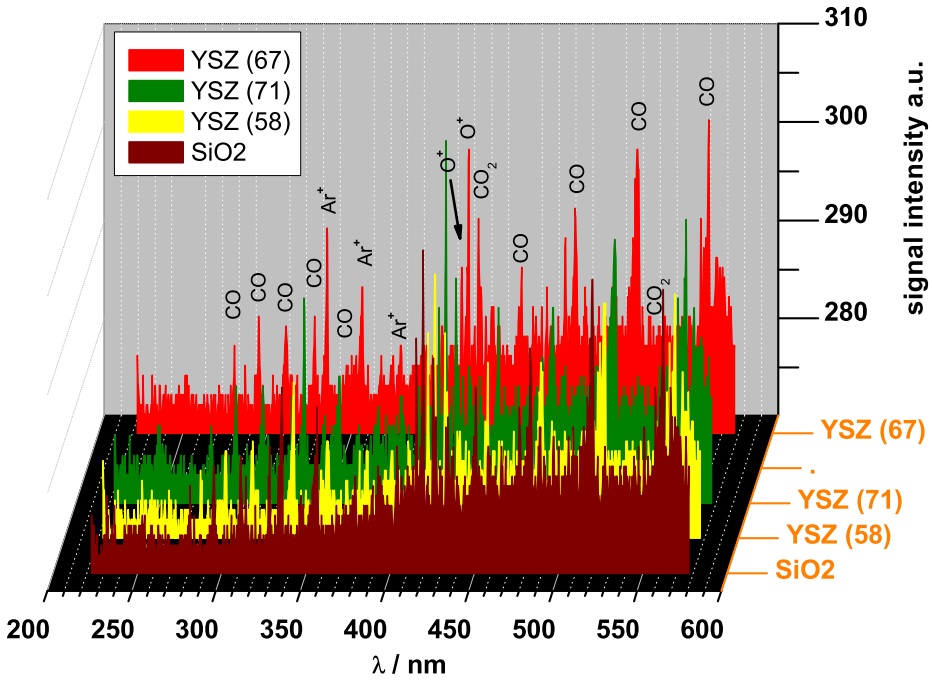

Figure 6.30: Comparison of all recorded optical emission spectra with the (1/1/13) gas flux setting at elevated temperatures. The SiO_2 measurement was recorded at a discharge frequency of 6 kHz, all YSZ related measurements at 7 kHz discharge frequency. Below 400 nm several Ar^+ emission lines are visible with higher signal intensity than the CO emission lines identified in the room temperature OES.

Chapter 7

Summary, Conclusions and Outlook

It was possible to ignite a dielectric barrier discharge with and without YSZ functional coating on fused silica dielectrics. An significant increase of the conversion rate of the carbon monoxide oxidation could be measured with QMS and was also visible due to the changes in OES. The impact of contamination by nickel at room temperature on the dielectrics could not be totally prevented, but the influence of the contamination could be reduced by establishing a cleaning route and changing the experimental order. The influences of different YSZ depositions could only be investigated at elevated temperatures of about 300°C due to the nickel contamination during first room temperature investigations. The data of the elevated temperature investigations show a hint that a larger surface area of YSZ which should be true for the non-reactive sputtered YSZ film (small grains and oxygen deficit during deposition) influences the reaction rate positively. This film showed the highest increase of the CO_2 signal intensity at 300°C. The dense high temperature YSZ deposition (58) showed less CO_2 signal increase, therefore the assumption that a larger surface area influences positively the oxidation rate seems reasonable.

It could be shown that depending on the frequency a higher energy input according to Planck's law takes place especially at frequencies of 6 kHz and 7 kHz. The catalytic rate enhancement has its highest values at frequencies of 3 kHz for all investigated gas flux settings. The rate enhancement is with the exception of the higher measured frequencies of the (2/1/12) setup higher than 100% with 100% being the CO_2 signal increase obtained with uncoated dielectrics.

The ignition voltages for discharges at elevated temperatures are lowered in comparison to the voltages needed at room temperature. Especially for

the YSZ deposited dielectric it was also observed that the ignition voltages for "cold" dielectrics (first ignition after preparation and gas flux adjustment) were higher than for "hot" dielectrics, for example if the discharge was switched off and ignited again after a few seconds. The reaching of an equilibrium discharge condition during room temperature measurements took longer with YSZ coated dielectrics then with uncoated fused silica dielectrics.

The CO_2 signal increase at a discharge temperature of about 200°C is not triggered by the presence of a YSZ coating, because uncoated fused silica dielectrics show the same temperature dependent increase. The CO_2 signal increase seems to be a conversion increase like often observed in heterogeneous catalysis when a special reaction rate increases due to the activation of a catalyst rapidly at a certain temperature.

Summarizing all observations it can be concluded that the deposition of a YSZ thin film on a fused silica dielectric enhances the carbon monoxide oxidation. This enhancement effect seems to be coming from either the plasma YSZ surface interaction which heats the YSZ surface to significant higher temperatures above room temperature or to a surface restructuring which takes places especially at room temperature conditions due to the plasma YSZ surface interaction. From the kinetic description either a partial pressure dependent reaction mechanism like the Eley-Rideal-Mechanism can be proposed or with the assumption that the YSZ supports lattice oxygen for the CO oxidation a Mars-van-Krevelen-Mechanism like reaction path can also be possible. The last mechanism would fit well into the concept and aim presented at the beginning of this work if carbon monoxide adsorbs at surface lattice oxygen atoms of the YSZ. Further research has to be performed to ascertain which kinetic model can be applied for the concept of heterogeneous plasma catalysis with an oxygen ion conducting catalyst.

From OES can be concluded that the investigated discharges are strongly influenced by the carbon monoxide. As long as the partial pressure of CO is high enough no Ar^+ emission lines can be detected. Oxygen emission lines can be found only rarely and with decreasing intensity at higher oxygen partial pressures. This might be a clue to increased concentrations of negatively charged oxygen ions.

During the experiments it was found that several circumstances influence the measurement routines and have an impact onto the experimental results. First the nickel contamination should be avoided due to the catalytic activity of nickel and its oxides. This should be achieved by preventing the Mond process which seems to be the cause for the contamination by replacement of all nickel containing pieces in the experimental chamber. Supplementary, the experiments should not be performed at room temperature because even a heating through sun light influenced the temperature and therefore the

pressure inside the extractor hub in the laboratory. An "room temperature" analysis about 5 to 10°C above the highest room temperature during measurement time, seems to solve this problem.

The strong CO_2 signal increase in the QMS at about 200°C should be caused by a material used inside the reactor chamber. This might be either the brass or in worse case the platinum electrodes at the backside of the dielectric base plates. The use of less metal parts inside the reactor chamber would help to clarify the real catalytic activity of YSZ.

After establishing the cleaning route of the dielectric base plates it was found that the oxidation rate increase undergoes an activation process. The interaction of the discharge and the surface of the thin film or the fused silica alters the plasma|surface interaction after a few hours of discharge in such a way that differences of over 10 % can occur. This was found during several experiments. To avoid this unwanted gap during measurements it would be good to prepare all dielectric plates after cleaning with a certain discharge condition to activate the surface of the YSZ films, respectively to enhance the plasma|dielectric interaction. If for example nickel contamination are responsible for the oxidation increase this will also help to prepare equal "starting points" for all dielectrics.

Chapter 8

Appendix

The appendix includes additional information that would interfere with the fluent reading of this work but is useful for readers who like to take a closer look on certain details.

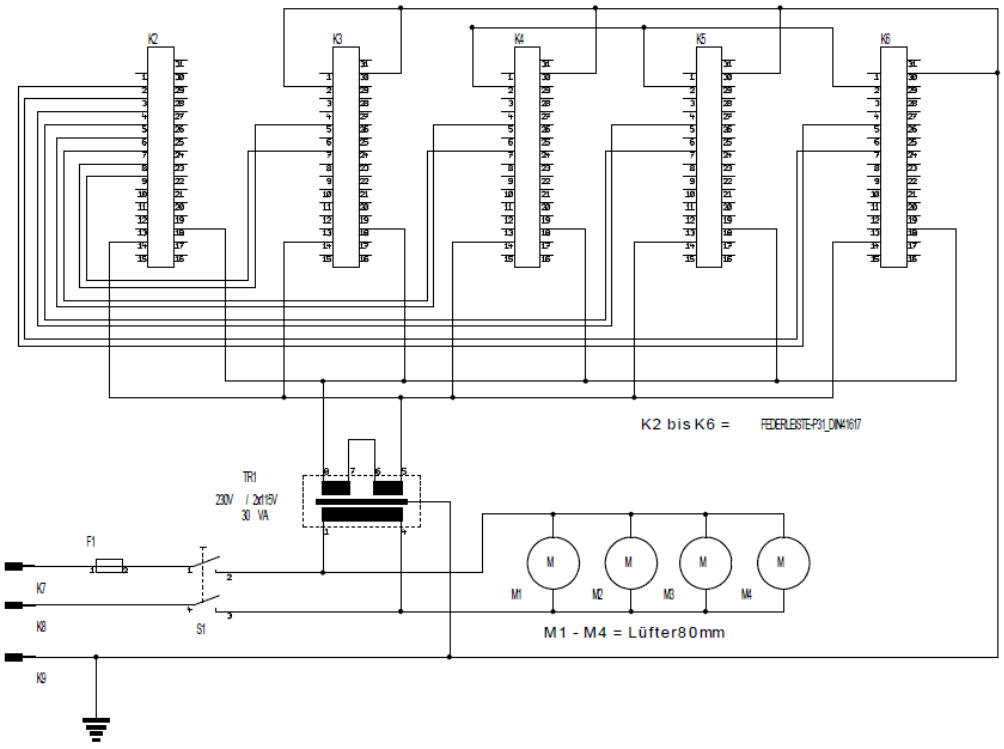

Figure 8.1: Schematic of the AC generator build for DBD discharge. Draft by H. Weigand.

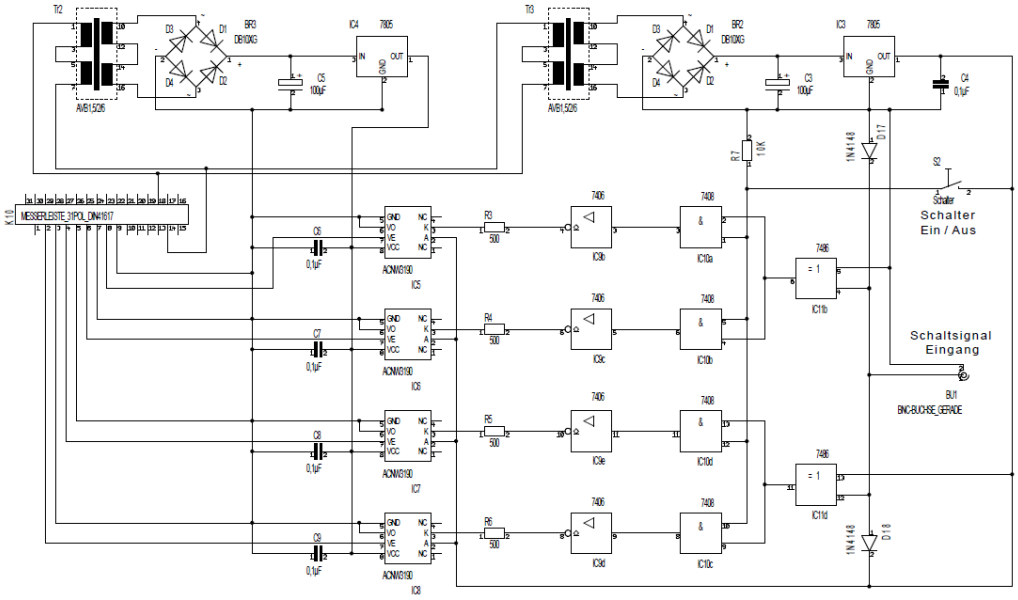

Figure 8.2: Schematic of the AC generator build for DBD discharge. Draft by H. Weigand.

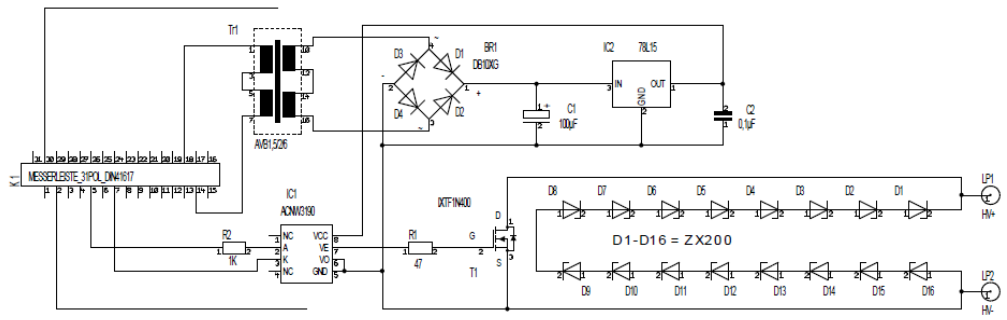

Figure 8.3: Schematic of the AC generator build for DBD discharge. Draft by H. Weigand.

Dielectric Base Plate System Holder

Figure 8.4 shows the structural difference of the bottom part of the holders with the differences of room temperature and high temperature holders. The different size of the holders was due to the first method of construction with one adjustable fused silica base plate holder.

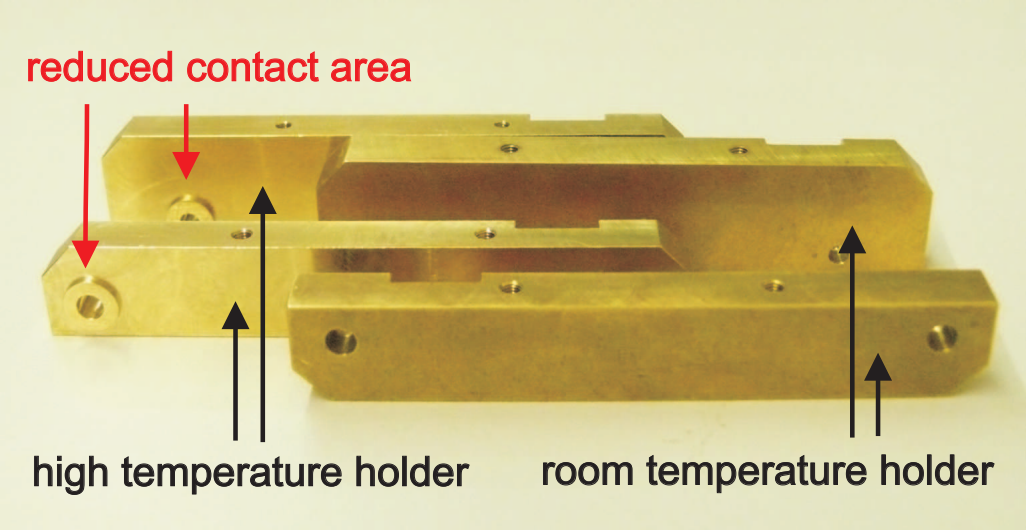

Figure 8.4: The figure shows the holders used for the furnace and the dielectric base plates. On the left side the high temperature holders can be seen with reduced contact area (red arrows) to the bottom of the brass reactor chamber. The room temperature holders are shown in the right side of the figure. They have no reduced contact area.

Bibliography

[1] W. Siemens, "Ozone Production in an Atmospheric-Pressure Dielectric Barrier Discharge," PoggendorfŠs Ann. Phys. Chem. 102, 66 (1857) **102**, 66 (1857).

[2] J. S. Townsend, "The conductivity produced in gases by the motion of negatively charged ions." Nature **62**, 340–341 (1900). http://dx.doi.org/10.1080/14786440109462605

[3] C. A. Skinner, "Simplified Theory of the Cathode Fall in Gases with Application to Plates And Wires," Phys. Rev. **12**, 143–157 (1918). http://link.aps.org/doi/10.1103/PhysRev.12.143

[4] P. M. Morse, "A Theory of the Electric Discharge Through Gases," Phys. Rev. **31**, 1003–1017 (1928). http://link.aps.org/doi/10.1103/PhysRev.31.1003

[5] V. A. Lisovsky and V. D. Yegorenkov, "Low-pressure gas breakdown in combined fields," Journal of Physics D: Applied Physics **27**, 2340 (1994). http://stacks.iop.org/0022-3727/27/i=11/a=014

[6] U. Kogelschatz, "Twenty years of Hakone symposia: From basic plasma chemistry to billion dollar markets," Plasma Processes and Polymers **4**, 678–681 (2007), 10^{th} International Symposium on High Pressure, Low Temperature Plasma Chemistry, Saga, Japan, Sep 04-08, 2006.

[7] U. Kogelschatz, "Collective phenomena in volume and surface barrier discharges," Journal of Physics: Conference Series **257**, 012 015 (2010). http://stacks.iop.org/1742-6596/257/i=1/a=012015

[8] X. Xu, "Dielectric barrier discharge – properties and applications," Thin Solid Films **390**, 237 – 242 (2001). http://www.sciencedirect.com/science/article/pii/S0040609001009567

[9] G. Fridman, M. Peddinghaus, H. Ayan, A. Fridman, M. Balasubramanian, A. Gutsol, A. Brooks, and G. Friedman, "Blood coagulation and living tissue sterilization by floating-electrode dielectric barrier discharge in air," Plasma Chemistry and Plasma Processing **26**, 425–442 (2006).

[10] H. L. Chen, H. M. Lee, and S. H. a. Chen, "Review of Packed-Bed Plasma Reactor for Ozone Generation and Air Pollution Control," Industrial & Engineering Chemistry Research **47**, 2122–2130 (2008). http://pubs.acs.org/doi/abs/10.1021/ie071411s

[11] C. W. Chen, H. M. Lee, S. H. Chen, H. L. Chen, and M. B. Chang, "Ultrasound-Assisted Plasma: A Novel Technique for Inactivation of Aquatic Microorganisms," Environmental Science & Technology **43**, 4493–4497 (2009).
http://pubs.acs.org/doi/abs/10.1021/es900345z

[12] G. Fu, A. Polity, N. Volbers, and B. K. Meyer, "Annealing effects on VO_2 thin films deposited by reactive sputtering," Thin Solid Films **515**, 2519–2522 (2006).

[13] Y. M. Lu, Y. B. He, B. Yang, A. Polity, N. Volbers, C. Neumann, D. Hasselkamp, and B. Meyer, "RF reactive sputter deposition and characterization of transparent $CuAlO_2$ thin films," Physica Status Solidi (c) **3**, 2895–2898 (2006).
http://dx.doi.org/10.1002/pssc.200669571

[14] T. Czerwiec, N. Renevier, and H. Michel, "Low-temperature plasma-assisted nitriding," Surface and Coatings Technology **131**, 267 – 277 (2000).
http://www.sciencedirect.com/science/article/pii/S0257897200007921

[15] G. Borcia, R. Cazan, and C. Borcia, "DBD Surface Modification of Polymers in Relation to the Spatial Distribution of Reactive Oxygen Species," Plasma Chemistry and Plasma Processing **31**, 729–740 (2011).

[16] C.-Y. Tsai, R.-S. Juang, and C. Huang, "Surface Modification of Polypropylene Membrane by RF Methane/Oxygen Mixture Plasma Treatment," Japanese Journal of Applied Physics **50** (2011).

[17] M. F. Gendre, M. Haverlag, and G. M. W. Kroesen, "Optical and electrostatic potential investigations of electrical breakdown phenomena

in a low-pressure gas discharge lamp," Journal of Physics D: Applied Physics **43**, 234 004 (2010).
http://stacks.iop.org/0022-3727/43/i=23/a=234004

[18] H.-Y. Jung, T.-H. Lee, O. Kwon, H.-W. Cheong, S. O. Steinmüller, J. Janek, and K.-W. Whang, "Realization of High Luminous Efficacy at Low Voltages in the Plasma Display Panel With SrO-MgO Double Layer," IEEE Electron Device Letters **31**, 686–688 (2010).

[19] K. H. Groh and H. W. Loeb, "State of the art of radiofrequency ion sources for space propulsion," Review of Scientific Instruments **65**, 1741–1744 (1994).
http://scitation.aip.org/content/aip/journal/rsi/65/5/10.1063/1.1144869

[20] R. L. Merlino, J. R. Heinrich, S.-H. Kim, and J. K. Meyer, "Dusty plasmas: experiments on nonlinear dust acoustic waves, shocks and structures," Plasma Physics and Controlled Fusion **54**, 124 014 (2012).
http://stacks.iop.org/0741-3335/54/i=12/a=124014

[21] K. Baba, T. Kaneko, and R. Hatakeyama, "Ion irradiation effects on ionic liquids interfaced with rf discharge plasmas," Applied Physics Letters **90**, 201 501 (2007).
http://scitation.aip.org/content/aip/journal/apl/90/20/10.1063/1.2739327

[22] S. Z. El Abedin, M. Poelleth, S. A. Meiss, J. Janek, and F. Endres, "Ionic liquids as green electrolytes for the electrodeposition of nanomaterials," Green Chemistry **9**, 549–553 (2007).

[23] T. Kaneko, K. Baba, and R. Hatakeyama, "Static gas-liquid interfacial direct current discharge plasmas using ionic liquid cathode," Journal of Applied Physics **105**, 103 306 (2009).
http://scitation.aip.org/content/aip/journal/jap/105/10/10.1063/1.3133213

[24] T. Kaneko, Q. Chen, T. Harada, and R. Hatakeyama, "Structural and reactive kinetics in gas-liquid interfacial plasmas," Plasma Sources Science & Technology **20** (2011), International Workshop on Plasmas with Liquids (IWPL), Matsuyama, Japan, Mar, 2010.

[25] M. Vennekamp and J. Janek, "Plasma electrochemical growth of ion-conducting AgBr and AgCl," Solid State Ionics **141**, 71–80 (2001), XIV. International Symposium on the Reactivity of Solids (XIV. ISRS), Budapest, Hungary, Aug 27-31, 2000.

[26] M. Vennekamp and J. Janek, "Plasma electrochemistry in radio frequency discharges - Oxidation of silver in a chlorine plasma," Journal of the Electrochemical Society **150**, C723–C729 (2003).

[27] M. Vennekamp and J. Janek, "Control of the surface morphology of solid electrolyte films during field-driven growth in a reactive plasma," Physical Chemistry Chemical Physics **7**, 666–677 (2005).

[28] S. A. Meiss, M. Rohnke, F. Rettig, R. Moos, and J. Janek, "Ion-Conducting Probes for Low Temperature Plasmas," Contributions to Plasma Physics **48**, 473–479 (2008).
http://dx.doi.org/10.1002/ctpp.200810076

[29] F. Chen and D. Arnush, "The floating potential of cylindrical Langmuir probes," Physics of Plasmas **8**, 5051–5052 (2001).

[30] F. Chen, "Langmuir probe analysis for high density plasmas," Physics of Plasmas **8**, 3029–3041 (2001).

[31] E. F. Mendez-Martinez, P. G. Reyes, D. Osorio-Gonzalez, F. Castillo, and H. Martinez, "Langmuir Probe and Optical Emission Spectroscopy Studies of Low-Pressure Gas Mixture of CO_2 and N_2," Plasma Science & Technology **12**, 314–319 (2010).

[32] F. F. Chen, J. D. Evans, and W. Zawalski, "Calibration of Langmuir probes against microwaves and plasma oscillation probes," Plasma Sources Science & Technology **21** (2012).

[33] Y. Torimoto, S. Yao, A. Harano, and M. Sadakata, "Formation of a DC Glow Discharge at Atmospheric Pressure Using Solid Electrolyte," Journal of Chemical Engineering of Japan **30**, 159–162 (1997).

[34] Y. Torimoto, A. Harano, T. Suda, and M. Sadakata, "Emission of O^- radical anions from a solid electrolyte surface into the gas phase," Japanese Journal of Applied Physics Part 2 - Letters **36**, L238–L240 (1997).

[35] Y. Torimoto, M. Nishioka, and M. Sadakata, "Emissions of O^- radical anions and electrons from silver on a solid electrolyte," Journal of Catalysis **209**, 256–259 (2002).

[36] M. Nishioka, Y. Torimoto, H. Kashiwagi, Q. Li, and M. Sadakata, "Features and mechanism of atomic oxygen radical anion emission from yttria-stabilized zirconia electrolyte," Journal of Catalysis **215**, 1–6 (2003).

[37] Y. Fujiwara, A. Kaimai, J. Hong, K. Yashiro, Y. Nigara, T. Kawada, and J. Mizusaki, "Emission characteristics of O^- ions from a bare surface of yttria-stabilized zirconia (YSZ) at elevated temperatures," Japanese Journal of Applied Physics Part 2 - Letters **41**, L657–L659 (2002).

[38] Y. Fujiwara, A. Kaimai, J. Hong, K. Yashiro, Y. Nigara, T. Kawada, and J. Mizusaki, "An oxygen negative ion source of a new concept using solid oxide electrolytes," Journal of the Electrochemical Society **150**, E117–E124 (2003).

[39] Y. Fujiwara, T. Sakai, A. Kaimai, K. Yashiro, T. Kawada, and J. Mizusaki, "Continuous emission of O^- ions into a vacuum from a bare surface of yttria-stabilized zirconia at elevated temperatures," Journal of Vacuum Science & Technology A **24**, 1818–1822 (2006).

[40] M. Rohnke, J. Janek, J. Kilner, and R. Chater, "Surface oxygen exchange between yttria-stabilised zirconia and a low-temperature oxygen rf-plasma," Solid State Ionics **166**, 89–102 (2004).

[41] S. Steinmüller, M. Rohnke, and J. Janek, "Low pressure oxygen direct current discharges with ion conducting yttria stabilized zirconia electrodes," Solid State Ionics **245-246**, 24 – 32 (2013). http://www.sciencedirect.com/science/article/pii/S0167273813002476

[42] H. Wagner, R. Brandenburg, K. Kozlov, A. Sonnenfeld, P. Michel, and J. Behnke, "The barrier discharge: basic properties and applications to surface treatment," Vacuum **71**, 417–436 (2003), Symposium on Plasma Surface Engineering held at the Spring Meeting of the German-Physical-Society, Regensburg, Germany, Mar 11-15, 2002.

[43] U. Kogelschatz, "Dielectric-barrier discharges: Their history, discharge physics, and industrial applications," Plasma Chemistry and Plasma Processing **23**, 1–46 (2003).

[44] A. A. Garamoon, D. M. El-zeer, A. Abd El-Ghany, D. Ghoneem, and F. El-Hossary, "Influences of the barrier types and arrangements on dielectric barrier discharge characteristics," European Physical Journal - Applied Physics **53** (2011).

[45] U. Kogelschatz, "Filamentary, patterned, and diffuse barrier discharges," IEEE Transactions on Plasma Science **30**, 1400–1408 (2002).

[46] U. Kogelschatz, "Applications of microplasmas and microreactor technology," Contributions to Plasma Physics **47**, 80–88 (2007), 3^{rd} International Workshop on Microplasmas (IWM 2006), Greifswald, Germany, May 09-11, 2006.

[47] U. Kogelschatz, B. Eliasson, and W. Egli, "Dielectric-barrier discharges. Principle and applications," Journal de Physique IV **7**, 47–66 (1997), XXIII. International Conference on Phenomena in Ionized Gases, Toulouse, France, Jul 17-22, 1997.

[48] R. Brandenburg, Z. Navratil, J. Jansky, P. St'ahel, D. Trunec, and H.-E. Wagner, "The transition between different modes of barrier discharges at atmospheric pressure," Journal of Physics D - Applied Physics **42** (2009).

[49] F. Aghamir, N. Matin, A. Jalili, M. Esfarayeni, M. Khodagholi, and R. Ahmadi, "Conversion of methane to methanol in an AC dielectric barrier discharge," Plasma Sources Science & Technology **13**, 707–711 (2004).

[50] S.-E. Yin, B.-M. Sun, X.-D. Gao, and H.-P. Xiao, "The Effect of Oxygen and Water Vapor on Nitric Oxide Conversion with a Dielectric Barrier Discharge Reactor," Plasma Chemistry and Plasma Processing **29**, 421–431 (2009).

[51] Z. Falkenstein, "Frequency dependence of photoresist ashing with dielectric barrier discharges in oxygen," Journal of Applied Physics **83**, 5095–5101 (1998).

[52] J. Li, S.-P. Bai, X.-C. Shi, S.-L. Han, X.-M. Zhu, W.-C. Chen, and Y.-K. Pu, "Effects of Temperature on Benzene Oxidation in Dielectric Barrier Discharges," Plasma Chemistry and Plasma Processing **28**, 39–48 (2008).

[53] S. Yu and M. Chang, "Oxidative conversion of PFC via plasma processing with dielectric barrier discharges," Plasma Chemistry and Plasma Processing **21**, 311–327 (2001).

[54] R. Li, Y. Yamaguchi, Y. Shu, T. Qing, and T. Sato, "Influence of dielectric barrier materials to the behavior of dielectric barrier discharge plasma for CO_2 decomposition," Solid State Ionics **172**, 235–238 (2004), 15^{th} International Symposium on the Reactivity of Solids, Kyoto, Japan, Nov 09-13, 2003.

[55] R. Li, Q. Tang, S. Yin, and T. Sato, "Plasma catalysis for CO_2 decomposition by using different dielectric materials," Fuel Processing Technology **87**, 617–622 (2006).

[56] G. Samara, "Low-Temperature Dielectric-Properties of Candidate Substrates for High-Temperature Superconductors - $LaAlO_3$ and ZrO_2 - 9.5 Mol-Percent-Y_2O_3," Journal of Applied Physics **68**, 4214–4219 (1990).

[57] T. Ozaki, T. Ogasawara, T. Kosugi, and T. Kamada, "Dielectric dispersion of SiO_2 glass at low temperatures," Physica B **263**, 333–335 (1999), 9^{th} International Conference on Phonon Scattering in Condensed Matter (Phonons 98), Lancaster, England, JUL 26-31, 1998.

[58] G. Ertl, "The Arduous Way to the Haber-Bosch Process," Zeitschrift für anorganische und allgemeine Chemie **638**, 487–489 (2012). http://dx.doi.org/10.1002/zaac.201190458

[59] G. Ertl, "Heterogeneous catalysis on atomic scale," Journal of Molecular Catalysis A: Chemical **182-183**, 5 – 16 (2002). http://www.sciencedirect.com/science/article/pii/S1381116901004605

[60] H.-J. Freund, G. Meijer, M. Scheffler, R. Schlögl, and M. Wolf, "CO Oxidation as a Prototypical Reaction for Heterogeneous Processes," Angewandte Chemie International Edition **50**, 10 064–10 094 (2011). http://dx.doi.org/10.1002/anie.201101378

[61] G. Hutchings, "Promotion in Heterogeneous Catalysis: A Topic Requiring a New Approach?" Catalysis Letters **75**, 1–12 (2001). http://dx.doi.org/10.1023/A

[62] M. Fernandez-Garcia, A. Martinez-Arias, A. Iglesias-Juez, A. Hungria, J. Anderson, J. Conesa, and J. Soria, "New $Pd/Ce_xZr_{1-x}O_2/Al_2O_3$ three-way catalysts prepared by microemulsion - Part 1. Characterization and catalytic behavior for CO oxidation," Applied Catalysis B - Environmental **31**, 39–50 (2001).

[63] A. Martinez-Arias, M. Fernandez-Garcia, A. Iglesias-Juez, A. Hungria, J. Anderson, J. Conesa, and J. Soria, "New $Pd/Ce_xZr_{1-x}O_2/Al_2O_3$ three-way catalysts prepared by microemulsion - Part 2. In situ analysis of CO oxidation and NO reduction under stoichiometric $CO+NO+O_2$," Applied Catalysis B - Environmental **31**, 51–60 (2001).

[64] X. Zhang, H. Shi, and B.-Q. Xu, "Comparative study of Au/ZrO_2 catalysts in CO oxidation and 1,3-butadiene hydrogenation," Catalysis

Today **122**, 330–337 (2007), Gold 2006 Meeting, Univ Limerick, Limerick, Ireland, Sep 03-06, 2006.

[65] R. Craciun, B. Nentwick, K. Hadjiivanov, and H. Knozinger, "Structure and redox properties of MnO_x/yttrium-stabilized zirconia (YSZ) catalyst and its used in CO and CH_4 oxidation," Applied Catalysis A - General **243**, 67–79 (2003).

[66] W. Dow, Y. Wang, and T. Huang, "Yttria-stabilized zirconia supported copper oxide catalyst. 1. Effect of oxygen vacancy of support on copper oxide reduction," Journal of Catalysis **160**, 155–170 (1996).

[67] W. Dow and T. Huang, "Yttria-stabilized zirconia supported copper oxide catalyst. 2. Effect of oxygen vacancy of support on catalytic activity for CO oxidation," Journal of Catalysis **160**, 171–182 (1996).

[68] T.-J. Huang, K.-C. Lee, H.-W. Yang, and W.-P. Dow, "Effect of chromium addition on supported copper catalysts for carbon monoxide oxidation," Applied Catalysis A: General **174**, 199 – 206 (1998). http://www.sciencedirect.com/science/article/pii/S0926860X98001938

[69] M. J. Lippits, A. C. Gluhoi, and B. E. Nieuwenhuys, "A comparative study of the effect of addition of CeO_x and Li_2O on gamma-Al_2O_3 supported copper, silver and gold catalysts in the preferential oxidation of CO," Topics in Catalysis **44**, 159–165 (2007).

[70] P. Esmaeilnejad-Ahranjani, A. Khodadadi, H. Ziaei-Azad, and Y. Mortazavi, "Effects of excess manganese in lanthanum manganite perovskite on lowering oxidation light-off temperature for automotive exhaust gas pollutants," Chemical Engineering Journal **169**, 282 – 289 (2011). http://www.sciencedirect.com/science/article/pii/S1385894711002713

[71] X.-Q. Wang, W. Chen, Q.-P. Guo, Y. Li, G.-H. Lv, X.-P. Sun, X.-H. Zhang, K.-C. Feng, and S.-Z. Yang, "Characteristics of NO_x removal combining dielectric barrier discharge plasma with selective catalytic reduction by C_2H_5OH," Journal of Applied Physics **106** (2009).

[72] C. Chang and T. Lin, "Elimination of carbon monoxide in the gas streams by dielectric barrier discharge systems with Mn catalyst," Plasma Chemistry and Plasma Processing **25**, 387–401 (2005).

[73] V. J. Rico, J. L. Hueso, J. Cotrino, V. Gallardo, B. Sarmiento, J. J. Brey, and A. R. Gonzalez-Elipe, "Hybrid catalytic-DBD plasma reactor for the production of hydrogen and preferential CO oxidation (CO-PROX) at reduced temperatures," Chemical Communications pp. 6192–6194 (2009).

[74] U. Roland, F. Holzer, and F. Kopinke, "Improved oxidation of air pollutants in a non-thermal plasma," Catalysis Today **73**, 315–323 (2002), 5^{th} Europacat Conference, Limerick, Ireland, Sep 02-07, 2001.

[75] A. M. Harling, V. Demidyuk, S. J. Fischer, and J. C. Whitehead, "Plasma-catalysis destruction of aromatics for environmental clean-up: Effect of temperature and configuration," APPLIED CATALYSIS B-ENVIRONMENTAL **82**, 180–189 (2008).

[76] T. Smith, "Diffusion Coefficients and Anion Vacancy Concentrations for the Zirconium-Zirconium Dioxide System," Journal of the Electrochemical Society **112**, 560–567 (1965).

[77] J. Park and R. Blumenthal, "Electronic Transport in 8 Mole Percent Y_2O_3-ZrO_2," Journal of the Electrochemical Society **136**, 2867–2876 (1989).

[78] M. Filal, C. Petot, M. Mokchah, C. Chateau, and J. Carpentier, "Ionic-Conductivity of Yttrium-doped Zirconia and the Composite Effect," Solid State Ionics **80**, 27–35 (1995).

[79] P. Manning, J. Sirman, R. DeSouza, and J. Kilner, "The kinetics of oxygen transport in 9.5 mol % single crystal yttria stabilised zirconia," Solid State Ionics **100**, 1–10 (1997).

[80] M. Weller, R. Herzog, M. Kilo, G. Borchardt, S. Weber, and S. Scherrer, "Oxygen mobility in yttria-doped zirconia studied by internal friction, electrical conductivity and tracer diffusion experiments," Solid State Ionics **175**, 409–413 (2004), 14^{th} International Conference on Solid State Ionics, Monterey, CA, Jun 22-27, 2003.

[81] M. Chen, B. Hallstedt, and L. Gauckler, "Thermodynamic modeling of the ZrO_2 - $YO_{1.5}$ system," Solid State Ionics **170**, 255–274 (2004).

[82] D. Vladikova, J. Kilner, S. Skinner, G. Raikova, and Z. Stoynov, "Differential impedance analysis of single crystal and polycrystalline yttria

stabilized zirconia," Electrochemica Acta **51**, 1611–1621 (2006), 6^{th} International Symposium on Electrochemical Impedance Spectroscopy, Cocoa Beach, FL, May 16-21, 2004.

[83] R. A. De Souza, M. J. Pietrowski, U. Anselmi-Tamburini, S. Kim, Z. A. Munir, and M. Martin, "Oxygen diffusion in nanocrystalline yttria-stabilized zirconia: the effect of grain boundaries," Physical Chemistry Chemical Physics **10**, 2067–2072 (2008).

[84] M. V. F. Schlupp, B. Scherrer, H. Ma, J. G. Grolig, J. Martynczuk, M. Prestat, and L. J. Gauckler, "Influence of microstructure on the cross-plane oxygen ion conductivity of yttria stabilized zirconia thin films," Physica Status Solidi A - Applications and Materials Science **209**, 1414–1422 (2012).

[85] J. Joo and G. Choi, "Electrical conductivity of YSZ film grown by pulsed laser deposition," Solid State Ionics **177**, 1053–1057 (2006).

[86] A. Infortuna, A. S. Harvey, and L. J. Gauckler, "Microstructures of CGO and YSZ thin films by pulsed laser deposition," Advanced Functional Materials **18**, 127–135 (2008).

[87] Pachner, Benjamin, *Herstellung und Charakterisierung von YSZ-Dünnschichten*, Diploma thesis, Justus-Liebig-Universität Gießen (2011).

[88] C. Wagner, "Adsorbed Atomic Species as Intermediates in Heterogeneous Catalysis," Advances in Catalysis **21**, 323 (1970).

[89] C. Vayenas, S. Bebelis, and S. Neophytides, "Non-Faradaic Electrochemical Modofication of Catalytic Activity," Journal of Physical Chemistry **92**, 5083–5085 (1988).

[90] S. Ladas, S. Kennou, S. Bebelis, and C. Vayenas, "Origin of Non-Faradaic Electrochemical Modification of Catalytic Activity," Journal of Physical Chemistry **97**, 8845–8848 (1993).

[91] C. G. Vayenas and S. I. Bebelis, "Electrochemical promotion," Solid State Ionics **94**, 267 – 277 (1997).
http://www.sciencedirect.com/science/article/pii/S0167273896005115

[92] C. G. Vayenas and S. Bebelis, "Electrochemical promotion of heterogeneous catalysis," Catalysis Today **51**, 581 – 594 (1999).
http://www.sciencedirect.com/science/article/pii/S0920586199000425

[93] M. N. Tsampas, F. M. Sapountzi, and C. G. Vayenas, "Electrochemical promotion of CO oxidation on Pt/YSZ: The effect of catalyst potential on the induction of highly active stationary and oscillatory states," Catalysis Today **146**, 351–358 (2009), 2^{nd} Conference on Applications of Electrochemical Promotion of Catalysis (EPOCAP), Oleron Isl, France, Sep-Oct, 2008.

[94] R. Imbihl, "Electrochemical promotion of catalytic reactions," Progress in Surface Science **85**, 241–278 (2010).

[95] G. Dilecce, P. F. Ambrico, and S. De Benedictis, "Optical diagnostics in dielectric barrier discharges at atmospheric pressure," Pure and Applied Chemistry **82**, 1201–1207 (2010), 19^{th} International Symposium on Plasma Chemistry (ISPC-19), Bochum, Germany, Jul 26-31, 2009.

[96] R. Geballe and M. Harrison, "Negative Ion Formation in Oxygen," Physical Review **85**, 372–373 (1952).

[97] A. Bell, "Concentrations of Atoms and Negative Ions of Oxygen in Drift Tubes and High-Frequency Electric Discharges," Industrial & Engineering Chemistry Fundamentals **10**, 373–379 (1971).

[98] B. Davis, "Energy Necessary to Ionize a Molecule by Impact of Negative Ions," Phys. Rev. (Series I) **24**, 93–102 (1907). http://link.aps.org/doi/10.1103/PhysRevSeriesI.24.93

[99] A. Kramida, Yu. Ralchenko, J. Reader, and and NIST ASD Team, NIST Atomic Spectra Database (ver. 5.1), [Online]. Available: `http://physics.nist.gov/asd` [2013, September 21]. National Institute of Standards and Technology, Gaithersburg, MD. (2013).

[100] H. Jia, H. Fujiwara, M. Kondo, and H. Kuraseko, "Optical emission spectroscopy of atmospheric pressure microwave plasmas," Journal of Applied Physics **104** (2008). http://scitation.aip.org/content/aip/journal/jap/104/5/10.1063/1.2975345

[101] A. Lofthus and P. H. Krupenie, "The spectrum of molecular nitrogen," Journal of Physical and Chemical Reference Data **6**, 113–307 (1977). http://link.aip.org/link/?JPR/6/113/1

[102] P. H. Krupenie, "The Spectrum of Molecular Oxygen," Journal of Physical and Chemical Reference Data **1**, 423–534 (1972). http://link.aip.org/link/?JPR/1/423/1

[103] J. J. Camacho, M. Santos, L. DÃŋaz, and J. M. L. Poyato, "Optical emission spectroscopy of oxygen plasma induced by IR CO_2 pulsed laser," Journal of Physics D: Applied Physics **41**, 215 206 (2008). http://stacks.iop.org/0022-3727/41/i=21/a=215206

[104] P. G. Reyes, E. F. Mendez, D. Osorio-Gonzalez, F. Castillo, and H. Martinez, "Optical Emission Spectroscopy of CO_2 Glow Discharge at Low Pressure," Physica Status Solidi (c) **5**, 907–910 (2008). http://dx.doi.org/10.1002/pssc.200778306

[105] B. Hobein, F. Tietz, D. Stover, and E. Kreutz, "Pulsed laser deposition of yttria stabilized zirconia for solid oxide fuel cell applications," Journal of Power Sources **105**, 239–242 (2002), 7^{th} Annual Ulmer Electrochemical Day, Ulm, Germany, Jun 26-27, 2000.

[106] K. Rodrigo, J. Knudsen, N. Pryds, J. Schou, and S. Linderoth, "Characterization of yttria-stabilized zirconia thin films grown by pulsed laser deposition (PLD) on various substrates," Applied Surface Science **254**, 1338–1342 (2007), Symposium on Laser Synthesis and Processing of Advanced Materials held at the E-MRS 2007 Spring Meeting, Strasbourg, France, 2007.

[107] X. Zhang, P. Berdahl, A. Klini, C. Fotakis, and S. S. Mao, "Transition of crystalline orientation of yttria-stabilized zirconia films grown by pulsed laser deposition," Applied Physics A - Materials Science & Processing **91**, 407–410 (2008).

[108] S. Heiroth, R. Frison, J. L. M. Rupp, T. Lippert, E. J. B. Meier, E. M. Gubler, M. Doebeli, K. Conder, A. Wokaun, and L. J. Gauckler, "Crystallization and grain growth characteristics of yttria-stabilized zirconia thin films grown by pulsed laser deposition," Solid State Ionics **191**, 12–23 (2011).

[109] N. Pryds, J. Schou, and S. Linderoth, "Large-area production of yttria-stabilized zirconia by pulsed laser deposition," in *COLA'05: 8^{th} International Conference on Laser Ablation* (2007), pp. 140–143, 8^{th} International Conference on Laser Ablation, Banff, Canada, Sep 11-16, 2005.

[110] B. Hobein, F. Tietz, D. Stover, M. Cekada, and P. Panjan, "DC sputtering of yttria-stabilised zirconia films for solid oxide fuel cell applications," Journal of the European Ceramic Society **21**, 1843–1846 (2001),

7^{th} International Conference on Electronic Ceramics and their Applications (ELECTROCERAMICS VII-2000), Portoroz, Slovenia, Sep 03-06, 2000.

[111] J. Cyviene, J. Dudonis, M. Laurikaitis, A. Rakauskas, and D. Milcius, "Synthesis of ZrO_2/Y_2O_3 by combined arc and magnetron sputtering technique," Surface and Coatings Technology **180-181**, 53 – 58 (2004). http://www.sciencedirect.com/science/article/pii/S0257897203011769

[112] P. Fedtke, M. Wienecke, M. Bunescu, T. Barfels, K. Deistung, and M. Pietrzak, "Yttria-stabilized zirconia films deposited by plasma spraying and sputtering," Journal of Solid State Electrochemisty **8**, 626–632 (2004), OSSEP Workshop on Ionic and Mixed Conductors, Aveiro, Portugal, Apr, 2003.

[113] A. L. Shaula, J. C. Oliveira, V. A. Kolotygin, C. Louro, V. V. Kharton, and A. Cavaleiro, "Protective YSZ-based thin films deposited by RF magnetron sputtering," Vacuum **83**, 1266–1269 (2009), 5^{th} European Topical Conference on Hard Coating, Caparica, Portugal, Jun 22-25, 2008.

[114] R. Nedelec, S. Uhlenbruck, D. Sebold, V. A. C. Haanappel, H.-P. Buchkremer, and D. Stoever, "Dense yttria-stabilised zirconia electrolyte layers for SOFC by reactive magnetron sputtering," Journal of Power Sources **205**, 157–163 (2012).

[115] S. Sonderby, A. J. Nielsen, B. H. Christensen, K. P. Almtoft, J. Lu, J. Jensen, L. P. Nielsen, and P. Eklund, "Reactive magnetron sputtering of uniform yttria-stabilized zirconia coatings in an industrial setup," Surface & Coatings Technology **206**, 4126–4131 (2012).

[116] Steinmüller, Sven Ole, *Erzeugung und Charakterisierung von Niedertemperaturplasmen mit ionenleitenden Elektroden*, Diploma thesis, Justus-Liebig-Universität Gießen (2007).

[117] T.-H. Lee, H.-W. Cheong, O. Kwon, K.-W. Whang, S. O. Steinmueller, and J. Janek, "The role of a diffusion barrier in plasma display panel with the high gamma cathode layer," Applied Physics Letters **99** (2011).

[118] H. Hayashi, T. Saitou, N. Maruyama, H. Inaba, K. Kawamura, and M. Mori, "Thermal expansion coefficient of yttria stabilized zirconia for various yttria contents," Solid State Ionics **176**, 613–619 (2005).

[119] H. Yamamura, Y. Yagi, and K. Kakinuma, "Dielectric Relaxations of Y-Doped ZrO_2 Single Crystal," Journal of the Ceramic Society of Japan **115**, 546–550 (2007).

[120] N. H. Perry, S. Kim, and T. O. Mason, "Local electrical and dielectric properties of nanocrystalline yttria-stabilized zirconia," Journal of Materials Science **43**, 4684–4692 (2008), 16^{th} International Symposium on the Reactivity of Solids, Minneapolis, MN, Jun 03-06, 2007.

[121] H. Yamamura, Y. Yagi, and K. Kakinuma, "Electrode Effects for Dielectric Properties of 8 mol% Y_2O_3 Stabilized ZrO_2," Electrochemisty **76**, 734–739 (2008).

[122] N. H. Perry, T. C. Yeh, and T. O. Mason, "Temperature Dependence of Effective Grain Core/Single Crystal Dielectric Constants for Acceptor-Doped Oxygen Ion Conductors," Journal of the American Ceramic Society **94**, 508–515 (2011).

[123] N. Baumann, E. Mutoro, and J. Janek, "Porous model type electrodes by induced dewetting of thin Pt films on YSZ substrates," Solid State Ionics **181**, 7–15 (2010).

[124] A. Toghan, M. Khodari, F. Steinbach, and R. Imbihl, "Microstructure of thin film platinum electrodes on yttrium stabilized zirconia prepared by sputter deposition," Thin Solid Films **519**, 8139–8143 (2011).

[125] J. Janek and C. Korte, "Electrochemical blackening of yttria-stabilized zirconia - morphological instability of the moving reaction front," Solid State Ionics **116**, 181–195 (1999).

[126] L. Mond, C. Langer, and F. Quincke, "Action of Carbon Monoxide on Nickel ," Journal of the Chemical Society, Transactions **57**, 749–753 (1890).

[127] J. McCarley, R. Saltzman, and R. Osborn, "Recording Nickel Carbonyl Detector," Analytical Chemistry **28**, 880–882 (1956).

Acknowledgment - Danksagung

Mein großer Dank gilt Herrn Prof. Dr. Jürgen Janek für die Möglichkeit, diese Arbeit unter seiner Betreuung anfertigen zu können. Durch seinen Kontakt zu der Arbeitsgruppe von Prof. Whang von der Seoul National University entwickelte sich die thematische Idee zu dieser Promotionsarbeit.

Ich danke daher ebenfalls der Arbeitsgruppe von Herrn Prof. Whang und im besonderen Herrn Tae-Ho Lee für die Zusammenarbeit während der Testmessungen an ersten DBD YSZ Dünnschicht Plasma Zellen.

Der Arbeitsgruppe von Prof. Dr. Bruno Meyer im I. Physikalischen Institut der Justus-Liebig-Universität Gießen und im besonderen Herrn Benjamin Pachner und Frau Dr. Angelika Polity danke ich für die Unterstützung bei der YSZ Dünnschichtherstellung.

Für die Unterstützung beim Bau des AC-Generators für die Plasmaentladung und für alle damit verbundenen Diskussionen danke ich Herrn Harald Weigand, der immer die Notwendige Geduld hatte.

Der gesamten Feinmechanikwerkstatt gilt mein großer Danke, da alle Mitarbeiter immer geholfen haben, mein störrisches Plasma in seinen apparativen Grenzen zu halten.

Mein besonderer Dank gebührt Herrn Dr. Marcus Rohnke, der mir während der gesamten Promotionsarbeit als Ansprechpartner zur Verfügung stand. Ich danke ebenfalls für das Vertrauen mich am Tof-SIMS anzulernen und eigenständig arbeiten zu lassen.

Mein besonderer Dank gilt ebenfalls meiner Mutter, die mich während der ganzen Zeit nach allen ihr zur Verfügung stehenden Möglichkeiten unterstützt hat.

Ich Danke allen Mitgliedern des PCI für die angeregten Diskussionen und Hilfen während meiner Promotionszeit. Hervorheben möchte ich dabei:

Markus Göttlicher mit dem ich so manches "Problem" im Plasmalabor lösen konnte.

Jochen Reinacher, der die ersten beiden YSZ Plasma Zellen Prototypen während seines Aufenthaltes an der Seoul National University in der Arbeitsgruppe von Prof. Whang untersuchte und dadurch bedingt auch im Büro die meisten Diskussionen mit mir führen durfte.
Rabea Dippel und Kerstin Sann, die immer ein offenes Ohr für mich hatten und am Leo Gemini Rasterelektronenmikroskop bzw. im Lithiumlabor hilfreich zur Seite standen.
Dr. Klaus Peppler, der mich bei den Messungen am Merlin Rasterelektronenmikroskop unterstützt hat.

Mein großer Dank gilt Tanja Hagedorn für das Korrekturlesen meiner Arbeit.

Mein größter Dank gilt meiner Freundin Luisa, die mir die richtigen Dinge zur richtigen Zeit sagte und mich immer wieder zur Fertigstellung dieser Arbeit motivierte.